



ALESSANDRA DAVÓLIO GOMES

**USING RESERVOIR SIMULATION TO
CONSTRAIN THE ESTIMATION OF DYNAMIC
PROPERTIES FROM 4D SEISMIC**

***USO DA SIMULAÇÃO DE RESERVATÓRIOS PARA
RESTRINGIR A ESTIMATIVA DE PROPRIEDADES
DINÂMICAS A PARTIR DA SÍSMICA 4D***

CAMPINAS

2013



UNIVERSIDADE ESTADUAL DE CAMPINAS
FACULDADE DE ENGENHARIA MECÂNICA
E INSTITUTO DE GEOCIÊNCIAS

ALESSANDRA DAVÓLIO GOMES

**USING RESERVOIR SIMULATION TO CONSTRAIN THE
ESTIMATION OF DYNAMIC PROPERTIES FROM 4D SEISMIC**

***USO DA SIMULAÇÃO DE RESERVATÓRIOS PARA RESTRINGIR
A ESTIMATIVA DE PROPRIEDADES DINÂMICAS A PARTIR DA
SÍSMICA 4D***

Thesis presented to the Mechanical Engineering Faculty and Geosciences Institute of the University of Campinas in partial fulfillment of the requirements for the degree of Doctor in Petroleum Sciences and Engineering in the area of Reservoirs and Management.

Tese apresentada à Faculdade de Engenharia Mecânica e Instituto de Geociências da Universidade Estadual de Campinas como parte dos requisitos exigidos para a obtenção do título de Doutora em Ciências e Engenharia de Petróleo na área de Reservatórios e Gestão.

Orientador: Prof. Dr. Denis José Schiozer

Co-orientador: Dr. Célio Maschio

Este exemplar corresponde à versão final da tese defendida pelo aluno Alessandra Davólio Gomes e orientada pelo Prof. Dr. Denis José Schiozer.

A handwritten signature in blue ink is written over a horizontal line. The signature is cursive and appears to be the name of the student, Alessandra Davólio Gomes.

CAMPINAS
2013

Ficha catalográfica
Universidade Estadual de Campinas
Biblioteca da Área de Engenharia e Arquitetura
Rose Meire da Silva - CRB 8/5974

D311u Davólio, Alessandra, 1980-
Using reservoir simulation to constrain the estimation of dynamic properties
from 4D seismic / Alessandra Davólio Gomes. – Campinas, SP : [s.n.], 2013.

Orientador: Denis José Schiozer.

Coorientador: Célio Maschio.

Tese (doutorado) – Universidade Estadual de Campinas, Faculdade de
Engenharia Mecânica e Instituto de Geociências.

1. Reservatório de petróleo. 2. Engenharia de petróleo. 3. Engenharia de
petróleo - Metodos de simulação. 4. Geofísica. 5. Prospecção sísmica. I. Schiozer,
Denis José, 1963-. II. Maschio, Célio. III. Universidade Estadual de Campinas.
Faculdade de Engenharia Mecânica. IV. Título.

Informações para Biblioteca Digital

Título em outro idioma: Uso da simulação de reservatórios para restringir a estimativa de
propriedades dinâmicas a partir da sísmica 4D

Palavras-chave em inglês:

Reservoir simulation

Petroleum engineering

Petroleum engineering - Simulation method

Geophysics

Seismic prospecting

Área de concentração: Reservatórios e Gestão

Titulação: Doutora em Ciências e Engenharia de Petróleo

Banca examinadora:

Denis José Schiozer [Orientador]

Osvair Vidal Trevisan

Alexandre Anozé Emerick

Álvaro Favinha Martini

Thierry Jean-Louis Marie Coleou

Data de defesa: 24-10-2013

Programa de Pós-Graduação: Ciências e Engenharia de Petróleo



UNIVERSIDADE ESTADUAL DE CAMPINAS
FACULDADE DE ENGENHARIA MECÂNICA
E INSTITUTO DE GEOCIÊNCIAS

TESE DE DOUTORADO

USING RESERVOIR SIMULATION TO CONSTRAIN THE
ESTIMATION OF DYNAMIC PROPERTIES FROM 4D SEISMIC

Author: Alessandra Davólio Gomes
Advisor: Prof. Dr. Denis José Schiozer
Co-advisor: Dr. Célio Maschio

A banca examinadora composta pelos membros abaixo aprovou esta tese:

A handwritten signature in blue ink, appearing to be "Denis José Schiozer", written over a horizontal line.

Prof. Dr. Denis José Schiozer, Presidente
DEP/FEM/UNICAMP

A handwritten signature in blue ink, appearing to be "Osvaldo Vidal Trevisan", written over a horizontal line.

Prof. Dr. Osvaldo Vidal Trevisan
DEP/FEM/UNICAMP

A handwritten signature in blue ink, appearing to be "Alexandre Anozé Emerick", written over a horizontal line.

Dr. Alexandre Anozé Emerick
CENPES/PETROBRAS

A handwritten signature in blue ink, appearing to be "Álvaro Favinha Martini", written over a horizontal line.

Dr. Álvaro Favinha Martini
E&P-ENGP/PR/GFR/PETROBRAS

A handwritten signature in blue ink, appearing to be "Thierry Jean-Louis Marie Coleou", written over a horizontal line.

Dr. Thierry Jean-Louis Marie Coleou
CGG

Campinas, 24 de outubro de 2013

DEDICATION

This work is dedicated to a great (and patient) partner: Ricardo.

ACKNOWLEDGMENTS

(*AGRADECIMENTOS*)

I believe that talking about feelings is better done in our mother language so, for the following, pardon my Portuguese.

Ao meu orientador, Prof. Denis Schiozer, pelas valiosas (e diversas) discussões e ideias. Inclusive, e talvez principalmente, por aquelas em que não concordamos de início! Também pelo seu entusiasmo para novas possibilidades, o que me incentivou a aceitar novos desafios.

Ao Célio Maschio, pela prontidão para discutir resultados e ideias. Pelas inúmeras dicas de programação, formatação de texto, manipulação de softwares e afins! Agradeço também por me convencer a submeter o primeiro artigo deste trabalho, que acabou se tornando o ponto de partida para a estruturação da tese!

Aos meus pais, Ignez e Neudeci, pelo imensurável apoio em todos os meus passos.

Ao meu esposo, Ricardo, grande incentivador deste trabalho! Além de contribuir diretamente com instalações de softwares e correção de textos, reconheço que o bem que sua companhia me faz tem uma parcela considerável em todas as minhas realizações. Obrigada pelo companheirismo e pelo colorido que traz à minha vida!

À toda minha família, em especial àqueles que estão mais próximos: Adriana, Fabiano e minhas grandes paixões, Isabela e Felipe, que me ensinaram que pular corda é um ótimo exercício para esquecer (momentaneamente) uma tese pendente...

À minha família baiana a quem, apesar de incluída no parágrafo acima, gostaria de agradecer, de forma especial, todo o carinho e incentivo recebidos.

A todos os meus amigos, simplesmente por existirem em minha vida! Em especial, a duas figuras bastante presentes durante o desenvolvimento deste trabalho: Perin, pela arte e pelas dicas de Matlab e Marcos Sebastião, por sempre me ajudar em meus devaneios geofísicos e me confortar durante as tais crises do “tá tudo errado!”. Agradeço também ao Jean-Luc, que além da convivência, me proporcionou importantes aprendizados sobre geofísica. Além de ter me ajudado a montar a banca avaliadora! Merci!

Ao Henning Hoerber, por gentilmente disponibilizar uma das ferramentas mais úteis que conheço para gerar apresentações! (Thanks, Henning!)

Aos meus colegas do UNISIM, CEPETRO e DEP, por todo tipo de ajuda.

À PETROBRAS e à BG, pelo apoio financeiro.

*“The mind that opens to a new idea never returns
to its original size.”*

Albert Einstein (supposedly)

ABSTRACT

The focus of this work is to use reservoir engineering data from numerical flow simulation to improve the quantitative interpretation of 4D seismic signals. The idea is to use engineering knowledge to minimize possible incorrect information provided by 4D seismic before using it to update reservoir simulation models in a history matching procedure. In this work the integration between the two dataset is done in the pressure and saturation domain. So, the first part of the work presents a methodology to estimate pressure and saturation changes from 4D seismic through a petro-elastic inversion procedure. This procedure can be seen as a tool to apply the integration methodology of the second part which is one of the main contributions of this work. The integration methodology uses multiple simulation models to constrain the estimation of pressure and saturation from 4D seismic. As a result, less noisy maps were obtained, allowing a better interpretation of the reservoir changes. Following the traditional sequence, the estimated saturation map is then used as input to the history matching process presented in the third part of the work. It was shown that the history matching procedure provides better results if the input data, in this case the saturation map, respects the expected mass balance, which was not the case for the dataset considered. Thus, a methodology to calibrate the volume of injected water associated to the saturation map provided by 4D seismic is presented in the last part of the work, which is another important contribution to be highlighted. To better control the results of all the methodologies here presented, a synthetic dataset was used in the entire work. Although satisfactory results were observed for this dataset, it is important to highlight that the main contributions of this work are not only the results, but the methodologies proposed, that present an innovative perspective for 4D seismic and reservoir engineering data integration.

Keywords: 4D seismic; reservoir simulation; history matching; time-lapse seismic integration.

RESUMO

O foco deste trabalho é usar dados de engenharia de reservatórios gerados através da simulação de fluxos para melhorar a interpretação quantitativa da sísmica 4D. A ideia é usar os conhecimentos de engenharia para minimizar possíveis informações incorretas geradas pela sísmica 4D, antes de usá-la para atualizar modelos de simulação de reservatórios em um procedimento de ajuste de histórico. Neste trabalho a integração entre estes dois conjuntos de dados é feita no domínio da pressão e saturação. Dessa forma, a primeira parte do trabalho apresenta uma metodologia para estimar variações de pressão e saturação a partir da sísmica 4D através de um procedimento de inversão petro-elástica. Este procedimento pode ser visto como uma ferramenta para aplicar a metodologia de integração da segunda parte, que é uma das principais contribuições deste trabalho. A metodologia de integração usa múltiplos modelos de simulação para restringir a estimativa de pressão e saturação a partir da sísmica 4D. Como resultado, observaram-se mapas menos ruidosos que permitem, portanto, uma melhor interpretação das variações ocorridas no reservatório. Seguindo a sequencia tradicional de trabalho, o mapa de saturação estimado foi então usado como dado de entrada em um processo de ajuste de histórico apresentado na terceira parte da tese. Foi mostrado que o procedimento de ajuste gera melhores resultados quando o dado de entrada, neste caso mapa de saturação, respeita o balanço de massa, o que não acontecia para os dados considerados. Assim, uma metodologia para calibrar o volume de água injetada associado ao mapa de saturação gerado pela sísmica 4D é apresentada na última parte do trabalho, que é outra contribuição importante a se destacar. Para melhor controlar os resultados de todas as metodologias aqui apresentadas foram usados dados sintéticos em todo o trabalho. Embora resultados satisfatórios tenham sido observados para este conjunto de dados, é importante destacar que as principais contribuições deste trabalho não são apenas os resultados observados, mas as metodologias propostas, que apresentam uma perspectiva inovadora para integração entre dados de sísmica 4D e engenharia de reservatórios.

Palavras-Chave: sísmica 4D; simulação de reservatórios; ajuste de histórico; integração entre simuladores de fluxo e sísmica 4D.

TABLE OF CONTENTS

1. INTRODUCTION.....	1
1.1. Motivation.....	3
1.2. Objective.....	4
1.3. Premises.....	4
1.4. Description of the work.....	5
1.4.1. Paper 1: “ <i>Pressure and saturation estimation from P and S impedances: a theoretical study</i> ”	5
1.4.2. Paper 2: “ <i>A methodology to constrain pressure and saturation estimation from 4D seismic using multiple simulation models and observed data</i> ”	6
1.4.3. Paper 3: “ <i>Local history matching using 4D seismic data and multiple models combination</i> ”	7
1.4.4. Paper 4: “ <i>A methodology to calibrate water saturation estimated from 4D seismic</i> ”	8
2. PAPER 1: <i>Pressure and saturation estimation from P and S impedances: a theoretical study</i>.....	9
3. PAPER 2: <i>A methodology to constrain pressure and saturation estimation from 4D seismic using multiple simulation models and observed data</i>.....	25
4. PAPER 3: <i>Local history matching using 4D seismic data and multiple models combination</i>.....	39
5. PAPER 4: <i>A methodology to calibrate water saturation estimated from 4D seismic</i>.....	53
6. CONCLUSIONS.....	73
7. FUTURE WORKS.....	77
REFERENCES.....	79
APPENDIX A : Complementary results of the paper “<i>Pressure and saturation estimation from P and S impedances: a theoretical study</i>”	87

APPENDIX B : Complementary results of the paper “Local history matching using 4D seismic data and multiple models combination”.....109
APPENDIX C : Complementary results of the paper “A methodology to calibrate water saturation estimated from 4D seismic”.....113

1. INTRODUCTION

Reservoir simulation is one of the main tools used for dynamic reservoir characterization and management. Thus, one of the principal tasks of geoscientists and reservoir engineers is to build reliable models, which is not an easy task due to the complexity present in this kind of problem. The complexity comes mainly from the lack of geological information required to build such models. The confidence in the simulation models can be improved by incorporating dynamic data in a history matching procedure.

Traditional history matching procedures use well information such as pressure, oil, water and gas rates, to update the static model properties such as permeability, porosity, faults transmissibility and so on. The use of well data is generally insufficient to give confidence to simulation models because the process is an inverse and ill-posed problem.

The use of time-lapse seismic (also called 4D seismic) in history matching procedures is relatively new, but has become increasingly common in the recent years. The main contribution that this data brings is the areal information regarding the dynamic properties variations (such as pressure and saturation changes) observed due to production. Thus, instead of having only production profiles at very few points in the reservoir (well locations), spatial variations of dynamic properties also become accessible. This type of information can be used to update reservoir models in several ways, from qualitative interpretation, which helps to better map the uncertainties, to quantitative incorporation of seismic information inside the objective function (that measures the quality of the matching) of a history matching procedure. Another issue to be considered when 4D seismic is used to update reservoir models, is which seismic attribute should be used. In general, there are three possibilities (Figure 1): (1) time-lapse seismic can be incorporated into the history matching in its original domain, *i.e.*, in the form of seismic amplitudes; (2) it can be inverted to seismic impedances; and (3) it can be converted to pressure and saturation data. Although there are several works in the literature proposing different methodologies to integrate 4D seismic in the history matching, there is not a standard procedure to follow concerning the optimization algorithm to use, or the choice of the integration domain.

Usually the procedure for integrating 4D seismic data and reservoir information can be split into two independent steps: the first is related to the efforts of geophysicists to manipulate 4D seismic data and interpret the changes of reservoir properties and the second is the engineer driven process of including this new information in the reservoir simulation model (by running a history matching procedure, for instance).

This work is based on the idea that the integration between 4D seismic and simulation data should be done not only by following the traditional sequence, where 4D seismic is an input for a history matching. The idea is to use engineering knowledge to minimize possible incorrect information provided by 4D seismic before adding it to the matching procedure. Thus, this work proposes two methodologies that use simulation results to condition the estimation of dynamic properties from 4D, which are later used in a history matching procedure.

All of this work was developed to perform the integration between the two datasets in the pressure and saturation domain (Figure 1). The reason for working in this domain is determined by the fact that the values of these physical quantities can be controlled better than the elastic properties of rock (such as impedance); *i.e.*, it is easier to establish feasible limits of pressure and saturation for a given production scenario than it is to determine corresponding limits of impedances. Thus, working in this domain allows a clear view of the methodologies presented here.

Thereby, this thesis is structured in four papers (figure 2), the first of which describes the 4D inversion procedure proposed to estimate pressure and saturation from time-lapse seismic. The second paper proposes the first methodology of integration that uses reservoir simulation results to constrain the estimation of pressure and saturation maps to flow conditions. The third paper then proposes a history matching procedure that uses the previously estimated saturation map to perform a local history matching. Due to noise in seismic data and errors in the characterization of static properties, the estimated saturation map shown in paper 2 presented a volume of injected water larger than the expected. Thus, in the fourth and last paper, its effects on the history matching results of paper 3 are discussed and a methodology to calibrate the volume of water is proposed.

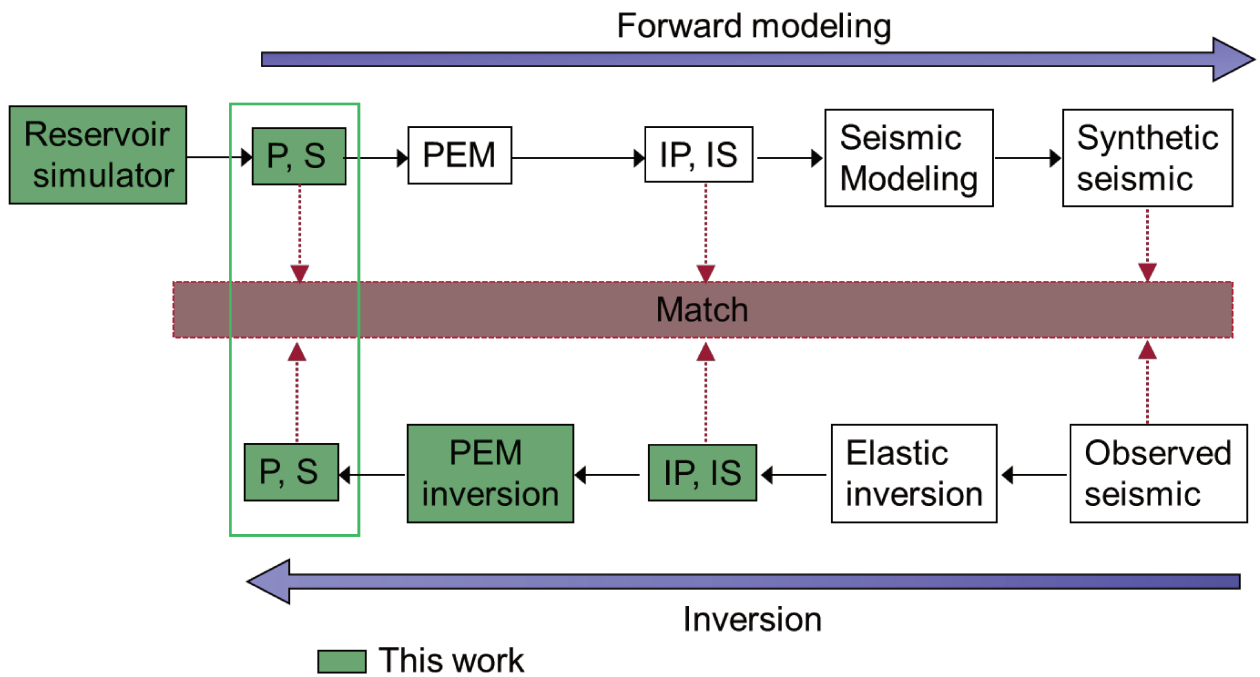


Figure 1: Possible domains of integration between 4D seismic and simulation data. As illustrated by the green boxes, in this work P and S impedances (named IP and IS, respectively) are converted to pressure (P) and saturation (S) values.

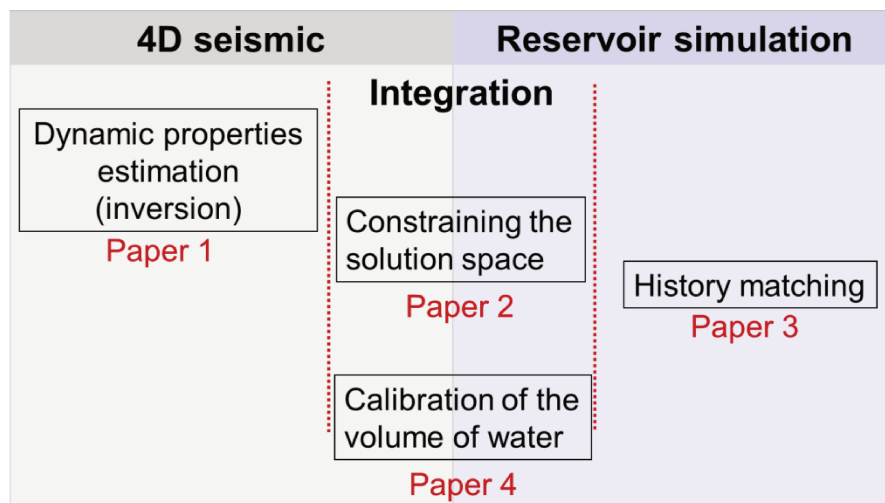


Figure 2: Structure of the thesis according to the main area of concentration of each paper.

1.1. Motivation

The motivation of this work is to generate more reliable reservoir models by improving the integration between reservoir simulation and 4D seismic. Since reservoir simulation models

can be seen as one of the main tools for reservoir management, the accuracy of these models is directly related to more efficient field operations and better financial return.

1.2. Objective

The objective of this work is to develop a methodology that uses reservoir behavior prediction from a flow simulator to improve the quantitative interpretation of 4D seismic data. Thus, the work proposes a quantitative integration that allows the estimation of dynamic properties from 4D signals, in agreement with information available from engineering data such as simulation results and volume of injected water. The goal is to generate a more reliable quantitative interpretation of 4D seismic, to be used as input to update reservoir simulation models, achieving a safer model updating when performing a history matching.

1.3. Premises

- In order to verify the efficiency and accuracy of the proposed methodologies, all the work was developed using synthetic data. Two simulation models were considered, called base and reference models. The base model represents the available knowledge of the reservoir, so it has a lack of information on the static properties (uncertainties). The reference model represents the true earth model, namely the answer that all the processes aim to reach.
- The synthetic seismic data considered in this work are P and S impedances, which are generated by running a petro-elastic model with the reference model properties and scale. Some noise was added to the impedances in order to mimic real problems (more details in paper 2). No seismic amplitudes were generated so no kind of elastic inversion was run.
- All data are at the same scale. All the simulation models considered in this work and seismic data were created at the same grid (110 x 90 x 5 blocks).
- As the seismic data (P and S impedances) are at the reservoir scale, they have 5 layers. So, when the term “map information” is used, it can be interpreted as volume, or five maps information (one for each layer).

- The base survey of the 4D seismic is considered to be acquired before production starts, so the dynamic properties of the reservoir (pressure and saturation) are considered to be known at the initial time (it has no uncertainties).
- No presence of gas (waterflood example above bubble pressure).
- Case studied: sandstone reservoir.
- The dynamic properties considered in this work are pressure and water saturation.

1.4. Description of the work

This thesis is structured in four scientific papers. This section presents a summary of each paper, highlighting the main contributions and how they are connected in the building of the whole thesis. The thesis also comprises three appendixes with complementary analyses and results of the papers; the relations between the papers and the appendixes are described in this section as well.

The papers in full extension are presented in the following chapters.

1.4.1. Paper 1: “*Pressure and saturation estimation from P and S impedances: a theoretical study*”

*Alessandra Davolio, Célio Maschio, Denis José Schiozer
Journal of Geophysics and Engineering, August 2012, v.9, p.447-460*

The first paper of this work presents a theoretical study of the proposed petro-elastic inversion process, which estimates pressure and saturation from time-lapse seismic. The estimation is achieved by an optimization procedure solved by a gradient-type method. As stated in the premises, this work considers synthetic data so, this paper presents a discussion that starts with an ideal dataset (free of error or noise) to explain the necessity of using two seismic attributes (P and S impedances). Then, some uncertainties in the static properties and errors in the seismic data were gradually considered and the inversion behavior was analyzed. When errors/uncertainties were considered, it was possible to verify the importance of using a 4D approach in the inversion scheme instead of a 3D inversion. The main goal of this paper is to better understand the inversion itself and the robustness and confidence of the optimization algorithm used; hence, it presents discussions on the objective function behavior, initial guess and

uniqueness of solution. To be able to visualize these issues, all the results presented are related to single reservoir blocks. This is possible because the inversion is run independently for each grid block.

The main contribution of this paper to the thesis is the implementation of a 4D inversion algorithm to obtain pressure and saturation from time-lapse seismic and the understanding of its advantages and limitations.

Appendix A presents some complementary results from paper 1. The same issues discussed in paper 1 for a single reservoir location are presented in Appendix A for an entire reservoir model so that the inversion results can be analyzed for different combinations of static and dynamic properties (namely different reservoir locations). The results presented in Appendix A were extracted from the work of Davolio et al (2011), which is attached at the end of the same appendix.

1.4.2. Paper 2: “A methodology to constrain pressure and saturation estimation from 4D seismic using multiple simulation models and observed data”

*Alessandra Davolio, Célio Maschio, Denis José Schiozer
Journal of Petroleum Science and Engineering, April 2013, v. 105, p. 51-61
Presented at SEG/SPE/AAPG Workshop “New advances in integrated reservoir surveillance”, California, 24-29 June 2012*

This paper proposes a methodology to constrain the inversion process presented in paper 1 to flow conditions. It is well known that seismic data carry errors due to a number of causes, from the acquisition methods to specific data processing procedures that can yield wrong reservoir data estimation. The central idea of the proposed methodology is that before using 4D seismic data in a history matching process, especially quantitatively, this data can be conditioned to some known engineering information. As in any optimization process, the solution space of the proposed inversion procedure can be constrained by known limits. For instance, in our case, they could be considered as general constraints of water saturation, connate water and one minus the residual oil saturation. But, instead of using these general values, the methodology proposes to extract minimum and maximum values for saturation and pressure from the simulation of multiple reservoir models. The multiple models are generated through the combination of the most important reservoir attributes, mapped as uncertainties. So, the limits imposed to the 4D seismic

are derived from the knowledge available at the current stage of the characterization process. The results presented show that the dynamic properties estimated through these constraints are less noisy and have more confidence to be further applied qualitatively or quantitatively in a history matching procedure. The main contribution of this work is the proposed methodology that allows checking the information extracted from 4D seismic to verify that it is in agreement with the uncertainties mapped in the characterization process.

1.4.3. Paper 3: “Local history matching using 4D seismic data and multiple models combination”

*Alessandra Davolio, Célio Maschio, Denis José Schiozer
Presented at the EAGE/SPE Europec Annual Conference & Exhibition, London, United Kingdom, 10–13 June 2013*

The third paper proposes a history matching methodology that uses the water saturation distribution obtained from 4D seismic data (resulting from paper 2) to update local properties. The idea behind the process is the use of saturation changes estimated from 4D seismic as local information for each injector well. The procedure proposed uses several model realizations as input, which are the same as those used in paper 2. The updating step is then made by a “copy and paste” procedure of the grid properties, such as porosity and permeability that are represented by geostatistical images. Then, the methodology replaces the base model properties with those extracted from the best model chosen for each region. The results showed that the updated model yielded a saturation map that is closer to the one observed from seismic. Thus, the main contribution of this paper is an easy-to-implement procedure that generates an updated model that reproduces the changes observed in 4D seismic and presents updated properties with geological aspects. So, it can be seen as an alternative to the sophisticated algorithms that incorporate geostatistical images in the history matching process.

The results of paper 2 are maps of saturation and pressure, so, for the dataset considered in this work, both maps would be available to perform the history matching. However, as presented in Appendix B, a satisfactory pressure map was achieved after a calibration of the global reservoir properties, which justifies the use of only the saturation map in the history matching presented in paper 3. See Appendix B for more details on pressure behavior.

1.4.4. Paper 4: “A methodology to calibrate water saturation estimated from 4D seismic”

*Alessandra Davolio, Célio Maschio, Denis José Schiozer
To be submitted to a journal*

Although the local history matching proposed in paper 3 yielded an updated model that better follows the map provided by 4D seismic, this model presents more injected water than it should. The increase in the amount of injected water in the updated model was caused by the saturation map used as input in the matching procedure, since the volume of injected water associated to this saturation map was larger than the known injected volume (due to errors during the inversion caused by noise in seismic data and errors in the static properties). Thus, the updating process (local history matching procedure) is working properly, but the input parameter for this process needs to be calibrated so that the matching process yields a more reliable updated model. In this sense, this last paper presents a methodology to calibrate the volume of injected water presented in the estimated saturation map. This methodology can be seen as an extension of the methodology proposed in paper 2.

Paper 4 presents a discussion concerning the improvement in the estimated saturation map, followed by a comparison of the history matching results when different saturation maps are used as input (with and without the calibration).

The main contribution of this paper is to show the importance of having a better estimation of saturation changes from 4D seismic to update reservoir models.

There are some complementary results regarding this paper in Appendix C, which include an analysis of how the methodologies of papers 2 and 4 improve the optimization response and the well curves after applying the history matching.

2. PAPER 1: *Pressure and saturation estimation from P and S impedances: a theoretical study*

Alessandra Davolio, Célio Maschio, Denis José Schiozer

Journal of Geophysics and Engineering, August 2012, v.9, p.447-460

Pressure and saturation estimation from P and S impedances: a theoretical study

Alessandra Davolio, Célio Maschio and Denis José Schiozer

Department of Petroleum Engineering, FEM, UNICAMP/CEPETRO, São Paulo, Brazil

E-mail: davolio@dep.fem.unicamp.br, celio@dep.fem.unicamp.br and denis@dep.fem.unicamp.br

Received 14 October 2011

Accepted for publication 8 June 2012

Published 16 August 2012

Online at stacks.iop.org/JGE/9/447

Abstract

This work represents the first step of a study to integrate time lapse seismic and reservoir engineering data where a petro-elastic inversion from seismic data to pressure and saturation is presented. This inversion is made through an optimization procedure. In order to better understand and validate the initial step of the methodology, synthetic data (initially free of noise and errors) have been used. Through this ideal set of data, it was possible to show that pressure and saturation can be extracted from P and S impedances using only one seismic survey (3D inversion). It is also shown that this 3D approach is not robust when errors are assumed in reservoir data and it fails when, for instance, uncertainty in porosity data occurs. Thus, an improvement is made and the algorithm is rewritten based on 4D differences that diminish the wrong reservoir data effect. For both algorithms (3D and 4D), we have presented a discussion of the objective function behaviour concerning the use of P and S impedances simultaneously, the initial guess and the solution space. A sensitivity analysis discussing the influence of porosity and the dynamic properties on P and S impedances for 3D and 4D approaches is also presented. After understanding the inversion process behaviour for an ideal data set, an analysis of its results assuming different combinations of pressure and saturation variations and including some errors in the data set used is presented in the last subsections.

Keywords: 4D seismic, estimation of pressure and saturation, petro-elastic inversion

(Some figures may appear in colour only in the online journal)

Nomenclature

IP	P impedance.	ϕ	Porosity.
IS	S impedance.	η	Coefficient of internal deformation.
K_{dry}	Effective bulk modulus of dry rock.	ρ	Bulk density.
K_{sat}	Effective bulk modulus of the rock with pore fluid.	ρ_{min}	Density of mineral material making up rock.
K_{min}	Bulk modulus of mineral material making up rock.	ρ_{fl}	Fluid density.
K_{fl}	Bulk modulus of the pore fluid.	μ_{dry}	Effective shear modulus of dry rock.
OF	Objective function.	μ_{sat}	Effective shear modulus of the rock with pore fluid.
P_{eff}	Effective pressure.		
Pre	Pore pressure.		
S_w	Water saturation.		
S_o	Oil saturation.		
V_p	P-wave velocity.		
V_s	S-wave velocity.		

Subscript

seis	Attribute derived from seismic.
sim	Attribute computed from reservoir simulation results.

1. Introduction

The use of time lapse seismic data to improve reservoir simulation models is becoming more frequent. The spatially dense information that comes from 4D seismic data complements well production data, helping in the reservoir model calibration. Tuttle *et al* (2009) and Castro *et al* (2009) have shown successful integration of these two sets of data. There are different domains where this integration can be done. In the amplitude (or impedance) domain, for instance, the reservoir simulation data are converted to seismic attributes through forward modelling and these synthetic seismic data are matched with the acquired seismic data (Dadashpour *et al* 2009, Fahimuddin *et al* 2010). Another way to perform the integration is by converting 4D seismic data into pressure and saturation and matching them with simulated values (Souza *et al* 2011). The last is a more complex procedure and there is no standard process to extract pressure and saturation from seismic data.

The selection of the inversion process and the seismic attributes to be used to obtain pressure and saturation information are not well established in the literature. Dadashpour *et al* (2008) presented a nonlinear inversion scheme that estimates pressure and saturation from synthetic zero offset seismic data. The work presented by Souza *et al* (2010) has shown the difficulty of obtaining this dynamic information from one set of seismic data (an acoustic impedance volume), mainly because of the problem of multiple answers present in this inversion problem. One way to handle this is to add another seismic attribute into the process that has a different response to the dynamic property changes. Several works combine different sets of seismic data to recover pressure and saturation information. Tura and Lumley (1999) showed that it is possible to estimate changes in pressure and saturation through IP and IS (P and S seismic-derived impedances). Landro (2001) defined a methodology based on time lapse difference of intercept and gradient to differentiate pressure and saturation effects from 4D seismic data. MacBeth *et al* (2006) also proposed a methodology to identify pressure and saturation changes using time lapse seismic data; their methodology is able to use any kind of seismic attributes (two or more) since they have a different response to pressure and saturation changes.

In the work of Tura and Lumley (1999), the estimation of the dynamic properties from 4D seismic data is done through a crossplot of the attributes. The procedure consists of first identifying regions (through forward modelling) in the crossplot of IP and IS that correspond to three production scenarios: (1) only saturation changes, (2) only pressure changes and (3) saturation and pressure changes. Then the seismic impedance values are mapped according to these regions and consequently classified as one of the three scenarios mentioned. The methodology proposed in this work, which will be better detailed in the following sections, also uses IP and IS to estimate the dynamic property variation but the estimation is done through an optimization process, aiming to quantify the results obtained.

This work represents the first steps of a theoretical study that aims to convert seismic data into pressure and saturation

values to be incorporated in a history matching process through a feedback loop in a future work. It is known that this conversion is not a simple procedure since it is subject to many sources of errors like different scale data, noise, uncertainty in the static properties, etc. So, here we are proposing an initial study that starts from an ideal set of data, free of any kind of error, in order to validate and verify the limitations of the inversion procedure. Thus, a discussion is presented concerning the simultaneous use of P and S impedances in the objective function, the possibility of using only one seismic vintage and the necessity of using time lapse seismic data to estimate pressure and saturation. Then, after understanding the inversion behaviour, some results are presented concerning different scenarios of production, i.e. different time lapse variation of pressure and saturation and also when a non-ideal data set is assumed by including some uncertainties and errors.

2. Synthetic seismic data

2.1. Petro-elastic modelling (PEM)

The inversion algorithm is based on an optimization procedure where the differences between the seismic attributes and the simulation-derived seismic attributes are minimized. To generate seismic attributes from simulation data, a PEM, which is a set of relationships that relate fluid/rock and elastic properties, is required. The seismic attributes that are used in the inversion are compressional and shear impedances, called here IP and IS, respectively. Considering ρ , V_p and V_s as the density, compressional and shear wave velocities of the medium, the impedances can be written as

$$IP = V_p \rho, \quad (1)$$

$$IS = V_s \rho. \quad (2)$$

Seismic velocities depend on rock-saturated bulk (K_{sat}) and shear (μ_{sat}) moduli according to the equations

$$V_p = \sqrt{\frac{K_{sat} + \frac{4}{3}\mu_{sat}}{\rho}}, \quad (3)$$

$$V_s = \sqrt{\frac{\mu_{sat}}{\rho}}. \quad (4)$$

The medium density can be written as

$$\rho = (1 - \phi)\rho_{min} + \phi\rho_{fl}, \quad (5)$$

where ϕ is the porosity, ρ_{min} is the mineral density and ρ_{fl} is the fluid density which is defined according to the equation

$$\rho_{fl} = \rho_o S_o + \rho_w S_w \quad (6)$$

where S is the saturation and the subscripts stand for oil and water.

The most used approach to determine the rock-saturated bulk and shear moduli are the Gassmann equations that are described as follows (Avseth *et al* 2005):

$$K_{sat} = K_{dry} + \frac{\left(1 - \frac{K_{dry}}{K_{min}}\right)^2}{\frac{\phi}{K_{fl}} + \frac{1-\phi}{K_{min}} - \frac{K_{dry}}{K_{min}^2}}, \quad (7)$$

$$\mu_{\text{sat}} = \mu_{\text{dry}}, \quad (8)$$

where K_{dry} , K_{min} and K_{fl} are the bulk moduli of the rock frame, the mineral and the fluid mixture. μ_{dry} and μ_{sat} are the shear moduli of the dry rock and the rock with pore fluid, respectively.

To compute the dry bulk and shear moduli, the known friable, or uncemented, sand model (Mavko *et al* 2003) is used in this work. This model makes use of the Hertz–Mindlin contact theory and a heuristic modified Hashin–Strikman lower bound, according to the equations:

$$K_{\text{dry}} = \left[\frac{\phi/\phi_c}{K_{\text{HM}} + 4\mu_{\text{HM}}/3} + \frac{1 - \phi/\phi_c}{K + 4\mu_{\text{HM}}/3} \right]^{-1} - \frac{4}{3}\mu_{\text{HM}}, \quad (9)$$

$$\mu_{\text{dry}} = \left[\frac{\phi/\phi_c}{\mu_{\text{HM}} + z} + \frac{1 - \phi/\phi_c}{\mu + z} \right]^{-1} - z, \quad (10)$$

where

$$z = \frac{\mu_{\text{HM}}}{6} \left(\frac{9K_{\text{HM}} + 8\mu_{\text{HM}}}{K_{\text{HM}} + 2\mu_{\text{HM}}} \right), \quad (11)$$

where K_{HM} and μ_{HM} are the bulk and shear moduli at critical porosity ϕ_c given by the contact Hertz–Mindlin theory

$$K_{\text{HM}} = \left[\frac{n^2(1 - \phi_c)^2 \mu_{\text{min}}^2 P_{\text{eff}}}{18\pi^2(1 - \nu)^2} \right]^{\frac{1}{3}}, \quad (12)$$

$$\mu_{\text{HM}} = \frac{5 - 4\nu}{5(2 - \nu)} \left[\frac{3n^2(1 - \phi_c)^2 \mu_{\text{min}}^2 P_{\text{eff}}}{2\pi^2(1 - \nu)^2} \right]^{\frac{1}{3}}, \quad (13)$$

where P_{eff} is the effective pressure; μ_{min} and ν are the mineral shear bulk modulus and Poisson ratio and n is the coordination number. Effective pressure follows the relation $P_{\text{eff}} = P_{\text{over}} - \eta \text{Pre}$, where P_{over} is the overburden pressure, Pre is the pore pressure and the parameter η is the coefficient of internal deformation which is assumed to be equal to 1 in this work.

The bulk modulus of the pore fluid is estimated by Wood's law given as

$$K_{\text{fl}} = \left[\frac{S_w}{K_w} + \frac{S_o}{K_o} \right]^{-1}, \quad (14)$$

where K_w and K_o denote oil and water bulk moduli, respectively. The fluid bulk moduli (K_w and K_o) are computed from the fluid bulk densities and fluid acoustic velocity through the equations of Batzle and Wang (1992). The bulk densities ρ_o and ρ_w can also be exported from the flux simulation and used as an input to compute bulk fluid modulus. A summary can be found in Mavko *et al* (2003). Note that in this work, it is assumed no gas is present.

2.2. Forward modelling

In order to validate the inversion scheme, synthetic seismic data are being considered in this work. As will be detailed later, the seismic attributes considered here are IP and IS. To build the synthetic impedance volumes, the PEM is run over a reference simulation model that represents the true earth modelling. This forward modelling uses as input pressure and saturation values, generated by the simulation, and computes

acoustic and shear impedances through the PEM for each simulation grid block. Apart from the dynamic property pair (Pre , S_w), the reservoir properties such as porosity, mineral compressibility, fluid properties and temperature are also needed.

Another simulation model is used in the inversion scheme, which refers to the engineering simulation model, here called the base model, built based on the reservoir characterization process and, therefore, assuming a lack of information that makes it different from the reference model. This lack of information can be, for instance, a missing channel, a wrong permeability field or a wrong facies modelling. These two models are generated according to the necessity of each study; in this case, they were different enough to produce considerable time lapse differences.

Initially, this work considers an ideal set of data, i.e.

- (i) Seismic impedance is generated at simulation scale (reference and base models have the same scale).
- (ii) Noise-free seismic data.
- (iii) Elastic inversion errors are not considered.
- (iv) No errors or uncertainties are assumed for the PEM and its input parameters. The same PEM is first used for the forward modelling to generate the synthetic impedance and then for the inversion process.
- (v) Water flooding example (no presence of gas).

In section 4, a discussion is presented for some cases where these ideal conditions are not totally assumed.

3. Preliminary studies

Before starting the discussion of the petro-elastic inversion itself, some verifications were made in order to check the importance of having more than one kind of seismic data (P and S impedances, in this case) when it is wanted to estimate pressure and saturation. Moreover, the influence of pressure, saturation and porosity in IP and IS was also verified for 3D and 4D data. Understanding these issues helps to control the inversion behaviour.

3.1. P and S impedances

An initial test based only on forward modelling was run to check and illustrate that the combination of P and S impedances would lead to a single pair (Pre , S_w), assuming the ideal set of data presented above. To achieve this, values of P and S impedances were computed through the PEM, varying pressure and water saturation within a known range. All other parameters (porosity, rock and fluid compressibility, temperature, etc) remained constant. These computed impedance values generated the solid red surfaces seen in figure 1. If a pressure and saturation pair is selected randomly, for instance, 24 MPa and 0.3, then the corresponding IP and IS values are 6367×10^3 and $3731 \times 10^3 \text{ kg s}^{-1} \text{ m}^2$, respectively. In the same figure, the red-dashed planes represent these constant impedances.

On the bottom of these images, the pressure and saturation pairs that correspond to the surface and plane intersection are

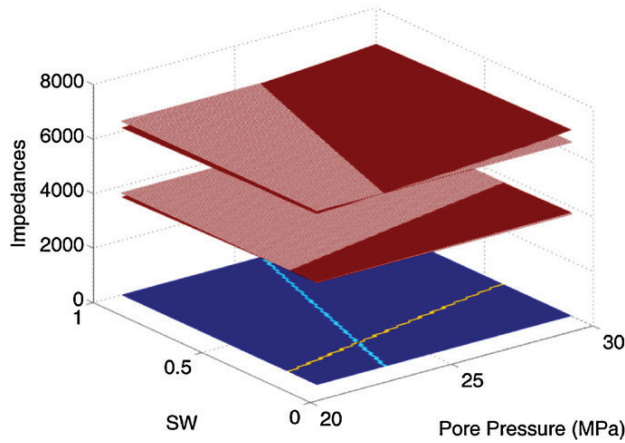


Figure 1. P and S impedance values computed through a petro-elastic model for all the pressure and saturation pairs in a range (20–30 MPa) and (0.1–10), respectively (red surface). Constant IP and IS planes computed from a randomly selected pressure and saturation pair (red-dashed). Light blue points on the bottom represent the intersection between the IP surface and the IP constant plane; the yellow points represent the same for IS.

highlighted. These points, in light blue, represent all pairs that would give $IP = 6367 \times 10^3 \text{ kg s}^{-1} \text{ m}^2$ and, in yellow, all pairs that would give $IS = 3731 \times 10^3 \text{ kg s}^{-1} \text{ m}^2$. In figure 1, it can be noted that the use of only IP to obtain pressure and saturation yields a multiple answer inversion problem. But, if both impedances are considered simultaneously, the solution set is now reduced to the intersection of these two sets of points, which, for this case, reduces to the single pair (24 MPa, 0.3).

So, it was shown that if the measured seismic attributes (impedances, in this case) and the PEM were perfect, without any noise, or error, the inversion procedure of converting IP and IS into pressure and saturation should convert to the right answer since there would be only a global minimum. It is also important to highlight that this simple illustration is valid

Table 1. Range of variation for the properties considered in the sensitivity analysis.

	Min	Ref. value	Max
ϕ	0.1	0.2	0.3
ρ_{\min} (g cm^{-3})	2.51	2.65	2.78
K_{\min} (GPa)	34.77	36.6	38.43
μ_{\min} (GPa)	42.75	45	47.25
η	0.9	1	1.1

for all pressure and water saturation pairs that belong to the range considered and depend on the PEM used.

3.2. Sensitivity analysis

The relationships between rock and fluid properties described through the PEM are not very simple and the influence of each unknown on the computed values of IP and IS is not easy to identify, especially due to the inter-dependence of them. So, a simplified uncertainty analysis is presented here, since it is not the scope of this work to deeply study this issue, in order to verify the influence of the independent rock and fluid properties used as input to the PEM described previously. To calculate these influences, one property was varied at a time and the respective percentage variations of IP and IS were saved. Each curve displayed in figure 2 corresponds to the variation of one property in the range described in table 1; the other properties remained constant (including the dynamic properties). Note that these ranges were defined within a feasible set of values, according to the sand reservoir model assumed.

From figure 2, it can be verified that porosity is the parameter that most influences impedance calculation. It is necessary to observe that the range of variation considered for porosity was wide, which consequently produces big variations in IP and IS, but even if a smaller range is considered, such as 20% for instance, the variation in impedances is still relevant and bigger than the ones observed for the other parameters.

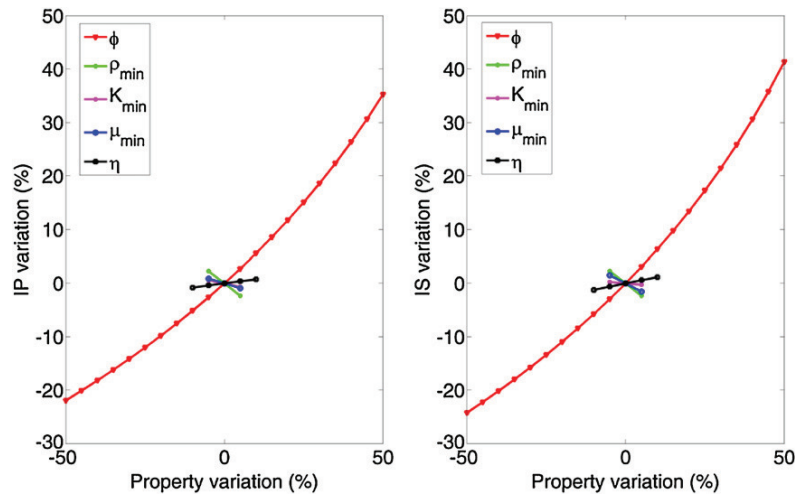


Figure 2. Sensitivity analysis of the PEM. Rock properties influence on IP and IS (property variation limits based on uncertainties associated with the reservoir characterization process).

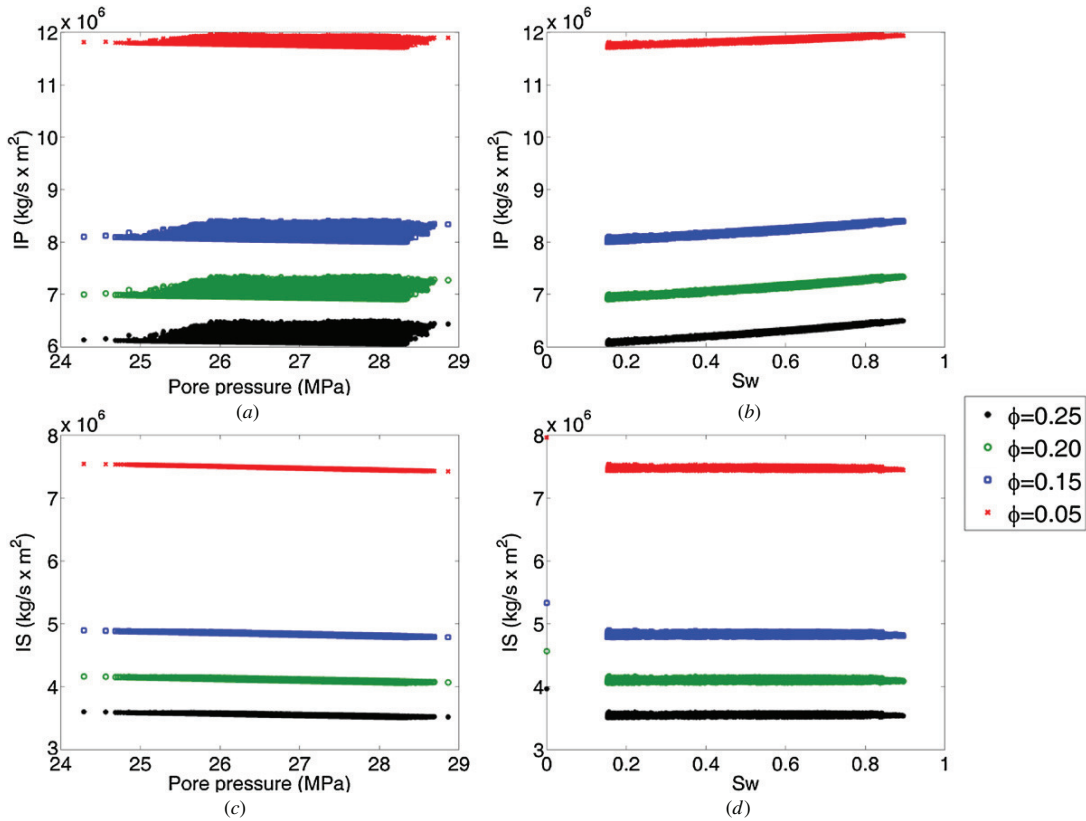


Figure 3. 3D data corresponding to the second vintage (after eight years of production) where each colour corresponds to different porosity. Crossplots of (a) $IP \times Pres$; (b) $IP \times S_w$; (c) $IS \times Pre$ and (d) $IS \times S_w$. Different porosity values yield different impedance ranges.

The same kind of sensitivity was done for temperature and fluid properties ($^{\circ}\text{API}$, salinity, oil and water densities) and even assuming a wide range of variation for these properties (-50% $+50\%$), the impedance variation observed was not bigger than 2%. As these results were not significant, they are not shown here.

The focus of this work is to discuss the inversion procedure to obtain dynamic properties from 4D seismic data, first considering an ideal set of data and after assuming some errors/noise. Thus, the discussion presented in the following sections aims to consider one source of error, which is the uncertainty on reservoir properties. As shown in this section, porosity is a very important property when calculating P and S impedances, so this property will be used to discuss the potentials and limitations of the inversion proposed.

3.3. Porosity influence on P and S impedances assuming dynamic property variation

This section proposes a sensitivity analysis to check the porosity influence on IP and IS for 3D and 4D data for different values of pressure and saturation. The procedure consists of computing both impedances through PEM, using pressure and saturation values generated from a reservoir simulation model at two production times (considering two seismic surveys) assuming different porosity values; the intention of using different values of porosity is to analyse the influence of

porosity on the results. The use of reservoir engineering simulated values was chosen in order to have a consistent time lapse difference for these unknowns. It is necessary to highlight that the model details of the static properties are not important for the analysis proposed here, because we just want to evaluate impedance variability for a given pressure and saturation pair assuming different porosities. So, the simulated block values are used as single points on the crossplots shown below.

The reservoir model used has an average initial pressure of 32 MPa and 15% of connate water saturation. After eight years of production, simulated values for different blocks belong to the pressure range (24–29 MPa) and the water saturation range (0.15–0.85). Figure 3 shows the impedances versus pressure and saturation crossplots for these data. The colours represent different porosities used to compute IP and IS. For one colour, each point represents a reservoir simulation grid block. This image shows the strong influence of porosity on both impedances, since there is a considerable distance between each colour point cloud.

The details of one of these cases can be seen in figure 4, where only the point cloud corresponding to $\phi = 0.15$ is displayed. This kind of display allows us to check some relations between both impedances and the dynamic unknowns (pressure and saturation) that were not clear in figure 3 because of the y-scale. Looking at figure 4(a), the vertical point dispersion of the cloud is due to different saturation

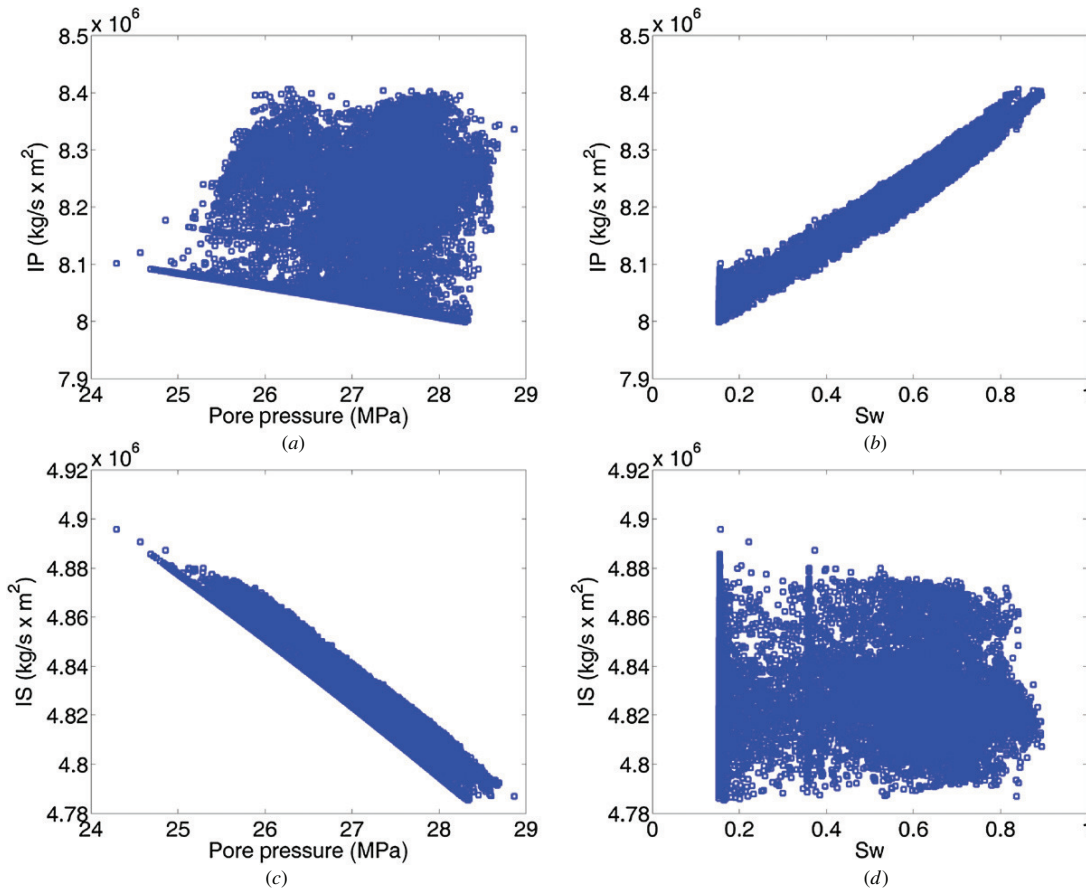


Figure 4. 3D data corresponding to the second vintage (after eight years of production); only the case where $\phi = 0.15$. Crossplots of (a) IP \times Pre; (b) IP \times S_w ; (c) IS \times Pre and (d) IS \times S_w .

values assumed, ranging from (0.15–0.85). This means that saturation has a strong influence on IP, because, for a fixed pressure, the range of possible values that IP can assume is wide. Doing the same analysis for pressure, it can be observed in figure 4(b) that the IP range is much smaller for a constant S_w than the one observed in figure 4(a). Therefore, saturation is more influential than pressure for these data. It is important to emphasize that the pressure range for this reservoir model is not as wide as the saturation range, in agreement with the expected behaviour of a predefined production strategy with controlled pressure drop (water flooding, for instance).

Making an equivalent analysis for shear impedance, in figures 4(c) and (d) the strong influence of pressure on IS can be seen in contrast to the weak influence of saturation (as expected), highlighted by the constant IS behaviour of the point cloud in figure 4(d). These different responses, or sensitivity, of IP and IS to pressure and saturation variations are good indicators that these two data should be used simultaneously in the inversion, as will be discussed in the following sections.

When time lapse differences are considered, the distance between each colour cloud observed in figure 3 becomes less significant, as shown in figure 5, where the colours represent the same porosity values considered previously. Now, these clouds are practically superimposed and have

a much smaller deviation among themselves than the ones observed in figure 3, which means that even if the porosity model is wrong, the 4D differences of IP and IS are going to be close to the true one, i.e. porosity errors will be minimized by the subtraction of the vintages.

Still in figure 5, the red point cloud is not really superimposed over the others, especially for figures 5(a) and (b), but this is not an important issue because, in this case, the porosity is too low, i.e. it can be considered a non-reservoir rock. In other words, if the porosity model is not able to identify reservoir and non-reservoir rocks, then not even the 4D differences should be able to give useful information about pressure and saturation variations.

Looking at any one of the four different porosity cases, some features can be observed in figure 5. One of them is the cloud dispersion of $\Delta\text{IP} \times \Delta\text{Pre}$ that occurs due to the variations of ΔS_w , which covers quite a wide range (0–0.7), showing that for the same ΔPre the P -impedance 4D variation can assume very different values. Therefore, ΔS_w is more influential than pressure on ΔIP . This is confirmed by the crossplot of $\Delta\text{IP} \times \Delta S_w$ where the point clouds are much less dispersed, showing a better correlation between these two properties.

Clearly, the same cannot be observed for the graph of $\Delta\text{IS} \times \Delta\text{Pre}$, as expected, since shear impedance is not

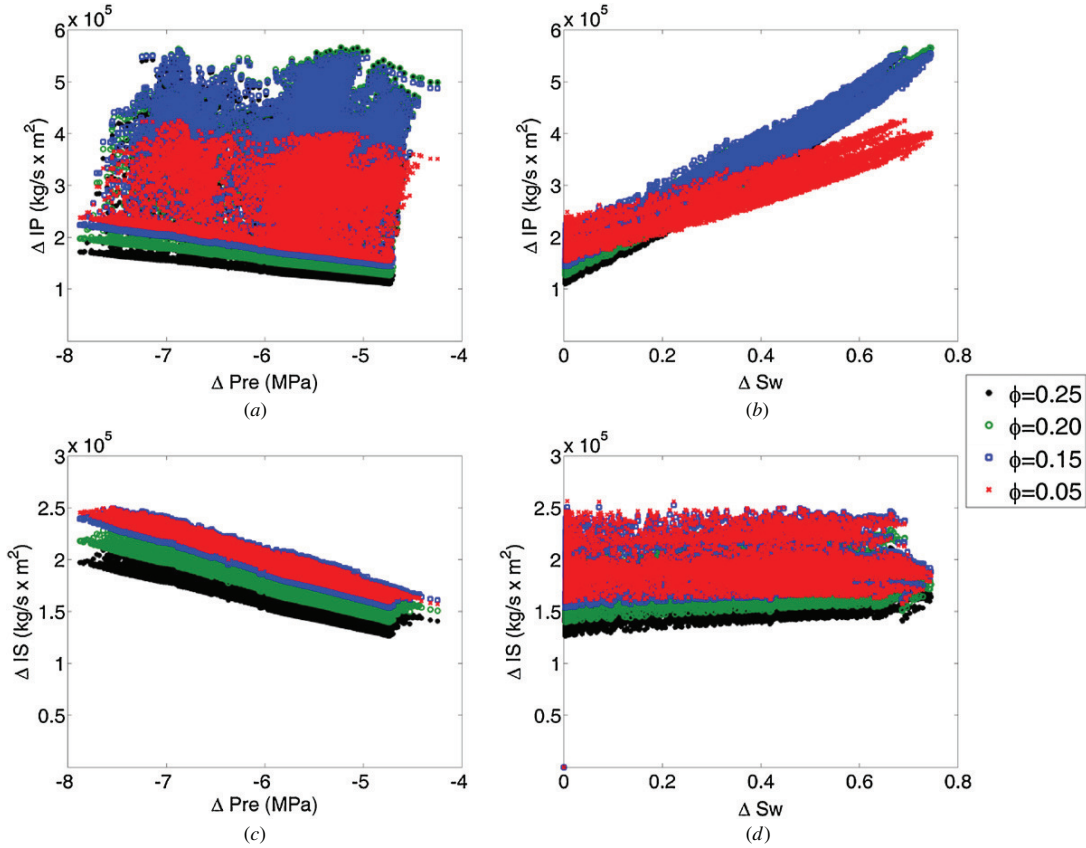


Figure 5. 4D data corresponding to monitor minus base (being the monitor after eight years of production). Crossplots of: (a) $\Delta IP \times \Delta Pre$; (b) $\Delta IP \times \Delta S_w$; (c) $\Delta IS \times \Delta Pre$ and (d) $\Delta IS \times \Delta S_w$. For time lapse differences, porosity does not have such a great influence on impedances as it has on 3D.

sensitive to saturation changes. For the same reason, the graph $\Delta IS \times \Delta S_w$ displays constant ΔIS behaviour when ΔS_w varies. On the other hand, the dispersion of any of the point clouds on this graph shows the influence of ΔPre on ΔIS , which is also confirmed by the good correlation presented in the crossplot of $\Delta IS \times \Delta Pre$.

The main points to highlight are (1) regarding 3D data, IP and IS modelling is very sensitive to porosity; (2) when time lapse data are considered, the porosity influence on ΔIP and ΔIS is much weaker compared to that observed for 3D data; (3) the variations observed on ΔIP and ΔIS due to dynamic property changes are more evident than those observed for porosity variation; (4) the strong correlations between $\Delta IP \times \Delta S_w$ and $\Delta IS \times \Delta Pre$ are a good indication that ΔIP and ΔIS can be used simultaneously to obtain ΔS_w and ΔPre .

4. Petro-elastic inversion

4.1. 3D inversion

The 3D inversion algorithm proposed here follows the idea presented in Souza *et al* (2010) and adds the shear impedance into the process in order to couple with the multiple

answer issue. The basic idea of the process is to minimize the difference between seismic impedance and synthetic impedance computed from a reservoir simulation model (figure 6). This minimization is done through an optimization process that uses simulated pressure and saturation values from the base model as an initial guess.

This work uses synthetic seismic data, so it is necessary to run a previous step to generate the synthetic impedance represented by the green box in figure 6.

The objective function of the optimization process is defined as

$$OF = \left\| \begin{array}{c} IP_{seis} - IP_{sim} \\ IS_{seis} - IS_{sim} \end{array} \right\|, \quad (15)$$

where IP_{seis} and IS_{seis} are the P and S impedances computed from seismic amplitudes, or in this case, it is the synthetic impedance computed considering the reference model and IP_{sim} and IS_{sim} are the P and S synthetic impedances computed with the base model simulation results.

As will be presented later, some tests were run comparing the inversion process when the objective function is defined by equation (15) and also when this equation is modified by removing the shear impedance from it. It is important to highlight that the procedures shown in figure 6 are all run at the reservoir simulation scale and the inversion is run on each grid

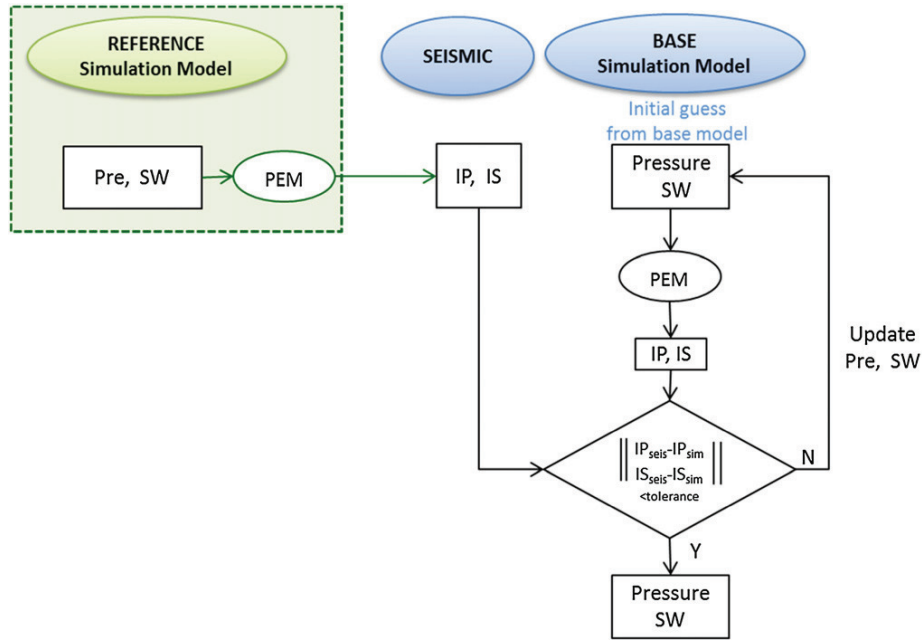


Figure 6. 3D inversion algorithm to obtain pressure and saturation from seismic impedance. The green box highlights the necessity of running a PEM to generate the synthetic seismic data used in this work.

Table 2. Inverting pressure and saturation values.

	Reference model (answer)	Base model (initial guess)	Inverted values OF = $f(IP)$	Inverted values OF = $f(IP, IS)$
Pre (MPa)	32	25	23.2559	32.00
S_w	0.55	0.8	0.10	0.55
Porosity	0.1474	0.1474	–	–

block independently. Also, the optimization algorithm used is an internal Matlab function called *fmincon* which is a gradient-based method for constrained problems. It is important to highlight that the convergence criteria are based not only on the minimization of the objective function but also on the size of the step between each answer found; if this size is smaller than a tolerance, then the algorithm ends.

In order to illustrate the objective function behaviour, we will consider single pressure and saturation pairs that we want to obtain from synthetic seismic data (as the inversion is run for each block separately, there is no problem to look at the inversion for only one block). As cited before, there are two different simulation models: the reference model (true earth model) and the base model (reservoir engineering model). Assuming that the simulation of these models gave the values listed in table 2 and that the inversion is constrained by the ranges $0.1 < S_w < 1$ and $5 < \text{Pre} < 50$ (MPa), then all possible values that the OF can assume, combining saturation and pressure with a step of 0.01 and 0.35, respectively, are defined by a surface that can be visualized in a 3D plot (OF, Pre, S_w).

Figures 7(a) and (b) show these corresponding surfaces for the case where $\text{OF} = f(IP)$ and $\text{OF} = f(IP, IS)$, respectively. The multiple response issue can be visualized on the bottom of these surfaces, where the contour plot is drawn. Note that

figure 7(b) clearly shows a global minimum in opposition to several local minima seen in figure 7(a). Another way of showing this is illustrated in figures 7(c) and (d). These images show two things: the first one is the set of coloured points corresponding to the lower objective function's values (hot colours stand for higher values) and the second is the three points given by the initial guess (cyan), the inversion solution (green) and the true answer (magenta). One could say that there is no doubt now that, if only IP was used, the optimization algorithm could be stuck in a local minimum as happened in the example shown in figure 7(c). Furthermore, the presence of shear impedance yields an optimization problem with a global minimum easily found by the optimization algorithm.

Davolio *et al* (2011) showed an application of this methodology in a synthetic reservoir model. In that paper, the case where only IP was considered is referenced by 'Algorithm 1' and when both impedances are used in the objective function, it is referenced by 'Algorithm 2'. The application of this algorithm in a noise-free data set shows that it is possible to obtain pressure and saturation if the second algorithm is used. The paper also shows that, if a simple perturbation is assumed in the porosity field (multiplying it by a constant), the 3D inversion algorithm fails and, therefore, a 4D approach should be used.

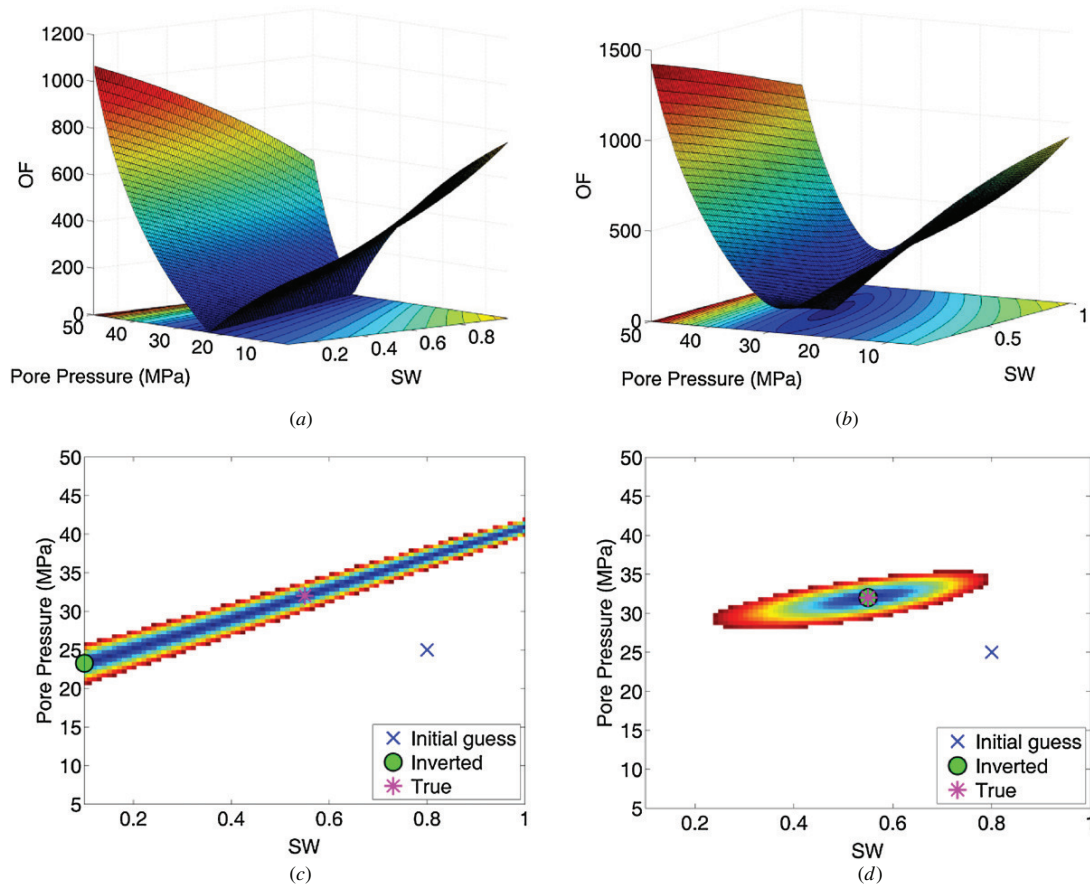


Figure 7. Top: objective function surfaces defined by all possible pressure and saturation pairs: (a) assuming $OF = f(IP)$; (b) assuming $OF = f(IP, IS)$. Bottom: lower values of the objective function, where hot colours stand for higher values; initial guess in cyan, inversion solution in green and the true answer in magenta; (c) assuming $OF = f(IP)$; (d) assuming $OF = f(IP, IS)$.

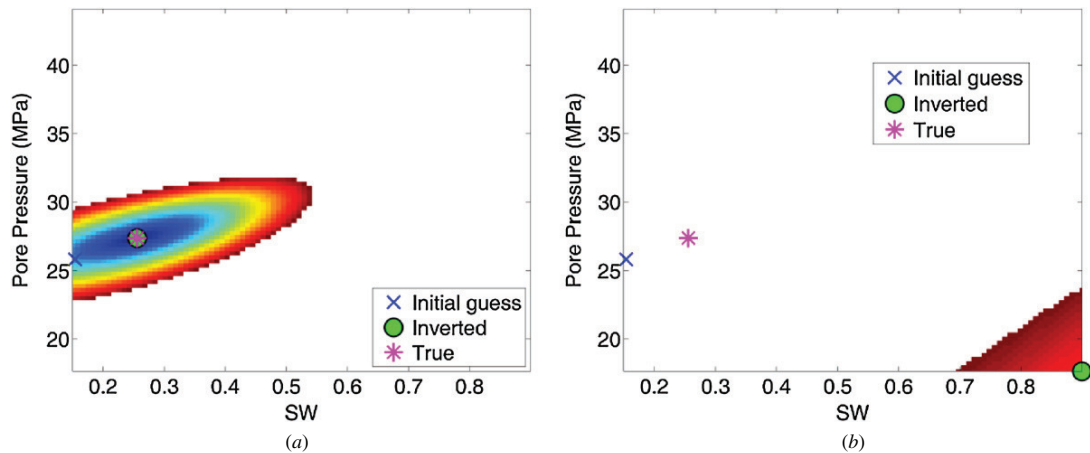


Figure 8. 3D inversion. (a) Assuming that the porosity is known: base = reference = 0.1956. For this case, the inversion was able to recover the true answer exactly. (b) Assuming a wrong porosity for the base model: reference = 0.1956 and base = 0.2590. For this last case, the inverted water saturation and pressure pair is far from the true answer.

4.2. 4D inversion

Now, convinced of the fact that both IP and IS should be used in the objective function in order to guarantee the existence

of a global minimum and also that the optimization algorithm is able to find it in an ideal set of data, the next step of our study is to start considering some errors, or uncertainties, in the modelling. The first uncertainty assumed concerns the porosity

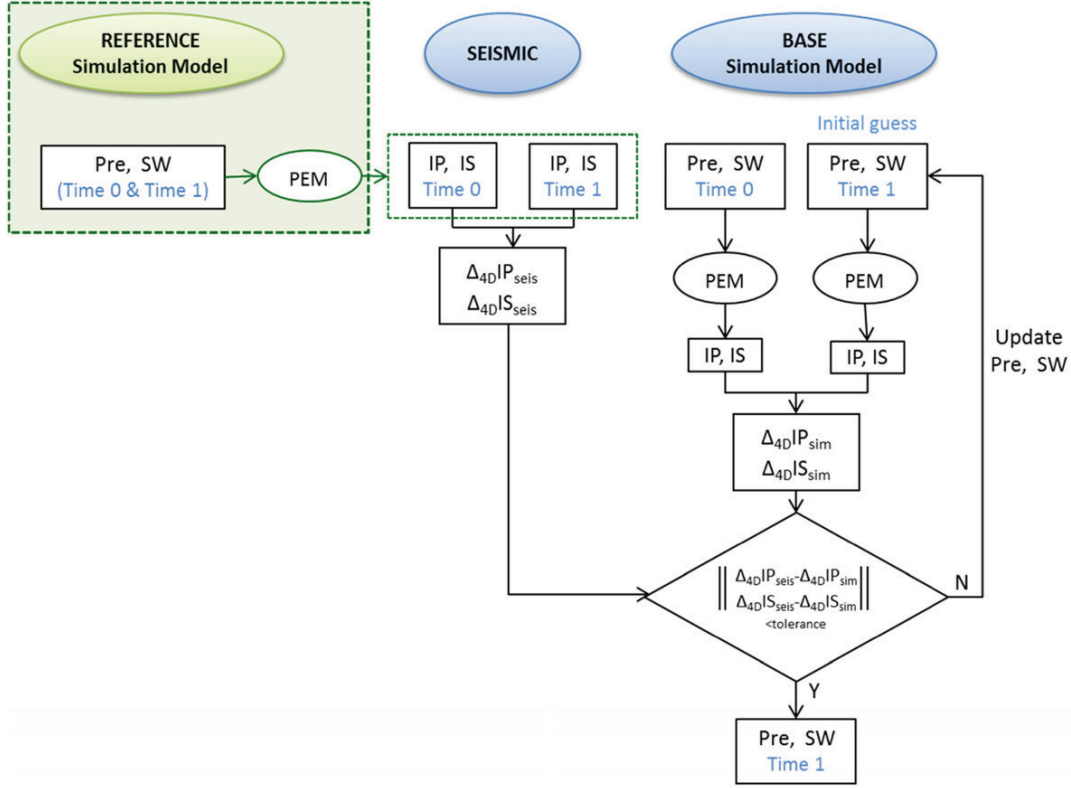


Figure 9. 4D inversion algorithm to obtain pressure and saturation from seismic impedances. The green box highlights the necessity of running a PEM to generate the synthetic seismic data used in this work.

Table 3. Base and reference model values used in the 4D inversion algorithm. The last column has the inverted values obtained through this new algorithm approach.

	Time 0		Time 1	
	Reference model	Base model	Reference model (answer)	Base model (initial guess)
Pre (MPa)	32.1016	32.1016	27.3938	25.8431
S_w	0.1500	0.1500	0.2556	0.1538

field, so now the base and reference models will have different porosity values.

As shown in a previous section, porosity has a strong influence on shear and acoustic impedances, indicating that if this parameter is wrong, the inversion procedure may fail. The images of figure 8 show a comparison of the inversion procedure using the 3D algorithm presented before for a single pair (S_w , Pre) for two cases: in figure 8(a) the porosity value is known and in figure 8(b) it is not. The base and reference model values are listed in table 3 under the ‘Time 1’ column. For the second case, the reference model porosity is 0.1956 and the base model porosity is 0.2590. From figure 8(b), it can be shown that the inversion does not work for such cases since the answer (magenta) is far from the global minimum.

The idea of 4D studies using seismic data is always related to 4D differences because it is expected that errors

from static properties (like porosity) will be diminished when the data are subtracted, thus highlighting dynamic effects, as discussed in section 3.3. So, the natural improvement of the algorithm proposed was to incorporate this approach in order to mitigate wrong porosity effects. The 4D inversion algorithm closely follows the same idea as the 3D, aiming to minimize the differences between seismic impedances and synthetic impedances computed from simulation data. As illustrated in the workflow of figure 9, the main difference now is that the algorithm deals with two seismic surveys (base = time 0 and monitor = time 1) and the objective function is written as

$$OF = \left\| \begin{array}{l} \Delta_{4D}IP_{seis} - \Delta_{4D}IP_{sim} \\ \Delta_{4D}IS_{seis} - \Delta_{4D}IS_{sim} \end{array} \right\|, \quad (16)$$

where the index *seis* stands for the seismic impedances, which, in this case, is a synthetic impedance computed through the reference model, and the index *sim* stands for the synthetic impedances computed using the base simulation model. Note that now the 4D difference is minimized, so the operator Δ_{4D} stands for the time lapse difference: monitor – base. One important assumption that is being used is the fact that the base 4D time corresponds to the reservoir initial time, which means that pressure and saturation are known at time 0. Another point to highlight is that as in the 3D approach, the 4D inversion is also run for each block independently.

The same data used to generate the images of figure 8 are now used to run the 4D inversion algorithm. The base and reference model values are listed in table 3 for the two 4D

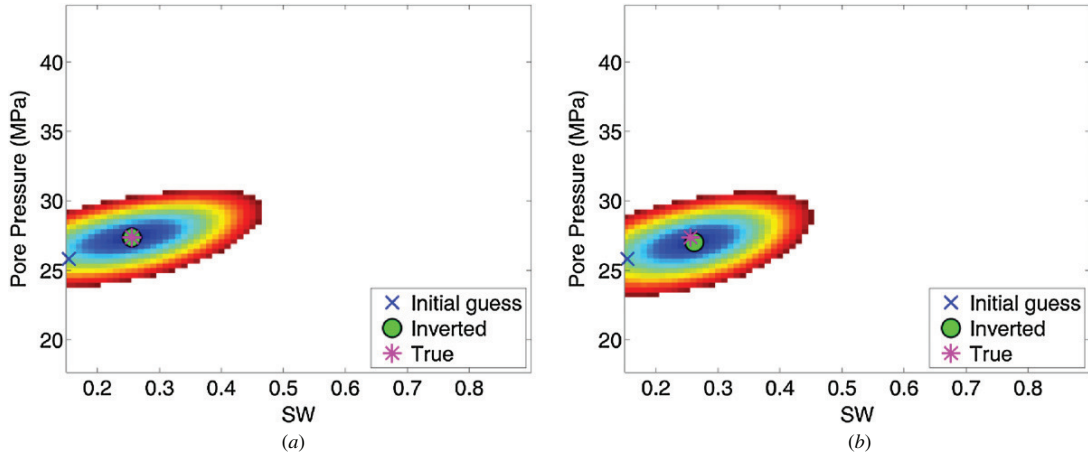


Figure 10. 4D inversion: (a) assuming that the porosity is known: base = reference = 0.1956. For this case, the inversion was able to recover exactly the true answer; (b) assuming a wrong porosity for the base model: reference = 0.1956 and base = 0.2590.

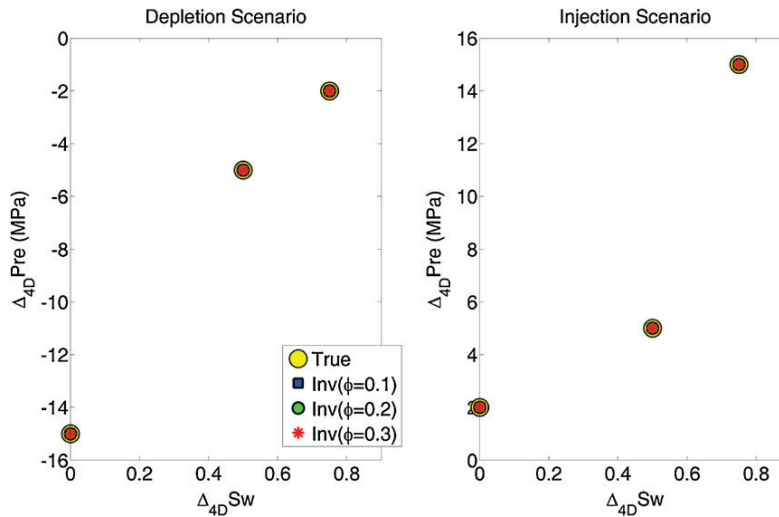


Figure 11. Depletion (left) and injection (right) scenarios. For each scenario, yellow circles are the answer the 4D inversion aims to reach and the inversion results assuming the porosity is known and has the values 0.1 (blue square), 0.2 (green circle) and 0.3 (red star).

times considered. Note that it is considered that the base 4D time corresponds to the reservoir initial time, which means that pressure and saturation are known at this time, yielding equal values for both reservoir models at time 0.

Figure 10 presents the results of the 4D inversion. For the case where the porosity is known (figure 10(a)), the 4D inversion algorithm yielded results very close to the true answer (the errors obtained correspond to the numerical errors of the optimization), as happened in the 3D inversion algorithm (figure 8(a)). However, when the porosity values are assumed to be wrong, the 4D approach makes the difference, yielding a pressure and saturation pair (figure 10(b)) much closer, although not exact, to the answer than the one seen in figure 8(b).

In order to check the algorithm, different initial guesses were tested but, since this optimization problem has a well-behaved objective function with a global minimum, this input does not make much difference.

Table 4. Production scenarios considered.

Depletion scenario		Injection scenario	
$\Delta_{4D}S_w$	$\Delta_{4D}Pre$ (MPa)	$\Delta_{4D}S_w$	$\Delta_{4D}Pre$ (MPa)
0	-15	0	+2
0.5	-5	0.5	+5
0.75	-2	0.75	+15

4.3. 4D inversion on different production scenarios

In order to have a more robust study, in this section, the 4D inversion results are presented for different production scenarios, i.e. different saturation and pressure pairs are evaluated.

The possible production scenarios are summarized in this work in six cases, as described in table 4. These six cases should cover the expected behaviour of the dynamic properties considering blocks located between production and injection

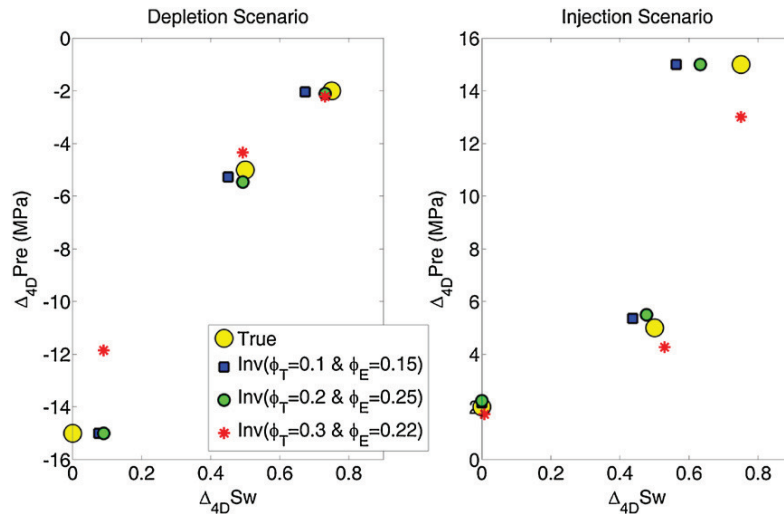


Figure 12. 4D inversion results for the same scenarios as figure 11, now assuming wrong porosities where ϕ_T is the true porosity and ϕ_E is the estimated porosity (the value assumed in the inversion).

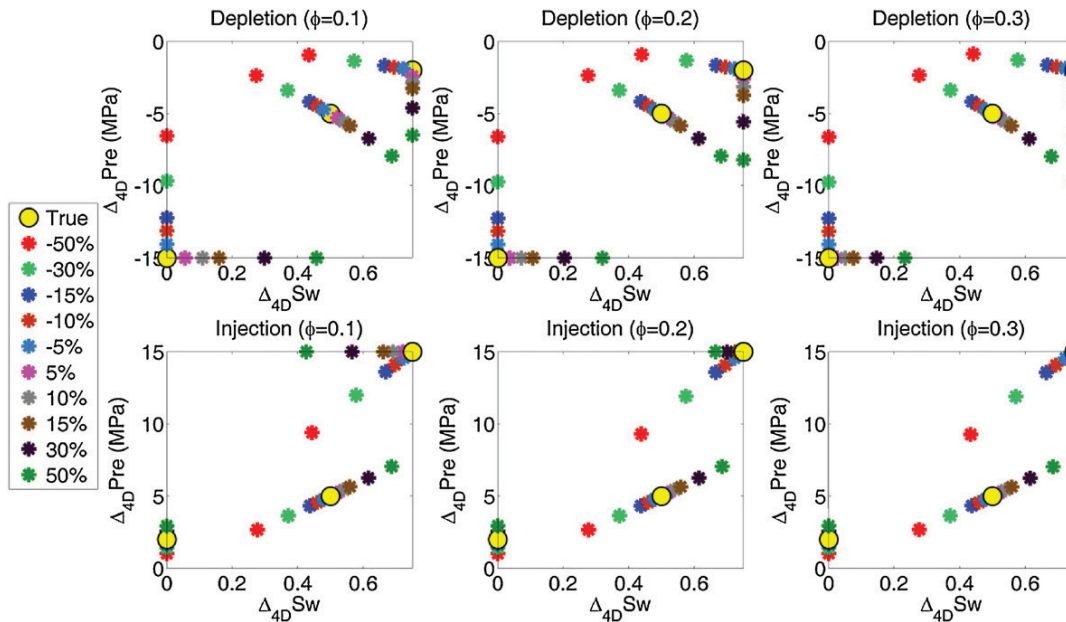


Figure 13. 4D inversion results assuming error on seismic impedances. The porosity is assumed to be known and the results show three cases: $\phi = 0.1$, $\phi = 0.2$ and $\phi = 0.3$. At the top are the depletion scenarios for each porosity and at the bottom are the injection scenarios also for each porosity. Each colour corresponds to a different perturbation applied on $\Delta_{4D}IP$ and $\Delta_{4D}IS$.

wells (close and far to the well locations). All these scenarios are illustrated by the yellow circles of figure 11. Note that for a better visualization of the different scenarios, the images in this subsection (and the following ones) show the 4D difference of the dynamic properties, instead of the second survey values as used before. Still in figure 11, the 4D inversion results for each scenario are plotted considering that porosity is known and assuming three different values: $\phi = 0.1$, $\phi = 0.2$ and $\phi = 0.3$. This image shows that no matter what the saturation, pressure and porosity values are, the 4D inversion provides correct values (just having the numerical error of the process)

when the ideal data set, with no errors or uncertainties, is considered.

Figure 12 presents the results for the same scenarios but now assuming that the porosity is not known (ϕ_T is the true porosity and ϕ_E is the estimated porosity); it shows the results for each scenario assuming that the estimated porosity was not totally correct. An important issue that can be observed in figure 12 is that looking at the inversion results for the same porosity case (red points, for instance), the quality of the estimated pressure and saturation variations depends on the scenario considered. One explanation for this

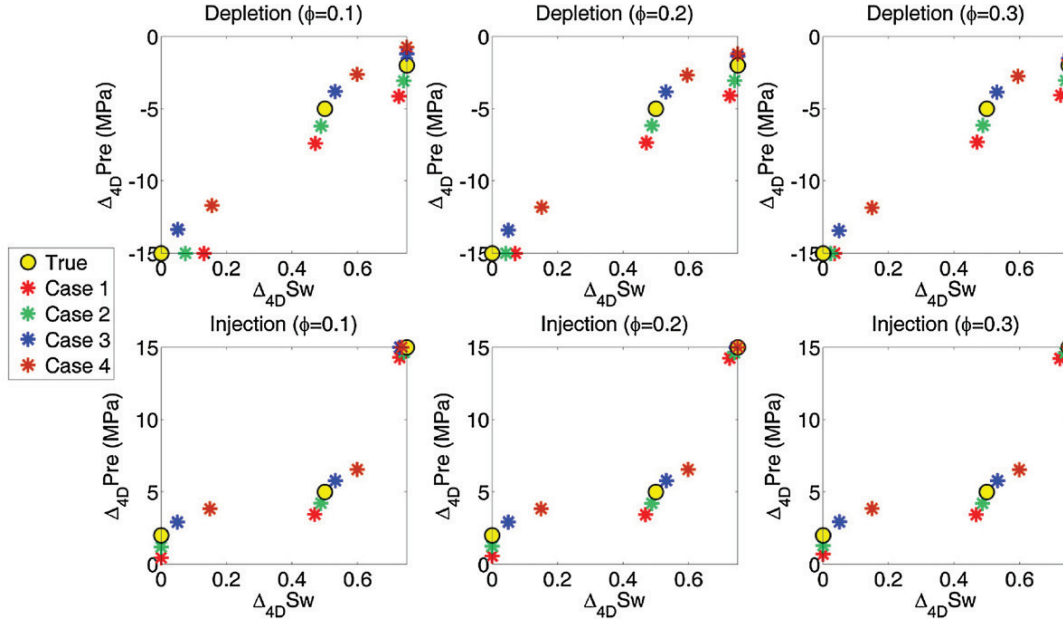


Figure 14. 4D inversion results assuming uncertainty in the reservoir initial conditions. The porosity is assumed to be known and the results show three cases: $\phi = 0.1$, $\phi = 0.2$ and $\phi = 0.3$. At the top are the depletion scenarios for each porosity and at the bottom the injection scenarios also for each porosity. Each colour corresponds to a different assumption regarding the reservoir initial conditions, as detailed in table 5.

may be that the error induced by the wrong porosity in the synthetic impedances (IP_{sim} and IS_{sim}) calculation overrides the effects that the dynamic property 4D variation has on them. Nevertheless, in general, the errors obtained are acceptable and it can be said that the 4D inversion works well in all scenarios and porosities.

4.4. 4D inversion assuming noise in seismic data

Another important source of error in the inversion process studied is the noise presented in seismic data. For the type of analysis that is being presented in this work, which looks at each point of the reservoir separately, the presence of noise in seismic data can be represented simply by a percentage perturbation on $\Delta_{4D}IP$ and $\Delta_{4D}IS$. So, these wrong values that the impedances assume can represent seismic noise, scale issues and even wrong modelling. Note that, when looking to the whole reservoir behaviour, these sources of errors need to be modelled more properly, since the spatial effects must be accounted for. Again, in this work, these effects just provide wrong point values of impedances since the algorithm is run for each reservoir simulation block.

In this sense, figure 13 shows the results of the 4D inversion assuming different perturbations on seismic impedances, also the porosity is considered known and the results are shown for three porosity cases (0.1, 0.2 and 0.3) for the depletion and injection scenarios described in table 4. Different colours stand for different perturbation applied to the time lapse difference of IP and IS, according to the legend. Again, it is observed that the quality of the inversion depends on the scenario assumed, which is expected since the success of the inversion will depend on the sensitivity of the impedance

Table 5. Five cases where the initial conditions are assumed to be wrong.

	S_w (time 0)	Pre (time 0) (MPa)
Case 1	0.1	30
Case 2	0.13	31
Case 3	0.2	33
Case 4	0.3	34
True value	0.15	32

variations for a certain variation of pressure and saturation. It is important to highlight that the solution set of the optimization was constrained by the limits of the scenarios considered ($\Delta_{4D}S_w = [0-0.75]$ and $\Delta_{4D}Pre = [-15-15]$ MPa); this fact justifies some results falling in the boundary. In general, it can be said that the results are acceptable for impedance errors up to 15%. For errors bigger than that, the results can still capture the trend expected (pressure or saturation decrease/increase), but the quantification of these values can be compromised; so additional research is necessary to verify how noisy data can be inverted with more confidence.

4.5. 4D inversion assuming uncertainty in the reservoir initial conditions

The last analysis shown in this work concerns the fact that the initial conditions of the reservoir are not known. Four cases were tested where the initial pressure and saturations used in the 4D inversion are the ones detailed in table 5, instead of assuming the correct values: $S_w = 0.15$ and Pre = 32 MPa. One thing to highlight is that at the initial time, pressure can be considered known, since the 4D acquisition occurs after some years of production and usually the reservoir pressure in the past is known, so the uncertainty is small. The connate

water value can be uncertain since the reservoir can have different facies that cannot be correctly located. This explains the small variation for pressure considered in table 5 around the true values and the chosen values for the initial saturation.

Figure 14 shows the results for these cases. The errors observed are acceptable, showing that even if these properties have some uncertainty, it should not interfere too much with the results (not as much as for noisy seismic data as shown in the previous section).

5. Conclusions

A theoretical study of a petro-elastic inversion to obtain pressure and saturation from seismic attributes was presented. Using an ideal set of data, free of any kind of noise or error in order to observe only the influence of the technical parameters, it was possible to show that pressure and saturation could be recovered from seismic data using only one seismic survey through the 3D inversion algorithm proposed, where P and S impedances were considered simultaneously. The necessity of a time lapse approach arises when errors start to be considered in the ideal set of data, assuming that the reservoir properties (initially represented only by porosity in this work to simplify the process) are unknown (which is the most common case).

The importance of the reservoir properties (represented in this work by porosity) to the petro-elastic modelling used was illustrated by a simple sensitivity analysis, from which it could be concluded that, for the PEM used, porosity has a high influence on 3D impedances and that this influence decreases when 4D differences are considered. Some tests of the 3D and 4D inversion algorithms proposed were presented and, in agreement with the sensitivity analysis, the 3D inversion failed when errors in porosity were considered and, as long as minimum knowledge about the porosity value is available, the 4D inversion yielded satisfactory results.

Different production scenarios were considered to validate the 4D inversion proposed. It was verified that for the ideal data set, the inversion results were practically exact for all scenarios analysed. If a not totally ideal data set is considered, assuming errors or uncertainties, it was observed that the quality of the inversion depends on the current scenario. Although, when uncertainties are considered in the porosity values and under the initial reservoir conditions, the inversion errors are still acceptable. When the time lapse difference of seismic impedances was disturbed up to 15%, the results of all scenarios were acceptable; if impedance differences are

disturbed more than that, the results can still capture the trend expected (pressure or saturation decrease/increase), but the quantification of these values can be compromised, and additional work is necessary to properly estimate pressure and saturation.

References

- Avseth P, Mukerji T and Mavko G 2005 *Quantitative Seismic Interpretation: Applying Rock Physics Tools to Reduce Interpretations Risk* (Cambridge: Cambridge University Press)
- Batzle M and Wang Z 1992 Seismic properties of pore fluids *Geophysics* **57** 1396–1408
- Castro S A, Caers J, Otterlei C M, Meisingset H, Høye T, Gomel P and Zachariassen E 2009 Incorporating 4D seismic data into reservoir models while honoring production and geologic data: a case study *Leading Edge* **28** 1498–1506
- Dadashpour M, Echeverría-Ciaurri D, Kleppe J and Landrø M 2009 Porosity and permeability estimation by integration of production and time-lapse near and far offset seismic data *J. Geophys. Eng.* **6** 325–44
- Dadashpour M, Landrø M and Kleppe J 2008 Nonlinear inversion for estimating reservoir parameters from time-lapse seismic data *J. Geophys. Eng.* **5** 54–66
- Davolio A, Maschio C and Schiozer D 2011 Incorporating 4D seismic attributes into history matching process through an inversion scheme *SPE142946 SPE EUROPEC/ EAGE Ann. Conf. and Exhibition (Vienna, Austria, 23–26 May)*
- Fahimuddin A, Aanonsen S and Skjervheim J A 2010 Ensemble based 4D seismic history matching: integration of different levels and types of seismic data *SPE131453SPE EUROPEC/ EAGE Ann. Conf. and Exhibition (Barcelona, Spain, 14–17 June)*
- Landrø M 2001 Discrimination between pressure and fluid saturation changes from time-lapse seismic data *Geophysics* **66** 836–44
- MacBeth C, Floricich M and Soldo J 2006 Going quantitative with 4D seismic analysis *Geophys. Prospect.* **54** 303–17
- Mavko G, Mukerji T and Dvorkin J 2003 *The Rock Physics Handbook: Tools for Seismic Analysis in Porous Media* (Cambridge: Cambridge University Press)
- Souza R M, Machado A F, Muneratto F P and Schiozer D J 2010 Iterative history matching technique for estimation reservoir parameters from seismic data *SPE131617SPE EUROPEC/ EAGE Ann. Conf. and Exhibition (Barcelona, Spain, 14–17 June)*
- Souza R M, Muneratto F P and Schiozer D J 2011 Quantitative integration of time-lapse derived information in a history matching procedure *SPE143009 SPE EUROPEC/ EAGE Ann. Conf. and Exhibition (Vienna, Austria, 23–26 May)*
- Tura A and Lumley D E 1999 Estimating pressure and saturation changes from time-lapse AVO data *SEG Expanded Abstracts*
- Tuttle C, Pelissier M, Barnes M, Tribe J and Persad K 2009 A seismically constrained reservoir modeling workflow: case study *Leading Edge* **28** 1492–7

3. PAPER 2: *A methodology to constrain pressure and saturation estimation from 4D seismic using multiple simulation models and observed data*

Alessandra Davolio, Célio Maschio, Denis José Schiozer

Journal of Petroleum Science and Engineering, April 2013, v. 105, p. 51-61

Presented at SEG/SPE/AAPG workshop “New advances in integrated reservoir surveillance”, California, 24-29 June 2012.



A methodology to constrain pressure and saturation estimation from 4D seismic using multiple simulation models and observed data

Alessandra Davolio*, Célio Maschio, Denis José Schiozer

Departamento de Engenharia de Petróleo, Faculdade de Engenharia Mecânica—UNICAMP, Caixa Postal 6052, 13.083-970 Campinas, São Paulo, Brazil

ARTICLE INFO

Article history:

Received 9 January 2012

Accepted 19 March 2013

Available online 2 April 2013

Keywords:

seismic and reservoir simulation integration

4D seismic

pressure and saturation estimation

reservoir simulation

ABSTRACT

The use of time-lapse seismic data to improve reservoir characterization is becoming a common practice in the oil industry. Nevertheless, the integration of datasets with different characteristics, such as flow simulation and seismic data, is still a challenge. One of the possible ways to perform the integration is the use of extracted pressure and saturation from 4D seismic in the history matching process. However, the quantitative use of pressure and saturation difference maps in the objective function needs more accurate estimation of these dynamic properties. Thus, this work proposes a methodology to use multiple simulation model realizations, generated through the combination of uncertain reservoir attributes, to guide an inversion process that evaluates pressure and saturation from 4D seismic, in order to provide estimations that are more reliable. The application of the methodology in a synthetic dataset showed promising results. The main contribution of this work is to show that it is possible to use available knowledge from flow simulation and reservoir characterization to constrain time-lapse data and extract from it more reliable information.

© 2013 Elsevier B.V. All rights reserved.

Contents

1. Introduction	51
2. Methodology	53
2.1. Petro-elastic inversion	53
2.2. Multiple flow simulation models	54
2.3. Using observed production data	54
3. Application	55
3.1. Reservoir model description	55
3.2. Model uncertainties	55
3.3. Reference and base model	55
3.4. Petro-elastic modeling	56
3.5. Synthetic seismic	58
3.6. Multiple models: limits extraction	58
4. Results and discussion	59
4.1. Case 1: inversion results using generic constraints	59
4.2. Case 2: inversion results using multiple models simulation	59
4.3. Case 3: inversion results using multiple model simulation and well dynamic data	60
4.4. Comments	60
5. Conclusions	60
Acknowledgments	61
References	61

1. Introduction

Nowadays, the use of time-lapse seismic data is a common practice for reservoir monitoring, since it may provide information

* Corresponding author. Tel.: +55 19 92070940.

E-mail address: davolio@dep.fem.unicamp.br (A. Davolio).

Nomenclature			
IP	P-impedance	V_s	S wave velocity
IS	S-impedance	ϕ	porosity
k_{dry}	effective bulk modulus of dry rock	η	coefficient of internal deformation
k_{sat}	effective bulk modulus of the rock with pore fluid	ρ	bulk density
k_{min}	bulk modulus of mineral material making up rock	ρ_{min}	density of mineral material making up rock
k_{fl}	bulk modulus of the pore fluid	ρ_{fl}	fluid density
OF	objective function	μ_{dry}	effective shear modulus of dry rock
P_{eff}	effective pressure	μ_{sat}	effective shear modulus of the rock with pore fluid
PEM	petro-elastic model		
Pre	pore pressure		
S_w	water saturation	<i>Subscript</i>	
S_o	oil saturation	<i>seis</i>	attribute derived from seismic
V_p	P wave velocity	<i>sim</i>	attribute computed from reservoir simulation results

that yields a better understanding of the reservoir and consequently, more efficient field operations and better financial return. There are several works in the literature describing successful applications of this technology (Castro et al., 2009; Helgerud et al., 2011; Tuttle et al., 2009).

Time-lapse seismic can provide not only information about dynamic properties (pressure and saturation changes) but it can also help to map static properties such as fault transmissibility or facies modeling. The work of Castro et al. (2009) is an example of the application of 4D seismic in both situations.

Another aspect to highlight, concerning the application of this kind of data, is how to integrate it with reservoir flow simulation. The information provided by 4D seismic can be used in a qualitative or quantitative way. The works of Helgerud et al. (2011) and Tuttle et al. (2009) are examples of qualitative application, where 4D seismic was used to determine barriers and baffles. The quantitative integration of time-lapse seismic and reservoir simulation data is usually made via history matching, by defining a procedure to match not only the well production and pressure data but also 4D seismic attributes.

Concerning seismic attributes, the matching is done between the observed seismic and the synthetic seismic derived from the simulation results. In this sense, the procedure can match seismic amplitudes, impedances or any other seismic-derived attribute. Several works, regarding this kind of application, can be found in the literature. Dadashpour et al.'s (2009) work is an example where a quantitative integration between production and seismic data is presented, given that the seismic is used in the form of zero offset amplitudes and gradients. Fahimuddin et al. (2010) compare the use of different seismic data when performing history matching in the ensemble Kalman filter framework. The authors conclude that, in the realistic case considered, the use of impedances yields better results than the ones obtained by using amplitudes. Another work that presents the quantitative use of 4D seismic in the impedance domain is that of Kazemi et al. (2010). In this case, the authors discuss techniques to normalize seismic derived impedances, to make the order of magnitude of these values comparable to the synthetic impedances computed from flow simulation.

It is also possible to extract information about pressure and saturation variations from time-lapse data and quantitatively match these estimated parameters with flow simulator results. Gervais and Roggero's (2010) work is an example, in which the authors propose a local parameterization technique and incorporate saturation information provided by the seismic data in an assisted history matching process. Jin et al. (2011) present another example of the use of saturation patterns extracted from 4D

seismic, in which the authors show a comparison of stochastic optimization methods to integrate quantitatively seismic and production data.

An effective estimation of saturation and pressure values from 4D seismic data is a more complicated task than extracting saturation patterns. Tura and Lumley (1999) showed that it is possible to estimate changes in pressure and saturation through P and S seismic impedances. Landro (2001) proposed a methodology based on mathematical expressions that combines 4D AVO attributes to extract pressure and saturation changes. In the same work, he demonstrates a successful application of his technique on the Gullfaks field. These results were also included in the discussion presented by Landro et al. (2001), which focuses on reservoir management, showing that time-lapse seismic improved the drainage understanding of the Gullfaks field. MacBeth et al. (2006) also proposed a methodology to identify pressure and saturation changes using time-lapse seismic data. Their methodology is able to use any kind of seismic attributes (two or more) since these attributes have a different response to pressure and saturation changes. The work of Dadashpour et al. (2008) present a petro-elastic inversion methodology that uses zero offset 4D seismic amplitudes to recover pressure and saturation changes. Davolio et al. (2012) also present a methodology to estimate dynamic properties from 4D seismic through the P and S seismic impedances. Different from Tura and Lumley (1999), the methodology of this work is based on an optimization process aimed at quantifying the results obtained.

There are many challenges to overcome when converting seismic data into pressure and saturation values. The main issues are noise/errors presented in acquired seismic data, together with errors/uncertainties in reservoir properties and modeling (petro-elastic modeling). Davolio et al. (2012) present a discussion about how some of these issues influence the estimation of dynamic properties from time-lapse seismic.

The methodology we are proposing in this work attempts to mitigate these influences by using known information (from engineering data) to guide the estimation of pressure and saturation changes from time-lapse data, avoiding unfeasible results (considering flow conditions) that can occur due to the problems mentioned. The methodology uses the combination of uncertain reservoir attributes to generate multiple reservoir models, from which limits are established for the unknown pressure and saturation. Then, these limits are used in a petro-elastic inversion algorithm to estimate pressure and saturation from 4D seismic. More specifically, these limits will constrain the solution space of the optimization procedure used to invert 4D data to pressure and saturation.

Observed well pressure and production data are also incorporated into the methodology, reducing the initial range of the reservoir response. The effects of this reduction are reflected on the estimated pressure and saturation values, since stricter limits are used in the inversion process.

If reservoir characterization and uncertain attributes selection are done properly, the limits extracted from multiple simulations can, for instance, restrict areas where the saturation front should reach, although that could be estimated from 4D seismic with some errors or noise. This kind of result is shown in the application presented in a synthetic dataset.

The focus of the proposed methodology is then to calibrate 4D seismic response using the knowledge available from reservoir simulation data as support for the inversion process. The main contribution of the work is to show how reservoir engineering data can be used to guide the inversion process by means of a robust and simple implementation method.

2. Methodology

The methodology proposed here has the objective of guiding the inversion process to estimate pressure and saturation from time-lapse seismic data, in order to obtain results that are more consistent with flow conditions (considering uncertainties). As illustrated in Fig. 1, the procedure consists of extracting limits for pressure and saturation from the simulation of multiple models (generated by flow simulation of scenarios that represent the combination of uncertain attributes). Then, these limits are used to constrain the solution space of the optimization process that estimates the dynamic parameters.

Well history data is also used to improve the methodology by selecting the models that provide production curves closer to the observed data. The reduced number of models consequently reduces the computed limit range that is used to constrain the estimation of pressure and saturation.

This section is divided into two parts: the first one describes the inversion process used to estimate pressure and saturation variations from 4D seismic data and the second one explains how the multiple models generated from the uncertainty analysis are used to constrain the inversion.

2.1. Petro-elastic inversion

The inversion procedure (Davolio et al. (2012) for more details) is based on an optimization process that minimizes the differences

between seismic impedances and synthetic impedances computed from flow simulation data in order to obtain pressure and saturation variations. To generate seismic attributes from reservoir simulation data, a petro-elastic model (PEM), which is a set of relationships that relates fluid/rock and elastic properties, is required.

The inversion is run at the flow simulation scale and is performed for every grid block independently (therefore, an upscaling/downscaling procedure is required to convert data from seismic scale to flow simulation scale). The input data are the 4D seismic, represented by two 3D surveys at time 0 (base) and time 1 (monitor), and the flow simulated pressure and saturation for both times. The procedure is run according to the following steps (see Fig. 2):

1. Go to the first grid block location.
2. At the current grid block, the initial guess (Pre, S_w) is taken from the simulated reservoir model at time 1.

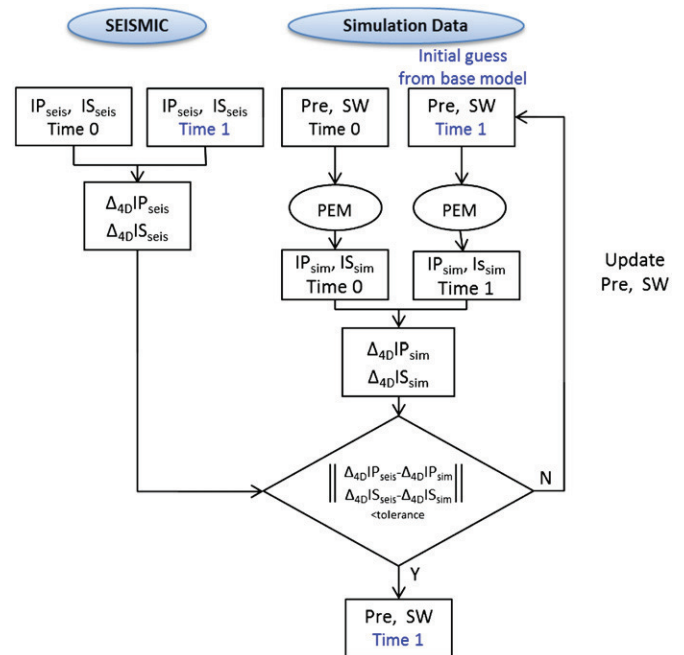


Fig. 2. 4D inversion algorithm to obtain pressure and saturation from seismic impedances.

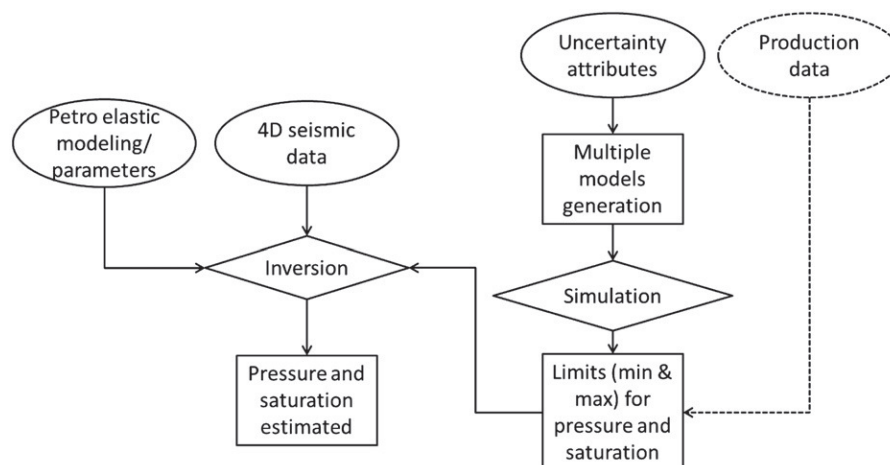


Fig. 1. General workflow of the proposed methodology. The simulation of multiple models (generated from the combination of uncertain attributes) together with production data defines limits (minimum and maximum) to be used in the inversion process, constraining the unknowns that will be estimated (pressure and saturation).

3. At the current grid block, compute IP and IS via PEM with the current values of (Pre, S_w).
4. Compute the objective function described in Eq. (1) for the current grid block. If the objective function value is smaller than a tolerance, go to step 5; if it is not, go to step 6.
5. The optimization finishes and the solution for the current block at time 1 is assumed to be the current pair (Pre, S_w). If it is not the last grid block location, go to the next block and return to step 2.
6. A gradient search algorithm updates the parameters (Pre, S_w) inside the constrained solution space and return to step 3.

The objective function depends on the difference of the time-lapse differences according to the equation:

$$OF = \left\| \begin{array}{l} \Delta_{4D}IP_{seis} - \Delta_{4D}IP_{sim} \\ \Delta_{4D}IS_{seis} - \Delta_{4D}IS_{sim} \end{array} \right\| \quad (1)$$

where the index *seis* stands for seismic impedances, the index *sim* stands for synthetic impedances computed from flow simulation results and the operator Δ_{4D} stands for time-lapse difference: monitor-base.

The constraints used in step 6 to limit the solution space are the key points of the proposed methodology. As described in the next section, this work proposes to define these constraints based on multiple reservoir simulation models.

The optimization algorithm used is a gradient-based method for constrained problems. Note that the way the problem was set, it is a simple and fast optimization problem with only two unknowns for each grid block. Therefore, a gradient method is being used, since there is no need for more sophisticated methods.

One important assumption that it is being used is based on the fact that the base 4D time corresponds to the reservoir at equilibrium conditions (initial time), which means that pressure and saturation are assumed to be known (or estimated with good accuracy) at time 0. Therefore, the final answer of the process is an estimation of pressure and saturation for the second survey (time 1).

Note that this procedure does not update any static reservoir property. The goal here is to extract pressure and saturation values from 4D seismic. These results should be further used in a history matching process, which will then update reservoir properties. Since history matching is not the focus of this work, this kind of application will not be shown here.

2.2. Multiple flow simulation models

One common approach for uncertainty analysis is the combination of different uncertain parameters such as porosity, permeability, faults transmissibility etc., and the generation of multiple simulation models. The proposed methodology aims to use the simulation results of all these models, in order to constrain the solution space of the inversion described in the previous section. The procedure consists of defining limits (minimum and maximum) for the unknown pressure and saturation at each reservoir block, and using them to constrain the solution space of the optimization process defined in Section 2.1. These limits are used more specifically in step 6.

Fig. 3 presents a scheme showing how these limits are extracted. The left side of the image illustrates an uncertainty analysis procedure assuming there are “*n*” uncertain attributes (which could be porosity, permeability, relative permeability etc.). After the combination of these attributes, “*m*” reservoir simulation models are built. After simulating all the models, “*m*” scenarios of pressure and saturation are generated. Thus, every single reservoir block location has “*m*” possible values of pressure and saturation. So, for every single location, the minimum and maximum values along all the possible “*m*” values are extracted.

The idea behind this methodology is to guide the inversion by using reservoir simulation results, avoiding pressure and saturation estimated values that are not compatible with the limits obtained from flow simulation considering the mapped reservoir uncertainties. Consequently, the methodology aims to avoid incorrect estimated values that can be generated due to noise/errors presented in seismic data and/or petro-elastic modeling and parameters, by constraining the solution space of the optimization process through the limits extracted.

If uncertainties are underestimated, as can be observed in several practical cases (generally described by unknown unknowns), flow simulation conditions can impose incorrect limits to the inversion process. In these instances, other iterations can be used to gradually improve the process.

2.3. Using observed production data

In addition to the use of the multiple models, it is possible to make an improvement in the methodology by using observed production data. The idea is to reduce the models dispersion by selecting only the ones that produce values close to the history data. If the models range is reduced, then tighter limits for pressure and

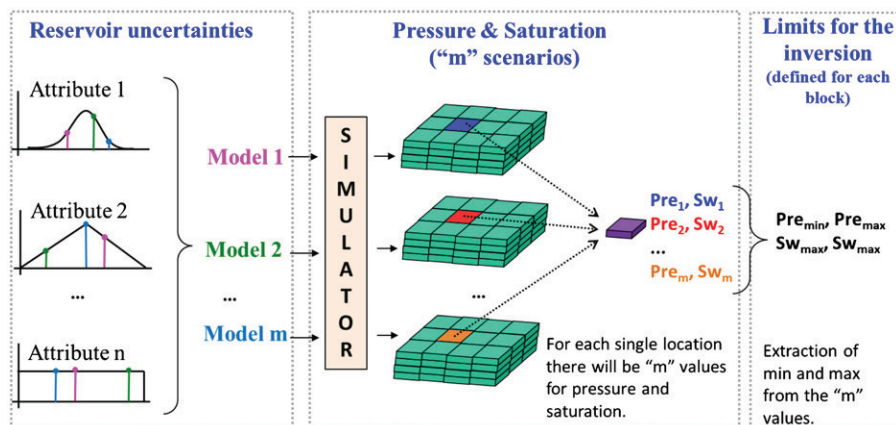


Fig. 3. General procedure used to define limits (minimum and maximum) of pressure and saturation for each reservoir block. 'Attribute 1', 'Attribute 2' and 'Attribute n' are generic representations of the reservoir uncertainty and 'Model 1', 'Model 2' and 'Model m' are generic reservoir models generated from the combination of the reservoir uncertainties.

saturation are expected, constraining the solution space of the inversion even more.

In this case, an additional step in the scheme presented in Fig. 3 is required in order to estimate the limits for the dynamic properties. It is necessary to do a selection of these models based on the distance between their simulation results and the history data. So, instead of using the “*m*” models generated, only certain selected models are used to determine minimum and maximum values for pressure and saturation.

The criterion used to exclude a model is based on the misfit (*M*) between observed (d_i^{obs}) and simulated data (d_i^{sim}), according to the equation below:

$$M = \sum_{i=1}^N (d_i^{obs} - d_i^{sim})^2 \quad (2)$$

where *N* is the number of observed data. In this work, the only available data is bottom-hole pressure. Models with misfit smaller than a given percentage, in relation to the model with the maximum misfit, are used to define the new limits of pressure and saturation.

3. Application

This section describes the dataset used to generate the results. In a real problem, the data needed to apply the proposed methodology is 4D seismic data (P and S impedances), the reservoir simulation model and the multiple model realizations resulting from an uncertainty analysis. This work uses a synthetic dataset, so, apart from the simulation model (called here base model) and the multiple realizations, there is another model (called here reference model) that is used to generate the synthetic seismic. Thus, the reference model represents the true earth model, and the base model represents the model available to the engineer. These models differ from each other by the uncertainty properties described in Section 3.2. Everything else (like grid definition, fault location etc.) is the same for both models.

As mentioned in the previous section regarding the inversion process (step 3), a petro-elastic modeling is used to generate the seismic attributes. The petro-elastic model described in Section 3.4 is used for two purposes: the first one is the forward modeling inside the inversion (step 3) and the second is the generation of the synthetic seismic dataset considered in this work, which is better detailed in Section 3.5.

3.1. Reservoir model description

The reservoir model considered in this work was discretized in a corner-point grid with $90 \times 110 \times 5$ blocks, 60 m in size in the *x*

and *y* directions ($5400 \times 6600 \text{ m}^2$) and 15 m (on the average) in the *z* direction. There are three facies characterized according to three permeability ranges. The reservoir also comprises four faults, as can be seen in Fig. 4. The reservoir is drained by eight vertical producer wells, which are supported by seven water injector wells (Fig. 4).

3.2. Model uncertainties

The uncertain attributes considered in this work, defined by multipliers are as follows:

- (1) Four faults transmissibility: three discrete values (0, 0.1 and 1).
- (2) Relative permeability curves (Corey exponents for the water phase) for each of the three facies.
- (3) Permeability ratio (vertical/horizontal).

Uniform distributions were used to start the procedure for each of these eight attributes.

The other two uncertain parameters are the porosity and horizontal permeability, both of which were generated by geostatistical techniques. Using the sequential Gaussian simulation technique (SGS), 200 realizations of porosity were generated, with the seismic P-impedance volume at time 0 (base survey) as a secondary variable. Each of these porosity fields was used later as a second variable for the SGS to generate 200 realizations of permeability.

Using the slice sampling technique (Neal, 2003), 400 simulation models were generated from the combination of the 10 uncertain attributes, which were sampled from uniform distributions. As uniform distribution was assumed, in principle, any other appropriate sampling technique could have been employed, such as Latin Hypercube for example, as presented by Maschio et al. (2010).

3.3. Reference and base model

As detailed in Section 3.5, a synthetic seismic is being used. To generate the seismic attributes, it is being considered a reference simulation model, which represents the true earth model.

Table 1
Reference and base model properties.

	Fault 1	Fault 2	Fault 3	Fault 4	K_z/K_x	Corey exp. Facies		
Reference	0.4	0.001	0.03	0.8	0.10	4.6	3.1	1.3
Base	0.1	0.1	0.1	0.1	0.26	1.8	2.8	1.4

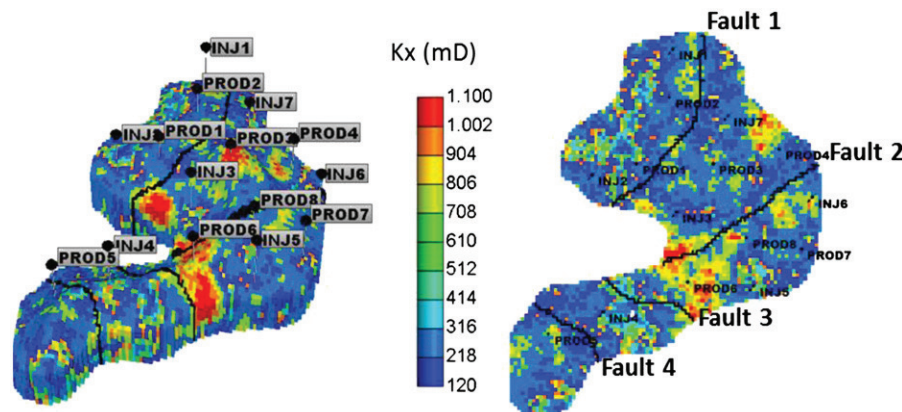


Fig. 4. Reservoir simulation model: 3D view (on the left) and 2D view of the third layer (on the right). The color represents the horizontal permeability field of the reference model. The reservoir has four main faults and the production is carried by eight vertical producer wells, supported by seven water injector wells. (For interpretation of the references to color in this figure legend, the reader is referred to the web version of this article.)

A second simulation model (the base model) is also used in the process, representing the reservoir model available to the engineer. This model represents the available knowledge about the reservoir. Hence, its reservoir properties (like porosity) are used as input in the inversion process, as well as its simulated pressure and saturation, which are used as the initial guess for the optimization process, as indicated in Fig. 2.

The base model was selected as one of the 400 model realizations generated after combining all the uncertainties. Thus, the differences between the two models concern the 10 uncertain parameters described previously. The values of the parameters defined as multipliers are presented in Table 1. The other two uncertain parameters are the permeability and porosity fields shown in Fig. 5 for the third reservoir layer. The porosity field of the base case was calibrated to the 3D seismic data, which allowed the capture of the general features of the true porosity field, although with little resolution.

As this work is focused on the process of extracting pressure and saturation variations from time-lapse seismic data, the most important question regarding the differences between the two models is the differences observed in the simulation results. In this sense, Fig. 6 displays pressure and saturation maps for the third layer of the reservoir for both models after six years of production. One of the most influential differences between the models is the sealing fault located in the middle of the reservoir (Fault 2), which is presented only in the reference model. This can be clearly visualized by comparing Fig. 6c and d, where the reference pressure map has two well defined regions (more and less pressurized) in opposition to the homogenous behavior of the pressure map of the base model.

In relation to the petro-elastic inversion, Fig. 6b and d represents the initial guess while the answer that the algorithm aims to reach is displayed in Fig. 6a and c.

3.4. Petro-elastic modeling

A petro-elastic modeling is required to generate seismic attributes from simulation data. The seismic attributes used in the inversion described in Section 2.1 are compressional and shear impedances, called here IP and IS, respectively. Considering ρ , V_p and V_s the density, compressional and shear wave velocities of the medium, respectively, the impedances can be written as:

$$IP = V_p \rho, \quad (3)$$

$$IS = V_s \rho. \quad (4)$$

Seismic velocities depend on rock-saturated bulk (k_{sat}) and shear (μ_{sat}) modulus according to the equations:

$$V_p = \sqrt{\frac{k_{sat} + (4/3)\mu_{sat}}{\rho}}, \quad (5)$$

$$V_s = \sqrt{\frac{\mu_{sat}}{\rho}}. \quad (6)$$

The medium density can be written as,

$$\rho = (1-\phi)\rho_{min} + \phi\rho_f, \quad (7)$$

where ϕ is the porosity, ρ_{min} is the mineral density and ρ_f is the fluid density which is defined according to the equation:

$$\rho_f = \rho_o S_o + \rho_w S_w \quad (8)$$

with S being the saturation and the subscripts standing for oil and water.

The most commonly used approach to determine the rock saturated bulk and shear modulus are the Gassmann equations

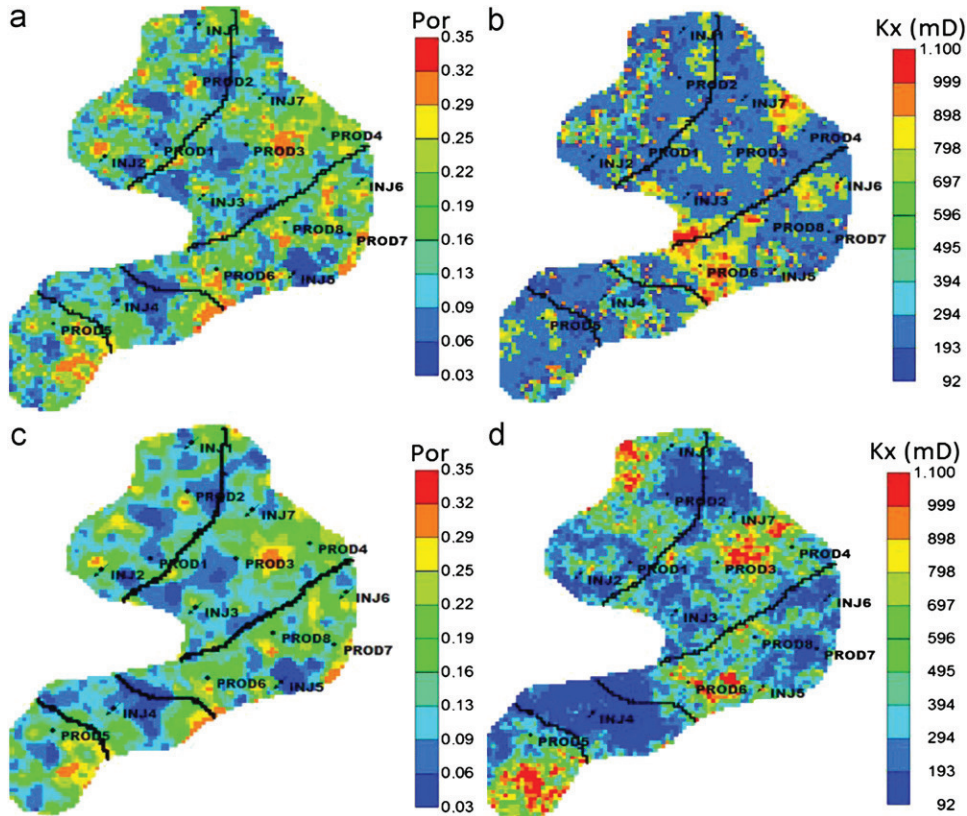


Fig. 5. Reference and base models properties for the third reservoir layer. Top: reference model porosity (a) and horizontal permeability (b). Bottom: base model porosity (c) and horizontal permeability (d).

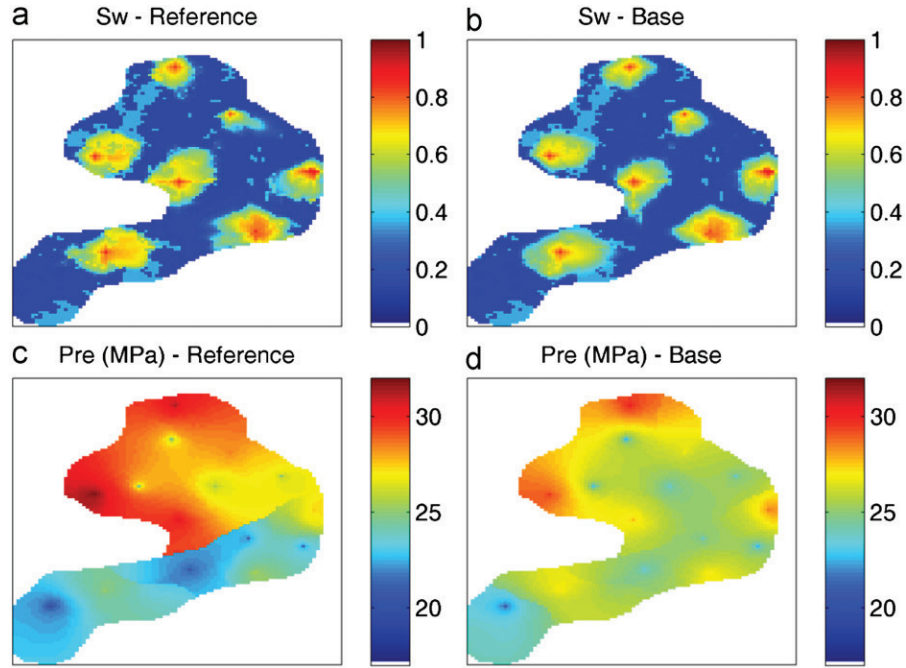


Fig. 6. Results of reference and base model simulation after six years of production for the third reservoir layer.

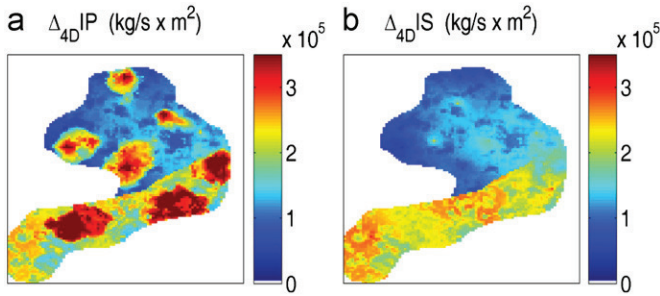


Fig. 7. Time-lapse difference of the synthetic seismic attributes without adding noise. (a) P-impedance. (b) S-impedance.

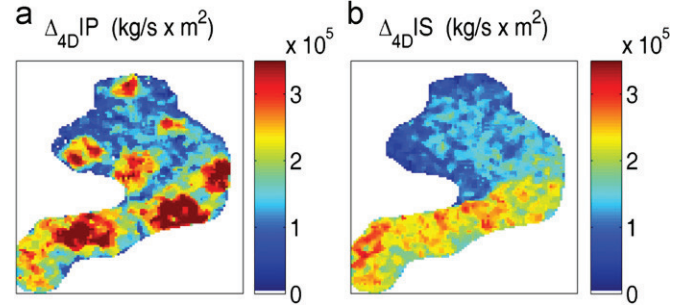


Fig. 8. Time-lapse difference of the synthetic seismic attributes after noise addition and filtering. (a) P-impedance. (b) S-impedance.

that are described as follows (Avseth et al., 2005):

$$k_{sat} = k_{dry} + \frac{(1 - (k_{dry}/k_{min}))^2}{(\phi/k_{fl}) + ((1-\phi)/k_{min}) - (k_{dry}/k_{min}^2)}, \quad (9)$$

$$\mu_{sat} = \mu_{dry}, \quad (10)$$

where k_{dry} , k_{min} and k_{fl} are the bulk moduli of the rock frame, the mineral and the fluid mixture. μ_{dry} and μ_{sat} are the shear moduli of the dry rock and the rock with pore fluid, respectively.

To compute the dry bulk and shear modulus, the known friable or uncemented sand model (Mavko et al., 2003) is used in this work. This model makes use of the Hertz–Mindlin contact theory and a heuristic modified Hashin–Strikman lower bound, according to the equations:

$$k_{dry} = \left[\frac{\phi/\phi_c}{k_{HM} + 4\mu_{HM}/3} + \frac{1-\phi/\phi_c}{k_{min} + 4\mu_{HM}/3} \right]^{-1} - \frac{4}{3}\mu_{HM}, \quad (11)$$

$$\mu_{dry} = \left[\frac{\phi/\phi_c}{\mu_{HM} + z} + \frac{1-\phi/\phi_c}{\mu_{min} + z} \right]^{-1} - z \quad (12)$$

where

$$z = \frac{\mu_{HM}}{6} \left(\frac{9k_{HM} + 8\mu_{HM}}{k_{HM} + 2\mu_{HM}} \right), \quad (13)$$

where k_{HM} and μ_{HM} are the bulk and shear moduli, respectively, at critical porosity ϕ_c given by the contact Hertz–Mindlin theory,

$$k_{HM} = \left[\frac{n^2(1-\phi_c)^2\mu_{min}^2 P_{eff}}{18\pi^2(1-\nu)^2} \right]^{(1/3)}, \quad (14)$$

$$\mu_{HM} = \frac{5-4\nu}{5(2-\nu)} \left[\frac{3n^2(1-\phi_c)^2\mu_{min}^2 P_{eff}}{2\pi^2(1-\nu)^2} \right]^{(1/3)}, \quad (15)$$

where P_{eff} is the effective pressure; μ_{min} and ν are the mineral shear bulk modulus and Poisson ratio and n is the coordination number. Effective pressure follows the relation $P_{eff} = P_{over} - \eta \times Pre$, where P_{over} is the overburden pressure, Pre is the pore pressure and the parameter η is the coefficient of internal deformation, which is assumed to be equal to one in this work.

The bulk modulus of the pore fluid is estimated by Wood's law given as:

$$k_{fl} = \left[\frac{S_w}{k_w} + \frac{S_o}{k_o} \right]^{-1} \quad (16)$$

where k_w and k_o denote the oil and water bulk moduli, respectively. The fluids bulk moduli (k_w and k_o) are computed from the fluid bulk densities and fluid acoustic velocity through the Batzle

and Wang (1992) equations. The bulk densities ρ_o and ρ_w can also be exported from the flow simulation and used as an input to compute bulk fluid modulus. A summary can be found in Mavko et al. (2003). Note that in this work it is assumed that there is no presence of gas.

3.5. Synthetic seismic

The input unknowns for the petro-elastic modeling can be single constants, or grid properties. The single constants can be temperature, overburden pressure, mineral properties (bulk and shear moduli, mineral density etc.) and fluid properties (salinity, density etc.). For the dataset considered in this work, the only grid properties used as input for the PEM are the porosity field, facies location and the dynamic properties (pressure and saturation). In other cases, it can have other parameters, such as, for instance, net pay.

To build the synthetic P and S impedances, the petro-elastic modeling is run using the reference model parameters. The same forward modeling that is done within the inversion process (with the base model properties) is previously applied to convert simulated pressure and saturation (from the reference model) into IP and IS for each simulation grid block. As the same PEM is used in both situations, this work assumes that errors are not being accounted for in the petro-elastic equations.

From the point of view of the inversion process, the most important error/uncertainty assumed in the considered dataset

concerns the porosity field (Fig. 5), since this property has a high influence when computing seismic attributes. A more detailed discussion about the influence of noise/errors in the inversion process is presented in Davolio et al. (2012). In this work, the authors show that, for the PEM considered (the same one considered here), porosity is the most influential attribute to compute seismic impedances, but even if this property is not totally known, it is still possible to estimate pressure and saturation information from seismic data (provided that 4D data is used, not 3D).

Two production times are considered in this work; the initial time (before production starts) and after six years of production, yielding a total of four impedance volumes representing the seismic data (P and S impedances for each survey).

With the purpose of having the synthetic data closer to real cases, an independent random noise of 1% of the average was added to each P and S impedance volume. To avoid the high frequency content that appears when computing time-lapse differences from these noisy attributes, a 2D median filter was applied to the noisy impedance volumes. Figs. 7 and 8 show the time-lapse difference for the synthetic attributes generated before and after disturbing them. Because of the median filter application, the perturbation observed in the impedances present different magnitudes for each reservoir location ranging from 1% to 50%, as shown in Fig. 9.

The dataset used in this work does not take into account scale differences between seismic and simulator data, which means that reference and base models are at the same scale. Another simplification made concerns the presence of gas, *i.e.*, the dataset corresponds to a water-flooding example (no presence of gas).

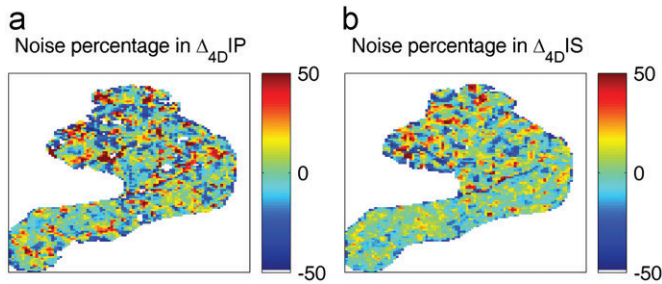


Fig. 9. Percentage of noise added in the synthetic impedances. (a) Noise percentage in $\Delta_{4D}IP$ and (b) noise percentage in $\Delta_{4D}IS$.

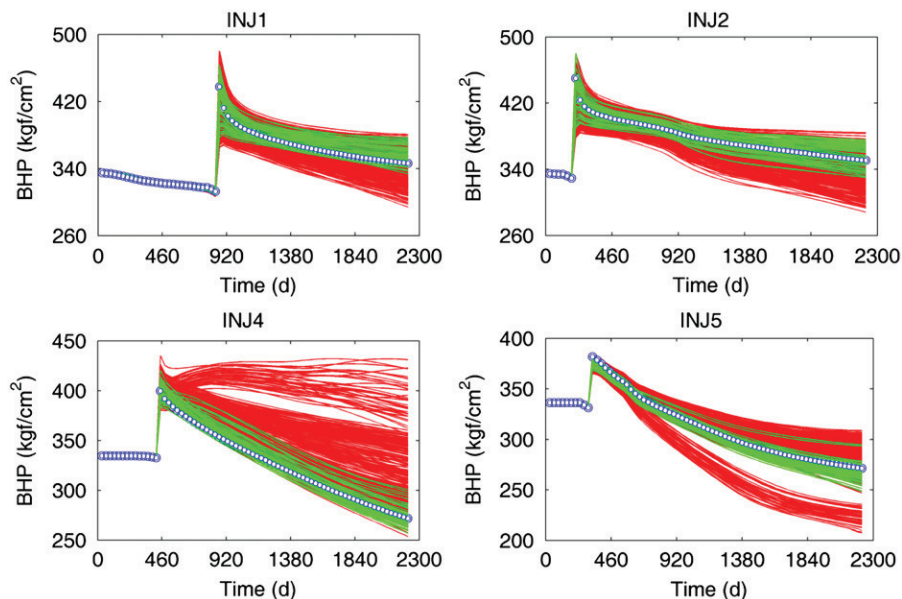


Fig. 10. Simulation results for well bottom-hole pressure for four injectors: green curves represent models kept after the exclusion criterion. (For interpretation of the references to color in this figure legend, the reader is referred to the web version of this article.)

of the inversion process; the results of this application are shown in Section 4.2.

The well bottom-hole pressure curves (for four injector wells) for the 400 simulated models are presented in Fig. 10, in red. They represent the initial dispersion of the models. The green curves represent the models closer to the history, after the application of the exclusion criteria. In this case, a cut-off value of 20% was used. This means that models with misfit greater than 20% with respect to the more misadjusted model are discarded. The number of models was then reduced to 64. The procedure of extracting minimum and maximum values was repeated for this reduced set of models and the results of using these limits in the inversion are presented in Section 4.3.

4. Results and discussion

The inversion procedure was run for three different cases; for each of them the optimization assumed different constraints for the variables of pressure and saturation. In case 1, generic, or usual, constraints were used. For the second case, new limits extracted from the 400 models were used to constrain the solution space; the same was done in case 3, considering only the 64 models that were selected according to the applied cut-off.

4.1. Case 1: inversion results using generic constraints

The constraints applied to pressure and saturation for the first case were established according to known reservoir simulation assumptions. For S_w the limits were the connate water saturation (lower limit) and one minus residual oil saturation (upper limit). For pressure, the injection pressure was used as the upper limit and the minimum well bottom-hole as the lower limit. The estimated pressure and saturation maps for the third layer can be seen at the top of Fig. 11. The errors are displayed at the bottom of the same image, computed through the difference: reference – estimated.

Knowing that the true answer is displayed in Fig. 6a and c, it could be said that the inversion did a good job, since the main features were captured, especially for the pressure map, where a nice improvement can be seen when compared to the initial guess (Fig. 6d).

Clearly, the estimated maps present a noisy aspect due to the errors presented in the synthetic seismic data, showing the necessity for the proposed methodology to use engineering data in order to minimize the noise influence on the estimated properties. These results are presented in the next section.

4.2. Case 2: inversion results using multiple models simulation

As mentioned previously, the combination of the uncertainties produced 400 models. From the simulation results of all these models, minimum and maximum values were extracted for pressure and saturation for each reservoir block. Therefore, the solution space of the optimization process is now constrained by these limits. Following the same layout as Fig. 11, the improvement of the estimated properties can be observed in Fig. 12 when these new constraints are applied. Comparing the error maps in Figs. 11c and 12c, a less noisy behavior of the new estimated saturation can be noted. Observe that, especially for regions where the water was

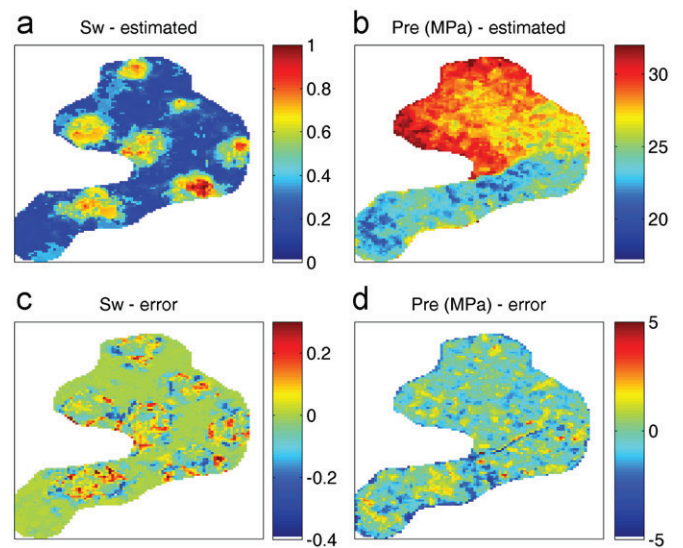


Fig. 12. Inversion results of case 2 for the second survey; layer 3. (a) Estimated water saturation. (b) Estimated pressure (MPa). (c) S_w error: estimated–reference. (d) Pressure error: estimated–reference.

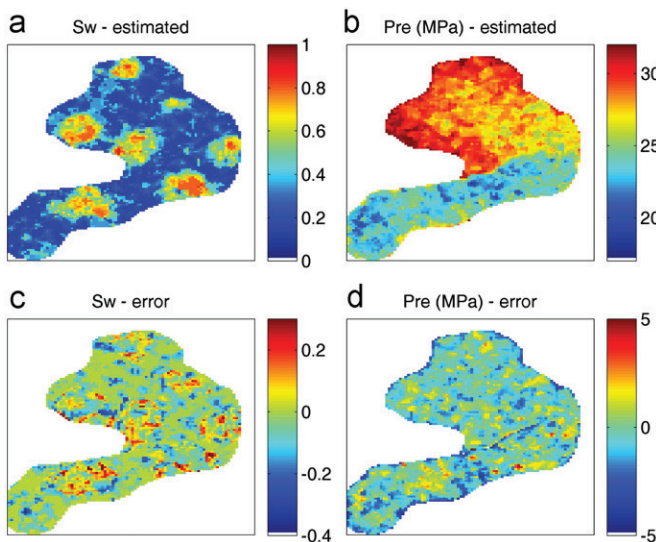


Fig. 11. Inversion results of case 1 for the second survey; layer 3. (a) Estimated water saturation. (b) Estimated pressure (MPa). (c) S_w error: estimated–reference. (d) Pressure error: estimated–reference.

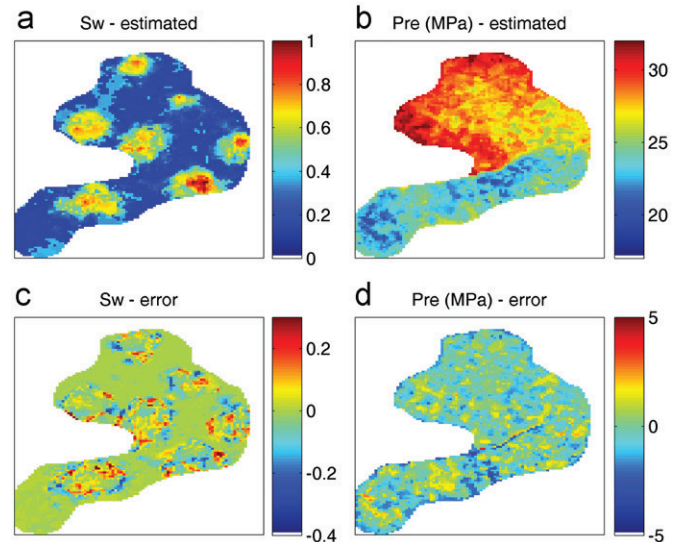


Fig. 13. Inversion results of case 3 for the second survey; layer 3. (a) Estimated water saturation. (b) Estimated pressure (MPa). (c) S_w error: estimated–reference. (d) Pressure error: estimated–reference.

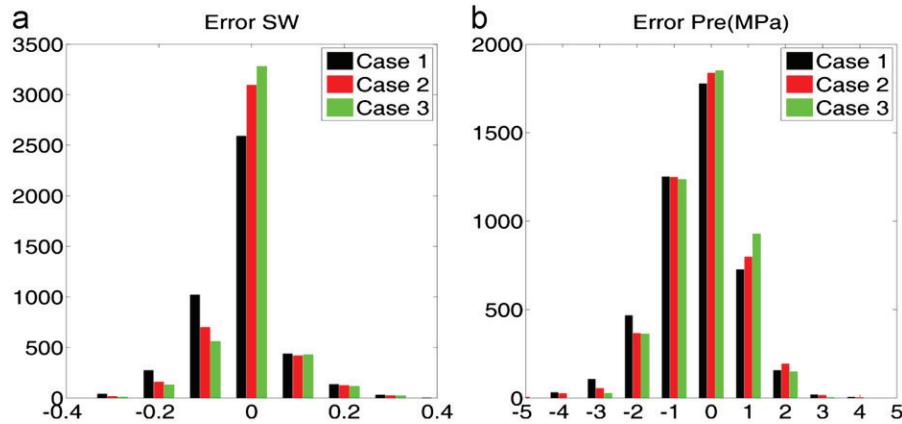


Fig. 14. (a) Histogram of the errors displayed in Figs. 11c, 12c and 13c. (b) Histogram of the errors displayed in Figs. 11d, 12d and 13d.

not supposed to reach, the new estimated saturation map presented more corrected values.

Although not as pronounced as the saturation maps, the new estimation of pressure has shown an improvement that can be better observed by comparing Fig. 11d and Fig. 12d.

4.3. Case 3: inversion results using multiple model simulation and well dynamic data

Reducing the number of simulation models by selecting only the ones closest to the history data automatically produces stricter limits to be used in the inversion process. As a result, it can be observed in Fig. 13 that these new limits, computed from the 64 selected models, allowed a reduction in the observed errors for both parameters (pressure and saturation).

Another way to compare the three results presented is by looking at the images displayed in Fig. 14, that show the histograms of water saturation and pressure errors for the three inversion results (built using the data of Figs. 11c, d, 12c, d and 13c, d).

Fig. 14a clearly shows the largest concentration of values close to zero for case 3 when compared to the other two cases, indicating that the inversion constrained by the new limits (obtained from 64 simulations) yielded the best results for saturation. Another interesting feature observed is the gradual improvement from case 1 to case 2 and then to case 3.

Although less pronounced, the same improvement can be observed for the pressure errors in Fig. 14b. Again, case 3 presented the largest concentration of points close to zero, indicating that this is the best estimation of pressure.

4.4. Comments

The focus of the proposed methodology is to use flow simulation information to guide the estimation of pressure and saturation from 4D seismic. Its relevance remains in the calibration of computed dynamic properties with flow conditions. This is an innovative aspect, since the works presented in the literature usually do not use engineering data (such as production profiles, uncertainty analysis etc.) for quantitative interpretation of time-lapse seismic anomalies.

It is important to emphasize that this work does not concern reservoir uncertainties mitigation. Nor is it proposing a new inversion technique to estimate the dynamic properties. Both techniques (uncertainties analysis and inversion) are used as tools to apply the proposed methodology.

The proposed methodology has the benefit of better exploring 4D seismic signals, since this helps in the quantification of the

saturation and pressure values by imposing limits that come from flow simulation (considering uncertainties). The limits imposed by the multiple models can, for instance, clean some areas in the estimated water saturation map where, according to the simulations, water should not have reached. This kind of result was observed in the synthetic example presented.

Although the application of the proposed methodology was successful for a synthetic model, there are some additional challenges to be addressed in real data. In cases where the uncertainty analysis is not done properly (e.g., having not taken into account an unknown unknown), for instance, the methodology might force the inversion limits to the boundaries. Therefore, the next step of the proposed methodology would be to verify the locations where this kind of behavior is observed and to evaluate whether the time-lapse seismic or the uncertainty analysis has some problems. This kind of integration will be useful, at least, to verify if the uncertain attributes are being correctly represented, and if the flow behavior, taking into account these uncertainties, is in agreement with the time-lapse signals, which can be indicative of the quality of the reservoir characterization.

5. Conclusions

A methodology to integrate time-lapse seismic data and reservoir simulation has been proposed. The process uses multiple simulation models, generated through the combination of uncertain reservoir attributes, to derive limits for pressure and saturation. These limits are later used to constrain an inversion scheme for estimating the dynamic properties from 4D seismic, avoiding values that are incompatible with flow conditions constrained by the characterization process.

The methodology was applied to a synthetic dataset, yielding a better estimation of the dynamic properties, especially for the water saturation front. The use of well dynamic data to reduce the models dispersion complemented the methodology, improving the results even more. The important contribution of this work remains in the quantitative use of available knowledge from reservoir characterization and flow simulation, tying them to observed changes in 4D seismic, and thus extracting, in a more reliable way, changes due to production (pressure and saturation changes).

The proposed methodology presented promising results, showing that the integration between seismic and simulation data can improve the reservoir dynamic properties characterization. It has an innovative aspect in the sense that the works in the literature concerning quantitative integration between the two different datasets usually incorporate seismic attributes into the history

matching. Here, the proposal is to calibrate the 4D signals response before running a history matching, in order to avoid incorporating too much incorrect information into the matching. Although an application of the estimated maps in a history matching process was not presented here (which is the next step in this type of methodology), what has been shown is that the proposed methodology can yield more robust pressure and saturation maps with less uncertainty, which can then be incorporated quantitatively into the history matching process.

The application of this methodology was successful for a synthetic model; however, there are some additional challenges for real data. Future work should attempt to extend the methodology to a statistical approach, in order to deal with more complex cases. In this case, instead of extracting minimum and maximum values, probability density functions (*pdf*) will be generated for each reservoir block from both engineering and 4D seismic data. The main idea is that by matching these *pdfs*, it will be possible to more effectively integrate 4D seismic and reservoir simulation in cases of greater complexity.

Acknowledgments

The authors wish to thank UNISIM, PETROBRAS, CEPETRO and Department of Petroleum Engineering for their support to this work. We also thank CMGL and Schlumberger for the software licenses.

References

- Avseth, P., Mukerji, T., Mavko, G., 2005. Quantitative Seismic Interpretation: Applying Rock Physics Tools to Reduce Interpretations Risk. Cambridge University Press, Cambridge.
- Batzle, M., Wang, Z., 1992. Seismic properties of pore fluids. *Geophysics* 57 (11), 1396–1408.
- Castro, S.A., Caers, J., Otterlei, C.M., Meisingset, H., Hoye, T., Gomel, P., Zachariassen, E., 2009. Incorporating 4D seismic data into reservoir models while honoring production and geologic data: a case study. *Leading Edge* 28 (12), 1498–1506.
- Dadashpour, M., Landrø, M., Kleppe, J., 2008. Nonlinear inversion for estimating reservoir parameters from time-lapse seismic data. *J. Geophys. Eng.* 5, 54–66.
- Dadashpour, M., Echeverría-Ciaurri, D., Kleppe, J., Landrø, M., 2009. Porosity and permeability estimation by integration of production and time-lapse near and far offset seismic data. *J. Geophys. Eng.* 6, 325–344.
- Davolio, A., Maschio, C., Schiozer, D., 2012. Pressure and saturation estimation from P and S impedance: a theoretical study. *J. Geophys. Eng.* 9, 447–460.
- Fahimuddin, A., Aanonsen, S., Skjervheim, J.A., 2010. Ensemble based 4D seismic history matching: integration of different levels and types of seismic data. SPE131453. In: Proceedings of the Annual Conference Exhibition of SPE EUROPEC/EAGE. 14–17 June, Barcelona, Spain.
- Gervais, V., Roggero, F., 2010. Integration of saturation data in a history matching process based on adaptive local parametrization. *J. Pet. Sci. Eng.* 73, 86–98.
- Helgerud, M.B., Miller, A.C., Johnston, D.H., Udoh, M.S., Jardine, B.G., Harris, C., Aubuchon, N., 2011. 4D in the deepwater Gulf of Mexico: Hoover, Madison and Marshall fields. *Leading Edge* 30 (9), 1008–1018.
- Jin, L., Alpak, F.O., Hoek, P.V., Pirmez, C., Fehintola, T., Tendo, F., Olaniyan, E., 2011. A comparison of stochastic data-integration algorithms for the joint history matching of production and time-lapse seismic data. In: Proceedings of the Annual Technical Conference Exhibition of SPE146418. 30 October–2 November, Denver, Colorado, USA.
- Kazemi, A., Stephen, K.D., Shams, A., 2010. Seismic history matching of Nelson using time-lapse seismic data: an investigation of 4D signature normalization. SPE131538. In: Proceedings of the Annual Conference Exhibition of SPE EUROPEC/EAGE. 14–17 June, Barcelona, Spain.
- Landrø, M., 2001. Discrimination between pressure and fluid saturation changes from time-lapse seismic data. *Geophysics* 66, 836–844.
- Landrø, M., Stronen, L.K., Slheim, O.A., Hilde, E., 2001. Time-lapse seismic as a complementary tool for in-fill drilling. *J. Pet. Sci. Eng.* 31, 81–92.
- MacBeth, C., Florich, M., Soldo, J., 2006. Going quantitative with 4D seismic analysis. *Geophys. Prospect.* 54, 303–317.
- Maschio, C., Carvalho, C.P.V., Schiozer, D.J., 2010. A new methodology to reduce uncertainties in reservoir simulation models using observed data and sampling techniques. *J. Pet. Sci. Eng.* 72, 110–119.
- Mavko, G., Mukerji, T., Dvorkin, J., 2003. *The Rock Physics Handbook: Tools for Seismic Analysis in Porous Media*. Cambridge University Press, Cambridge.
- Neal, R.M., 2003. Slice sampling. *Ann. Stat.* 31 (3), 705–767.
- Tura, A. and Lumey, D., 1999. Estimating pressure and saturation changes time-lapse AVO data. SEG Technical Program Expanded Abstr. pp. 1655–1658.
- Tuttle, C., Pelissier, M., Barnes, M., Tribe, J., Persad, K., 2009. A seismically constrained reservoir modeling workflow: case study. *Leading Edge* 28 (12), 1492–1497.

4. PAPER 3: *Local history matching using 4D seismic data and multiple models combination*

Alessandra Davolio, Célio Maschio, Denis José Schiozer

Presented at the EAGE/SPE Europec Annual Conference & Exhibition, London, United Kingdom, 10–13 June 2013.



SPE 164883-MS

Local History Matching Using 4D Seismic Data and Multiple Models Combination

Alessandra Davolio, Célio Maschio, Denis José Schiozer, UNICAMP

Copyright 2013, Society of Petroleum Engineers

This paper was prepared for presentation at the EAGE Annual Conference & Exhibition incorporating SPE Europec held in London, United Kingdom, 10–13 June 2013.

This paper was selected for presentation by an SPE program committee following review of information contained in an abstract submitted by the author(s). Contents of the paper have not been reviewed by the Society of Petroleum Engineers and are subject to correction by the author(s). The material does not necessarily reflect any position of the Society of Petroleum Engineers, its officers, or members. Electronic reproduction, distribution, or storage of any part of this paper without the written consent of the Society of Petroleum Engineers is prohibited. Permission to reproduce in print is restricted to an abstract of not more than 300 words; illustrations may not be copied. The abstract must contain conspicuous acknowledgment of SPE copyright.

Abstract

Nowadays there are several methodologies to incorporate quantitatively 4D seismic data in the history matching of reservoir simulation models. Most of them add a map attribute derived from 4D seismic, which can be impedance maps, saturations etc., in the objective function of the optimization process. In these cases, the goal is to match the dynamic information provided by 4D seismic with simulation response in the whole reservoir area, or the whole area covered by seismic data. In this work, it is proposed a history matching methodology that uses 4D seismic information locally for each injector (and the associated producers) individually, trying to match the water front movement related to each injector with the observed dynamic changes.

In order to guarantee consistency with geology, the matching is done by combining static properties that comes from different simulation models. These models are generated through a combination of the most important uncertain parameters in an uncertainty analysis procedure, geologically consistent, that should be run previously. Then, the matching procedure is based on the computation of the water saturation errors at some sub-regions defined around the injector for multiple scenarios; the error is computed between water saturation derived from 4D seismic and each model simulation result. The models which presented the smallest error for each sub-region are selected and a new simulation model is built by combining the static properties extracted from the selected models at each sub-region. Before calculating the saturation errors the volume of water computed from 4D seismic is calibrated to the volume of injected water providing a more robust calibration. The methodology was applied to a synthetic case where porosity and permeability were the main uncertainties updated by the methodology proposed. Since these properties were generated through geostatistic realizations, the adjusted model kept the geological features. The promising results observed in the synthetic case showed that the methodology can be a good alternative for history matching, since it is an easy to implement procedure and it does not require sophisticated optimization algorithms to incorporate 4D seismic into the process.

Introduction

Reservoir simulation is one of the main tools used for reservoir management. Thus, one of the main tasks of geologists and reservoir engineers is to build reliable models, which is not an easy task, due to the complexity present in this kind of problem. The complexity comes mainly from the lack of geological information needed to build such models. This issue can be minimized by matching dynamic data (well production, 4D seismic, etc) in a history matching procedure, which is an ill posed inversion process with several possible solutions. As it is a difficult and important task, several works can be found in the literature approaching the problem with different optimization algorithms, discussing how to use the dynamic data available to be matched and so on. There two relevant issues that has been subject of active research in the last ten years. One is the quantitative incorporation of 4D seismic data in the history matching procedure and the other is the development of history matching methodologies that generates models geologically consistent.

The works of Caers (2003) and Hoffman and Caers (2005) are good examples of history matching methodologies geologically consistent. In Caers (2003) it is proposed the multiple-point geostatistics method where geological information is jointly integrate with well production data through a geological training image. An extension of this approach is presented in Hoffman and Caers (2005) where the authors propose a methodology to use the same kind of probability perturbation method (using the training

images) but now performing regional perturbations. Consequently, the reservoir can be split into regions and the method allows different amount of properties change for different parts of the model, being that no discontinuities are formed along the borders.

The two methodologies mentioned above originally consider only well data to perform the matching, however an application of the probability perturbation method proposed by Caers (2003) that also includes 4D seismic data quantitatively can be seen in Castro et al (2009), for the Oseberg field, and Tolstukhin et al (2012) for the Ekofisk field.

Landa and Kumar (2011) and Stephen et al (2005) are other examples of history matching process that consider well production and 4D seismic data jointly to perturb the model properties; their methodologies also keep the integration with geological information. Both of them perform the history matching with a probabilistic approach but with different algorithms. Landa and Kumar (2011) uses a Monte Carlo type sampling algorithm and Stephen et al (2005) uses the Neighbourhood Algorithm (NA).

This work proposes a new methodology to run a local history matching using 4D seismic data quantitatively. Multiple models are used to perform the local matching in a simple process of comparing the errors between 4D seismic data and the reservoir model realizations. Differently of the methods usually find in the literature, as the one mentioned before, in the methodology proposed here no optimization process is performed. Another point is that it assumes that an uncertainty analysis was run previously so that it generated several model realizations. These realizations are used to update the reservoir properties, hence the model obtained after the matching will keep some geological consistence. In order to validate the methodology an application in a synthetic dataset is presented. The main contribution of this work remains in the simple approach proposed which can be an alternative to the sophisticated algorithms mentioned before.

Methodology

It is common nowadays to run statistical analysis to better understand the effect of uncertainties on reservoir behavior; as a result of this kind of procedure, several model realizations are generated by combining the most important uncertainties. The goal of the methodology proposed in this work is to harness these models together with 4D seismic to run a local history matching procedure that updates the reservoir properties without losing their geological aspect. The proposed approach aims to use the data provided by 4D seismic locally, by performing a local matching, considering each injector region, trying to adjust the movement of the water front.

The 4D seismic data considered in this work consist of water saturation difference map ($\Delta_{4D}Sw_{seis}$), generated by an inversion process such as the one described in Davolio et al (2012a). Thus, the local matching is done by dividing the reservoir into regions according to the location of the injector wells and its correspondent water saturation error map observed. Then, local properties such as porosity, permeability etc., are modified in order to minimize water saturation errors between the data provided by 4D seismic and the simulation model. The local modification of the static properties is done by using several model realizations. A more detailed description of the whole matching process is presented below. Note that the operator Δ_{4D} stands for the time lapse difference: property at time 1 – property at time 0 (time 0 and 1 correspond to two seismic surveys).

- 1- Simulate the n models generated by an uncertainty analysis procedure run previously and calculate the water saturation time lapse difference for each model ($\Delta_{4D}Sw_{sim,i}$, for $i=1:n$);
- 2- Simulate the base model and calculate the water saturation time lapse difference ($\Delta_{4D}Sw_{base}$);
- 3- Compute water saturation error map of the base model:

$$Error_{base} = \Delta_{4D}Sw_{seis} - \Delta_{4D}Sw_{base}; \quad (1)$$

- 4- Select an injector well and define regions around it according to the error map computed in step 3;
- 5- For each region and each of the n model realization calculate the quadratic error:

$$QE = \sum_{ijk} (\Delta_{4D}Sw_{seis}^{ijk} - \Delta_{4D}Sw_{sim}^{ijk})^2, \quad (2)$$

being that i,j,k are the block coordinates inside the region.

- 6- For each region select the model which presents the smallest quadratic error computed in step 5;
- 7- For the models selected in step 6, cut the local properties inside each region;
- 8- Replace the base model properties inside each region for the properties extracted in step 7;
- 9- Simulate the new base model and analyze the error map (equation 1), if the errors are acceptable select another injector and go to step 2, if not, redefine de regions and go back to step 5.

In order to use water saturation maps provided by 4D seismic data quantitatively, as described above, it is important to calibrate this information with engineering data. In this sense, an additional procedure is run before the step 3 defined above. It consists of computing the amount of injected water according to the water saturation map provided by 4D seismic and dividing this value by the known volume of injected water. The result is a correction factor that should be applied to the 4D seismic data by dividing the water saturation map by this number.

Another important fact to highlight is that the methodology described above should be used for local properties, so if there are global properties, such as relative permeability, that plays an important role in the reservoir response, then a global matching should be applied before starting the local matching.

Since it is not the focus of this work to perform a complex global match, a simple manual matching procedure based only in well data is proposed. The procedure treats each set of global property at a time and it consists of building hundreds of models through the derivative tree technique (Schiozer et al, 2004), where all the levels of one set of parameters are combined. Then, the quadratic error between each well production curve of each model and history data is computed according to the equation:

$$QE_{well} = \sum_{s=1}^m (obs_s - sim_s)^2, \quad (3)$$

where m is the number of production data and obs_s is the history. After that, for each model is calculated an average of the quadratic error of all wells, then the 20 models (which correspond to 10% of the amount of models used in this work) that produced the smallest average are selected. Finally a histogram showing the frequency of occurrence of each level for the 20 selected models is built and the analysis of the histograms indicates the value (defined by the levels) that should give the best match. Once a parameter is adjusted the model keeps this value and the procedure is repeated for the next global parameter to be matched.

One more thing to comment about the methodology proposed concerns the different scales of simulation and seismic data. In the data considered in this work, this is not an issue because the synthetic 4D seismic was generated at the simulation scale. However, in more realistic cases, this issue needs to be addressed; the simplest way would be to convert seismic data to the simulation scale. The efficiency of the methodology will depend on how much information is left after the scale transfer.

Application

The data required to apply the proposed methodology are 4D seismic data (converted to water saturation maps), the reservoir simulation model (base model) and the multiple model realizations resulted from an uncertainty analysis. This work uses a synthetic dataset, so, apart from the base model and the multiple realizations, there is also the reference model that represents the true earth model used to check the accuracy of the history matching proposed. This model was also used to generate the synthetic 4D seismic, which was disturbed by adding some noise. Follow below the description of all the data used.

Reservoir model description

The reservoir model considered in this work was discretized in a corner-point grid with $90 \times 110 \times 5$ blocks, 60m in size in x and y direction (5400×6600 m) and 15m (on the average) in z direction. There are three facies characterized according to three permeability ranges. The reservoir also comprises four faults, as can be seen in figure 1. The reservoir is drained by eight vertical producer wells, supported by seven water injector wells.

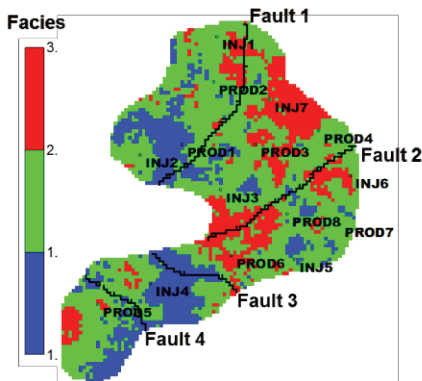


Figure 1: Reservoir model.

Table 1: Base and reference model global properties.

	Fault 1	Fault 2	Fault 3	Fault 4	Kz/Kx	Corey exp.		
						Facies		
Reference	0.4	0.001	0.03	0.8	0.100	4.6	3.1	1.3
Base	0	0.1	0	1	0.096	4.4	4.2	1.0

Model uncertainties

There are a total of ten uncertain parameters considered in this work, being that eight of them are defined as multipliers as follow:

- Four faults transmissibility;
- Relative permeability curves (Corey exponents for the water phase) for each of the three facies;
- Permeability ratio (vertical/horizontal).

The other two uncertain parameters are porosity and permeability; both were generated by geostatistical techniques. Using the sequential Gaussian simulation technique (SGS), 200 realizations of porosity were generated having the seismic P-impedance volume at time 0 (base survey) as a secondary variable. Each of these porosity fields was used later as a second variable for the SGS to generate 200 realizations of permeability.

Base and reference model

The differences of the base and reference models are the 10 uncertainties described above. The base model was built by a random combination of the ten uncertainties described above. The values of the parameters, for both models, defined as multipliers

are presented in table 1. The other two uncertainties are the porosity and permeability fields that can be seen on figure 2. The reference model properties were not built by the same geostatistic procedure mentioned before, i.e., they do not belong to the set of 200 realizations. Thus it can be observed relevant differences in the images especially for permeability.

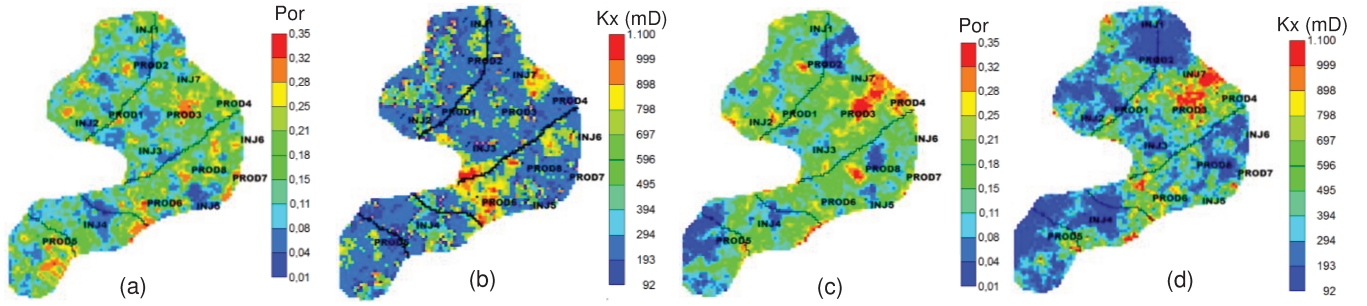


Figure 2: Reference and base models properties for the third reservoir layer. Reference model porosity (a) and horizontal permeability (b). Base model porosity (c) and horizontal permeability (d).

Saturation from 4D seismic data

The 4D seismic data used in the history matching is the estimated volume (it is not a map because in this synthetic dataset the seismic data has the same scale of the simulation model, i.e., 5 layers) of the time lapse difference of water saturation. The base survey (time 0) corresponds to the initial reservoir state, before production start and the second seismic survey corresponds to the reservoir after 6 years of production. The estimation of water saturation differences was made by an inversion process conditioned to flow conditions according to the methodology described in Davolio et al (2012b) and it is shown in figure 3b. Due to the noise added to the synthetic seismic data the estimated water saturation front presents some errors (figure 3c) when compared to the true answer given by the reference model (figure 3a).

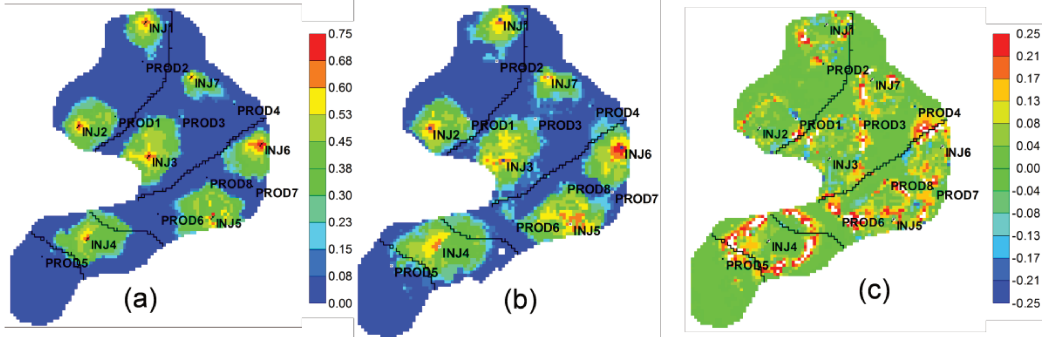


Figure 3: (a) Water saturation difference of the reference model ($\Delta_{4D}Sw_{ref}$). (b) Estimated water saturation difference from 4D seismic ($\Delta_{4D}Sw_{seis}$). (c) Error of the estimated water saturation difference: ($\Delta_{4D}Sw_{seis} - \Delta_{4D}Sw_{ref}$). All images correspond to the third layer.

Global matching

The case considered in this work has two important global properties: relative permeability (kr) and faults transmissibility. As mentioned before, in the global matching these two parameters are treated individually. In this work the procedure starts with the faults transmissibility. Four levels are considered for the four faults: level 0= 0, level 1= 0.001, level 2= 0.01 and level 3= 1. Thus, 256 models are created by combining all the possibilities through the derivative tree technique. Then, the quadratic error (equation 3) of the Bottom Hole Pressure (BHP) curves of each model for each well is computed. Although fault transmissibility is a global parameter, its influence is limited to some wells. The consequences of changing the transmissibility of fault 1, for instance, will not interfere considerably the production of PROD5. So, for each fault only the closer wells are considered to compute the average of the quadratic error. The well selected for each fault are:

- Fault 1: INJ1, INJ2, INJ3, INJ7, PROD1, PROD2, PROD3;
- Fault 2: INJ3, INJ6, PROD3, PROD4, PROD6, PROD8;
- Fault 3: INJ4, INJ5, PROD6;
- Fault 4: INJ4, PROD5

Hence, taking fault 1 as an example, the average of the quadratic error of only the 7 wells defined above is computed for each of the 256 models. Then, the 20 models that gave the smallest quadratic error are selected to do the histogram analysis. The same procedure is valid for the other three faults.

Once the faults transmissibility of the base model are updated, the next step is to repeat the same procedure for relative permeability. In this case five levels for the Corey exponent was considered, the values are: level 0= 1, level 1= 2, level 2= 3, level 3= 4 and level 4= 5. As there are three facies, after combining all the uncertainties levels through the derivative tree technique, 125 models are created. In this case the quadratic error is computed using the water rate curves (Q_w). After that, it is calculated an average of the quadratic error of all the 8 producer wells for each of the 125 models. And, again the 20 models that gave the smallest quadratic error are selected to do the histogram analysis. Note that, although some trend can be observed for the facies logs at the well location, it is not coherent to select the wells according to that for each facies (as it was done with the faults), because the flow depends on the facies in a neighborhood of the well not only at its position (the flow in a given facies influences wells located in other facies). This explains why all the 8 wells are considered simultaneously in this analysis.

Results

Global matching

The histograms shown in figure 4 were built using the 20 models selected by the average of the quadratic error of the BHP curves of the corresponding selection for each fault. Analyzing the results it can be said that for the faults 1, 3 and 4 the level 3 should be used, which correspond to a transmissibility multiplier value of 1 and that for fault 2 the most frequent level is 1, denoting that the transmissibility multiplier value for this fault should be 0.001.

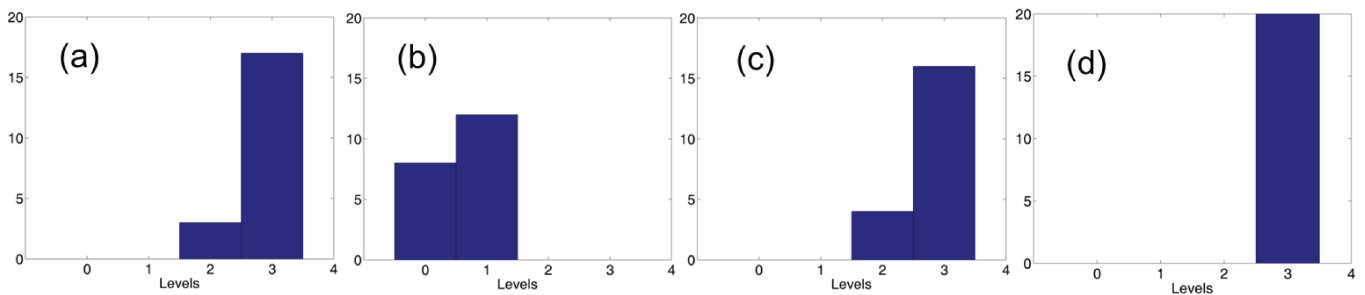


Figure 4: Frequency of occurrence of each level of transmissibility for the four faults: (a) fault 1, (b) fault 2, (c) fault 3 and (d) fault 4.

Following the analysis of the best 20 models, but in this case for Q_w curves, the second global match (for Kr) done produces the histogram displayed in figure 5. From the histograms it can be said that for facie 1 there is nothing to conclude since the frequency of occurrence of the 5 levels of the Corey exponent are similar, so the value of the base model is kept. For facies 2, the results indicate level 2, so the Corey exponent is set as 3. For facies 3 the Corey exponent is 1, corresponding to level 0.

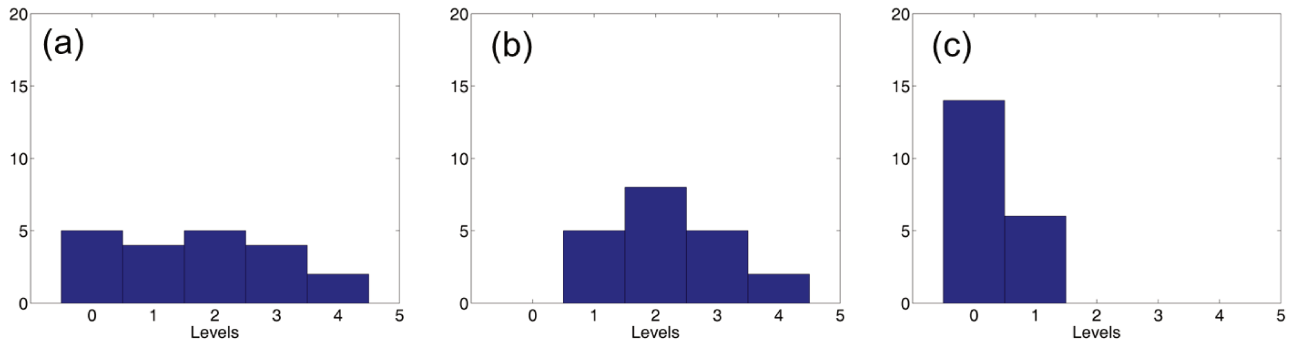


Figure 5: Frequency of occurrence of each level of the Corey exponent for the three facies: (a) facie 1, (b) facie 2 and (c) facie 3.

Table 2 summarizes the results of the global matching applied that updated the faults transmissibility and relative permeability curves.

Table 2: Base model after global matching properties

	Fault 1	Fault 2	Fault 3	Fault 4	Corey exp.		
					Facies		
Updated base model	1	0.001	1	1	4.4	3	1

Local matching

Now that the global properties are updated the proposed methodology for the local matching can be applied. One of the input data for the local matching is the set of model realizations that come from the uncertainty analysis. Let's consider that the global matching done previously reduced the uncertainties, so the faults transmissibility and the relative permeability curves are fixed now and. Since the ratio kz/kx is not such an important parameter for this model, the remaining uncertainties are porosity and absolute permeability. Thus, the number of model realizations is 200, being that the only difference between them are the correlated porosity and permeability fields. To start the local matching the first procedure is to analyze the error map of the time lapse difference of the water saturation provided by 4D seismic and the one computed from the base model (with the global properties updated).

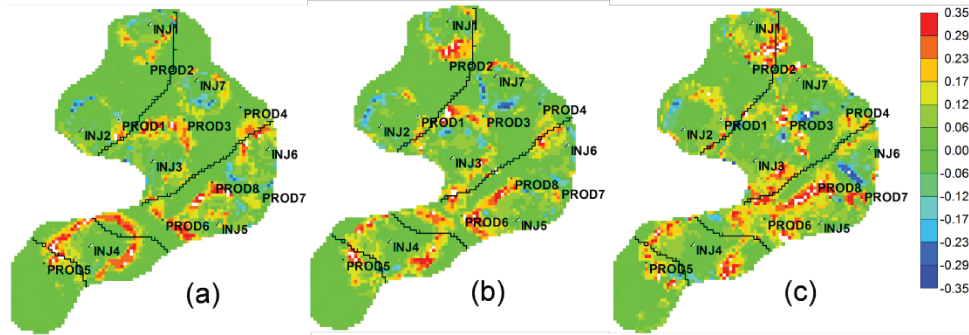


Figure 6: Error map between the data provided by 4D seismic and the base model after the global matching: $\Delta_{4D}Sw_{seis} - \Delta_{4D}Sw_{base_global}$. (a) Layer 3. (b) Layer 4. (c) Layer 5.

In the dataset used in this work seismic data is at the simulation scale, so this information is available at all the five layers of the model. Figure 6 shows the error map for the last three layers, which are the ones containing more water. From figure 6 it can be verified that the main water saturation error observed are related to the injectors: INJ3, INJ4, INJ5 and INJ1. Thus, these wells were selected to perform the local matching in order to update the porosity and permeability fields of the base model. Since the well INJ3 has a central location, its water front could reach several wells, so this injector was the first one used to define the regions where the properties should be modified. Four regions were defined around it, see in figure 7 regions R1a, R1b, R1c and R1d; being that each of them includes one producer: PROD1, PROD3, PROD6 and PROD8, respectively. Then, the other 3 regions seen in figure 7 (R2, R3 and R4) were also defined by including the corresponding producer of each injector as well as analyzing the error observed in the maps. Note that the regions should not overlap. The next step of the methodology is to compute the quadratic error (equation 2) within each region for the 200 models and then to update porosity and permeability inside each region by replacing these properties of the base model by the ones presented in the models that yielded the smallest quadratic error. Before computing the quadratic error of the time lapse difference of water saturation maps, the data provided by 4D seismic should be calibrated with the volume of injected water. Although this is an important step of the methodology the tests for this case did not present good results and some improvements need to be done to better evaluate volume differences.

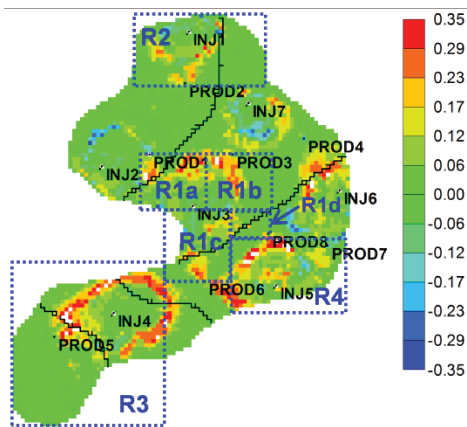


Figure 7: Regions where the local matching is performed.

The definition of the regions depends on the error map observed which depends on the resolution of the 4D seismic data. In this work the 4D data has the same vertical scale of the simulation model, so the regions can also be defined vertically. After some

tests it was verified that for some of the regions a much better matching was reached when each of these regions was split into five, *i.e.*, each layer is considered as another region. This kind of sub-division was made in the regions R3 and R4. Thus, for these two regions the quadratic error was computed for each layer separately which means that the properties (porosity and permeability) update for different layers can come from different models. For the regions around INJ3 (R1a, R1b, R1c, R1d) and around INJ1 (R2) the quadratic error was computed considering all the five layers together, so if, for instance, the model 37 was the one which presented the smallest error for the region R2 then the porosity and permeability values of the base model was replaced (just inside the region) by the ones from model 37 in all layers.

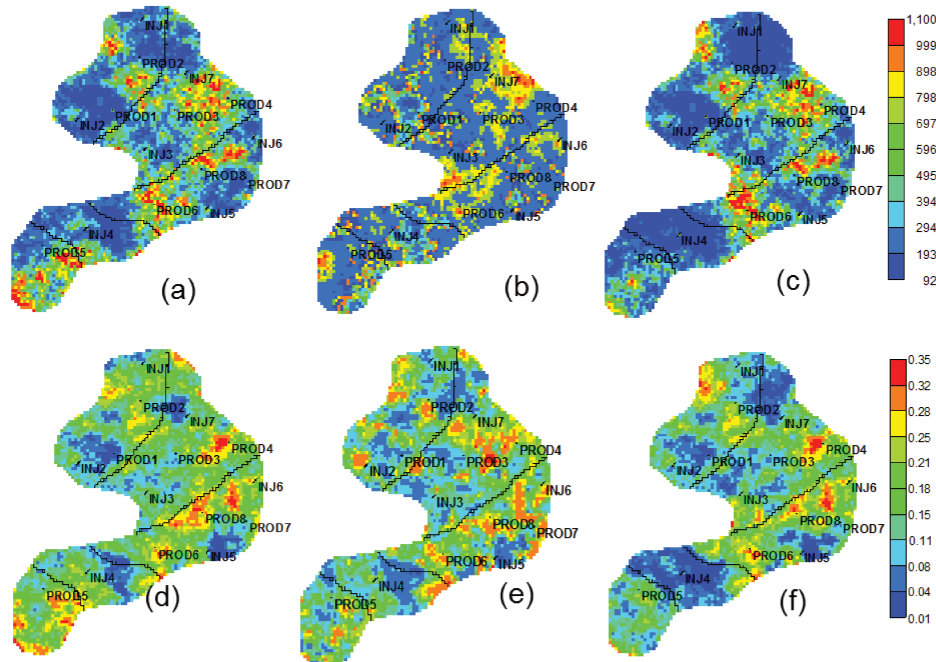


Figure 8: Permeability of the base model (a), the reference model (b) and the base model after the local matching (c). Porosity of the base model (d), the reference model (e) and the base model after the local matching (f). All the images correspond to the fourth model layer.

Figures 8c and 8f show the results of the local matching for permeability and porosity, respectively. In the same figure it is possible to check how the properties were modified by comparing with the base model images (figures 8a and 8d) and also to check if the results are closer to the reference model (figures 8b and 8e). It is important to note that the reference model properties were not generated through the same geostatistics procedure, more than that, all the 200 realizations of porosity and permeability are not very close to the reference model ones, especially for permeability, this explain the big difference between these properties and the ones of the base model. Another point to highlight is that the procedure tries to match the water saturation information that comes from 4D seismic which has some noise included, so the match cannot be perfect. Apart from these issues it is still possible to identify some similarities between the reference model properties and the ones updated after the local matching. An example is the zone of high permeability observed in the region R1c (figure 8c) that is better defined than the one of the base model. Another example is the low porosity zone between INJ1 and PROD2 that is also improved after the local matching.

Even not having a perfect agreement between the properties of the reference model and the model after the history matching, a substantial improvement can be verified in the error maps of water saturation. The images of figure 9 show the initial error maps, *i.e.*, the error between the data provided by 4D seismic and the initial base model. Note that the white areas observed inside the reservoir correspond to points where the error is outside the range of the color scale $[-0.35, 0.35]$, so these areas present the biggest errors. Following the same layout of figure 9, figures 10 and 11 display the results of the global matching and the final history matching performed (global+local), respectively. After the global matching (figure 10) some improvement can be observed in the error maps, but the error decrease of water saturation is actually relevant after the application of the local matching (figure 11). Although some errors can still be observed in the maps of figure 11, the local matching performed presented satisfactory results correcting the water front movement of the injectors selected. Note that the level of error reduction was similar for all the regions defined, this shows that the regions delimitation can be coarser like region R2 (defined as a regular region), or it can be more refined as it was done for regions R3 and R4 where the vertical subdivision was applied turning them into 5 sub-regions each. The choice of how to define the regions is then made according to the error observed and the resolution of the data available.

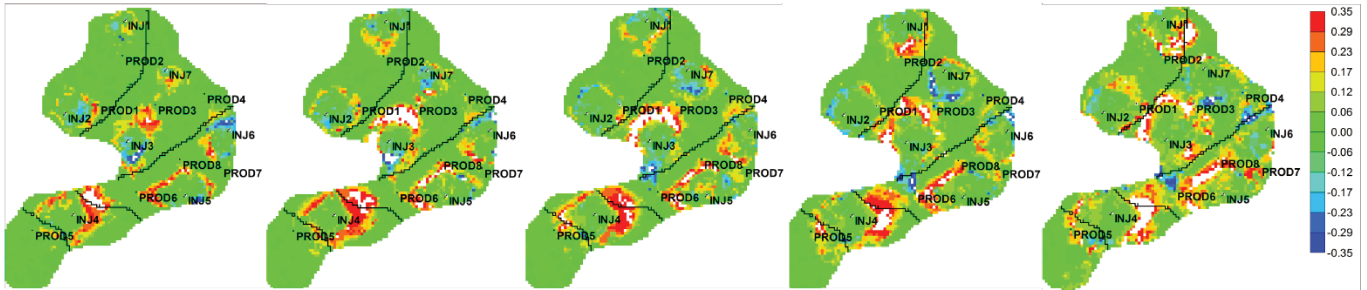


Figure 9: Error map between the data provided by 4D seismic and the base model: $\Delta_{4D}SW_{seis} - \Delta_{4D}SW_{base}$. From left to right are the maps of layers 1 to 5.

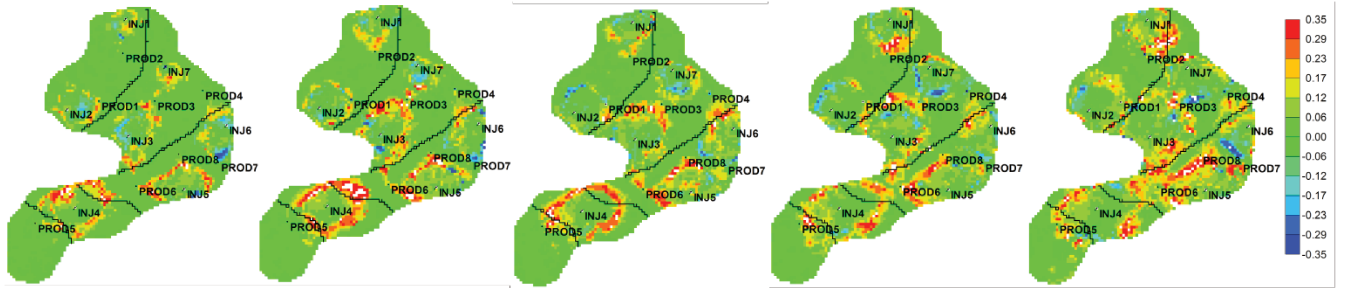


Figure 10: Error map between the data provided by 4D seismic and the base model after the global match: $\Delta_{4D}SW_{seis} - \Delta_{4D}SW_{global}$. From left to right are the maps of layers 1 to 5.

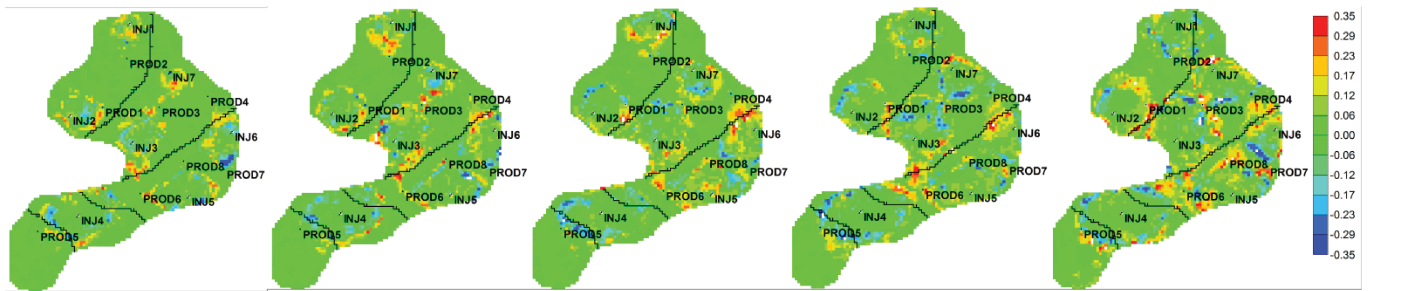


Figure 11: Error map between the data provided by 4D seismic and the base model after global and local matching: $\Delta_{4D}SW_{seis} - \Delta_{4D}SW_{final_base}$. From left to right are the maps of layers 1 to 5.

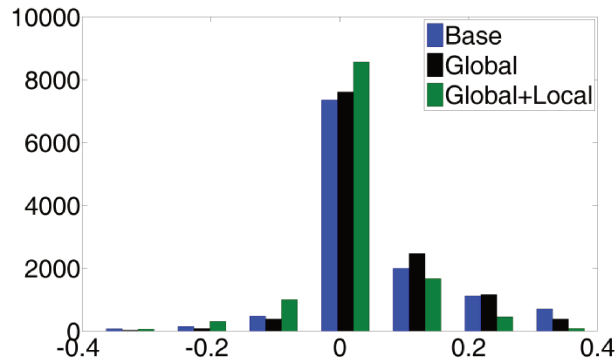


Figure 12: Histogram of the Sw errors map observed in figure 9 (blue), figure 10 (black) and figure 11 (green) that correspond to the Sw error of the initial base model, the model after the global matching and the model after global-local matching.

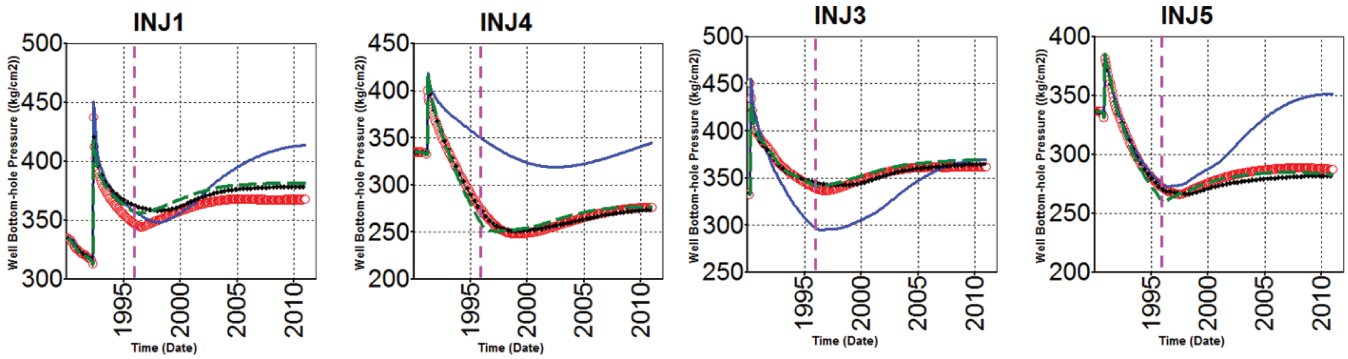


Figure 13: Bottom hole pressure curves [kgf/cm²] of four injectors. History data is in red circle, base model in solid blue, the model after global match in black diamond and the model after the global+local matching is in dashed green. The vertical magenta line divides the period in history and forecast.

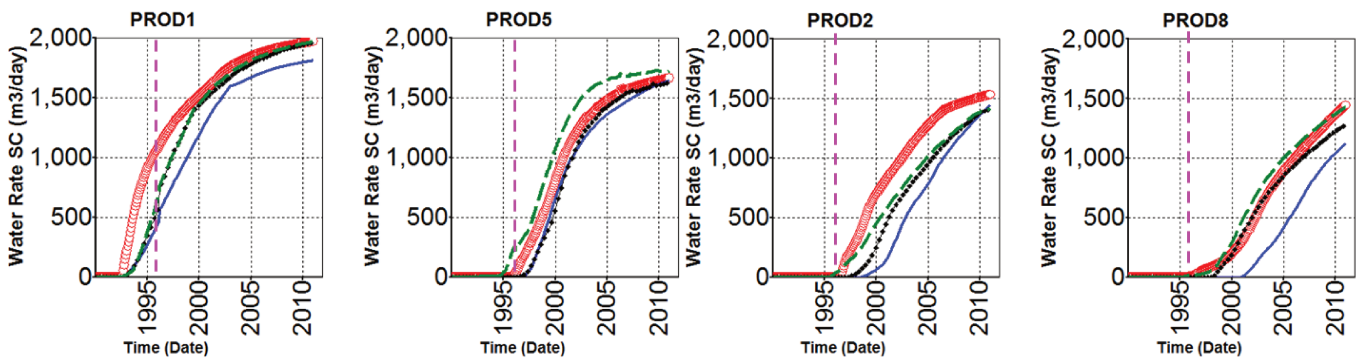


Figure 14: Water rate curves [m³/day] of four producers. History data is in red circle, base model in solid blue, the model after global match in black diamond and the model after the global+local matching is in dashed green. The vertical magenta line divides the period in history and forecast.

Figure 12 shows the histogram of the water saturation errors presented in figures 9, 10 and 11. This is just another way (a quantitative measure) to verify the improvement already observed in the error maps. The bigger concentration of values around zero together with the smaller concentration of higher errors, are confirming the improvement obtained after applying the local history matching.

Figures 13 and 14 show the pressure and production curves for some wells, including the forecast period (marked by the magenta line), remembering that the history matching was performed in 1996. In both figures it is possible to verify that the global matching presented better curves than the initial model. As the global match did a good job, few improvements were obtained in the curves after the application of the local matching. In this sense, the BHP curves presented in figures 13 show a pretty similar behavior between the global and global+local matching. For the water rate curves (figure 14) there are slight differences between the two adjusted models like, for instance, well PROD2 had its breakthrough corrected and PROD8 presented a better forecast behavior after the local matching.

The improvement in the water rate curves is mainly in the forecast period since the water had not reached the majority of the wells during the history (1990-1996); this behavior is also observed for the producers not shown here due to the limited space. It is important to highlight that even if a not so relevant improvement is observed in the production curves during the history period, the local matching, that diminish the errors observed in the maps, is still very important especially when new wells need to be planned since the necessity of reliable map information becomes more latent.

Final comments

The methodology proposed is a simple way to perform a history matching using quantitatively the information provided by 4D seismic. A good feature to highlight is that the procedure aims to harness the results of an uncertainty analysis run previously by a simple procedure of comparing water saturation errors of the several model realizations available, followed by a “cut and paste” property update. As a result, geological inconsistencies can be avoided. Thus, it is a simple way to incorporate geological uncertainties without running sophisticated algorithms like the ones proposed by Caers (2003), Caers and Hoffman (2005) and Stephen et al (2005). A pitfall of the methodology is that it does not ensure continuity in the boundaries of the regions and in some cases the geostatistic properties can be missed. One way to minimize this issue would be to delineate the regions according to

geological structures, instead of doing it based only on well location and error map. But, even though, the method will not guarantee total geostatistic coherence as the one proposed by Caers and Hoffman (2005), for instance, so it can be improved in future work.

Another feature of the methodology is that although this work considers 4D seismic data in the form of water saturation maps the methodology could be applied with another seismic attribute like acoustic impedance, for instance. Clearly, it would require an extra work which includes the conversion of simulation data to impedance and a previous study to match time lapse differences of impedance with water movement. In a way, the second issue is already addressed here when water saturation information is extracted from 4D seismic through an inversion process. So, the main point to add is the creation of impedances for all the simulation models used.

The synthetic dataset used in this work does not presented too much challenges with respect to the uncertainties of the model, in a sense that they were all known uncertainties (even porosity and permeability had their geostatic parameters not very far from the true) and just their values needed to be calibrated. However in more complex cases the uncertainties can be more difficult to define. Thus, 4D seismic could be first used in a qualitative way to better map these unknowns, after that a more consistent uncertainty analysis can be run yielding in better defined model realizations to be used in the local matching proposed in this work, when 4D seismic is quantitatively used. Another drawback of the lack of challenges regarding the uncertainties is that no much improvement could be seen in the production curves between the global and local matching applied. Again, in more realistic cases a good well history matching (and forecast) can be not so easy to reach and the local matching can be as important as it is for the error map reduction.

In general, the application of the methodology produced promising results, having as a main point the reduction of the water saturation errors by a simple procedure that yields model properties with some geological consistence.

Conclusion

A methodology that uses 4D seismic information to perform a local history matching was proposed. The main point to highlight is the simple way to incorporate uncertainties without running sophisticated algorithms. Moreover, after the match, geological features of the updated reservoir properties can be kept. In the application shown the history matching was done in two steps, firstly a calibration of the global properties of initial model was made by using well production curves. After that the local matching was performed incorporating 4D seismic information quantitatively. The results obtained with a synthetic dataset showed promising results with a significant improvement of the map information. There are two improvements that can be done in future works, one concerns the water volume calibration between seismic and simulation data and the other would be to investigate possible ways of guarantee geostatistic consistence in the borders of the regions.

Nomenclature

BHP	= Bottom-hole pressure
QE	= quadratic error computed for grid properties (equation 2)
QE _{well}	= quadratic error computed for well production curves (equation 3)
Q _w	= Water rate
Δ_{4D}	= Time lapse difference operator: property at time 1 minus property at time 0
SW _{seis}	= Water saturation estimated from 4D seismic
SW _{sim}	= Water saturation generated through the simulation of a reservoir model
SW _{base}	= Water saturation generated through the simulation of the base model
SW _{global}	= Water saturation generated through the simulation of the model after the global matching
SW _{base_final}	= Water saturation generated through the simulation of the model after the global+local matching

Acknowledgments

The authors would like to thank UNISIM, PETROBRAS, CEPETRO and Department of Petroleum Engineering for supporting this work.

References

- Caers, J., 2003. History matching under training-image based geological model constraints. SPE J. 7, 218-226.
- Castro, S. A., Caers, J., Otterlei, C. M., Meisingset, H., Høy, T., Gomel, P., and Zachariassen, E., 2009. Incorporating 4D seismic data into reservoir models while honoring production and geologic data: A case study. The Leading Edge. 28 (12), 1498-1506.
- Davolio, A., Maschio, C. and Schiozer, D., 2012a. Pressure and saturation estimation from P and S impedance: a theoretical study. J. Geophys. Eng. 9, 447-460.

Davolio, A., Maschio, C. and Schiozer, D., 2012b. Pressure and saturation estimation from 4D seismic constrained by reservoir flow simulation. Joint SEG/SPE/AAPG summer research workshop: new advances in integrated reservoir surveillance. La Jolla, CA, 24-29 June.

Hoffman, B. T., and Caers, J. 2005. Regional probability perturbations for history matching. *J. Petrol. Sci. Eng.* 46, 53-71.

Landa, J., L. and Kumar, D. 2011. Joint inversion of 4D seismic and production data. SPE146771. SPE Tech. Conf. Exhibition, Denver, CO, 30 October – 2 November.

Schiozer, D.J., Ligerio, E.L., Suslick, S.B., Costa, A.P.A., Santos, J.A.M., 2004. Use of representative models in the integration of risk analysis and production strategy definition. *J. Petrol. Sci. Eng.* vol. 44 (1–2), 131–141

Stephen, K., D., Soldo, J., MacBeth, C. and Christie, M. 2005. Multiple model seismic and production history matching: a case study. SPE 94173. SPE EUROPEC/EAGE. Ann. Conf. Exhibition, Madrid, Spain, 13-16 June.

Tolstukhin, E., Lyngnes, B. and Sudan H., H. 2012. Ekofisk 4D seismic – seismic history matching workflow. SPE 154347. SPE EUROPEC/EAGE. Ann. Conf. Exhibition, Copenhagen, Denmark, 4-7 June.

5. PAPER 4: *A methodology to calibrate water saturation estimated from 4D seismic*

Alessandra Davolio, Celio Maschio, Denis José Schiozer
To be submitted to a journal.

A methodology to calibrate water saturation estimated from 4D seismic

Alessandra Davolio, Célio Maschio and Denis José Schiozer

Department of Petroleum Engineering, FEM, UNICAMP/CEPETRO, São Paulo, Brazil

E-mail: davolio@dep.fem.unicamp.br, celio@dep.fem.unicamp.br and denis@dep.fem.unicamp.br

Abstract

Time-lapse seismic data can be used to estimate saturation changes within a reservoir. This is valuable information for reservoir management, as it can play an important role in reservoir simulation models updating. The process of updating reservoir properties, so-called history matching, can incorporate estimated saturation changes qualitatively or quantitatively. Especially for quantitative approaches, it is important to have reliable information from 4D seismic. Thus, in this work, a methodology to calibrate the volume of water present in the estimated saturation maps is proposed, as saturation maps can be wrongly estimated due to problems related to seismic signals (such as noise, errors associated to data processing and resolution issues). The idea is to condition the 4D seismic data to known information provided by engineering, in this case the known amount of injected water in the field. The application of the proposed methodology in an inversion process (previously published) that estimates saturation from 4D is presented, followed by a discussion concerning the use of such data in a history matching process. To validate the results, the methodology is applied to a synthetic dataset. The main results are: (1) a better estimation of saturation, namely reduction of noise and errors effects, yielding more reliable data to be used quantitatively or qualitatively and (2) an improvement in the properties update after using this data in a history matching procedure.

Keywords: time-lapse seismic, saturation estimation, volume calibration, history matching

Nomenclature

IP	P-impedance
IS	S-impedance
Sw	water saturation
Sw _c	connate water saturation
So _r	residual oil saturation
Pre	pore pressure
Pre _{ProdMin}	minimum pressure (producer wells)
Pre _{InjMax}	maximum pressure (injector wells)
Δ_{4D}	time-lapse difference operator
V _{inj}	volume of injected water (standard conditions)
V _{prod}	volume of produced water (standard conditions)
V _{current}	current volume of water present in the reservoir (standard conditions)

ϕ	porosity
Vb	volume of a grid block
nb	number of grid blocks
CF	volume correction factor
Bw	water formation volume factor

Subscript

<i>seis</i>	parameter derived from 4D seismic
<i>sim</i>	parameter computed from reservoir simulation results
<i>base</i>	parameter computed from the simulation results of the base model
<i>seis_cali</i>	parameter derived from 4D seismic with the volume calibrated
<i>t0</i>	parameter corresponding to the base survey

1. Introduction

Time-lapse seismic is becoming an important tool for reservoir monitoring as it provides a better understanding of the dynamic properties variations due to production within the reservoir. This is valuable information because it can be used to update reservoir models, which are an important tool for reservoir management (optimization strategy, planning infill drillings among others). There are several works in the literature showing successful use of 4D seismic (Johann et al, 2009, Tolstukhin et al, 2012, Castro et al, 2009).

The integration between 4D seismic and reservoir simulation is still a topic of intense research. There are several approaches that can be used, from qualitative interpretation of 4D seismic anomalies (Johann et al, 2009) that are further incorporated into reservoir simulation models, to quantitative use of 4D seismic data in an objective function of a history matching procedure (Brito et al, 2010, Landa and Kumar, 2011). Another branch of possibilities is the domain of integration of the two data, which can be generalized into three options: amplitude, impedance, saturation and pressure domains.

To perform the integration in the saturation and pressure domain, which is the focus of this work, it is necessary to estimate these properties from seismic amplitudes or impedances. Different methodologies can be applied to estimate saturation and pressure from 4D seismic attributes (Landro 2001, Lumley et al 2003, MacBeth et al 2006, Davolio et al 2012). Their differences concern the type of seismic attribute used to estimate the dynamic changes and how the data is manipulated to obtain these estimations.

Although these methodologies could be applied to any field that holds enough seismic data (usually pre-stack data is needed for base and monitor surveys), there are still some challenges to overcome concerning seismic signal related problems (such as noise, tuning and uncertainties in rock properties).

Thus, in order to be able to extract more reliable information from time-lapse seismic signals, another source of information can be used, for instance, engineering data (well production profiles, reservoir simulation data). Engineering data, such as reservoir simulation results, are normally used in forward modeling for feasibility studies, or to help in the understanding of observed 4D seismic anomalies. However, there are few works that effectively use this type of

information to constrain the estimation of dynamic properties from 4D seismic. The work of Huang et al (2011) is an example of such application; in this work the authors demonstrated that well production data (predominantly used for history matching) can be used to constrain the observed 4D seismic data and as a result, more robust information is extracted from seismic signals. Toinet et al (2011) can be cited as another example; in this case, the authors presented a workflow to perform a 4D pre-stack inversion that is constrained by a range of elastic properties variations computed from reservoir simulation results. In addition, reservoir model information was also included as a constraint to better locate water-bearing sands. Davolio et al (2013a) also presented a methodology that uses reservoir simulation results to constrain dynamic estimation from 4D seismic. But, different from Toinet et al (2011), in the work of Davolio et al (2013a), the constraints are used in a petro-elastic inversion that estimates saturation and pressure from seismic impedances.

The current work inclines toward the idea of using engineering information to constrain the estimation of dynamic properties from 4D seismic. More specifically, this work proposes a methodology to correct the volume of water present in estimated saturation maps from 4D seismic, based on the known volume of injected water in the field. This type of calibration is important, especially when employing a quantitative use of the estimated properties in a history matching procedure, since poor estimates used as input can lead to incorrect model updating. The volume calibration proposed here can be applied to saturation maps estimated from 4D seismic through one of the techniques mentioned previously. In this work, the saturation maps are estimated by the 4D petro-elastic inversion constrained to flow conditions proposed by Davolio et al (2013a). After analyzing the results of the calibration, a discussion about the importance of this type of information as input to a history matching procedure is also presented. To validate and demonstrate the benefits of the proposed methodology, the results are shown with synthetic data.

2. Methodology

The methodology presented here aims to calibrate the volume of injected water present in the water saturation (S_w) maps provided by 4D seismic with the known volume of injected water. The calibration is performed by applying a multiplicative correction factor in the S_w map provided by 4D seismic. The calibrated S_w values should belong to a feasible range, which is defined by the methodology proposed by Davolio et al (2013a). So, prior to running the volume calibration, it is necessary to estimate this range.

As displayed in figure 1, the methodology used to compute the feasible range starts by combining all the “ n ” uncertainties, or the most important “ n ” uncertainties of the reservoir model. Thus, “ m ” model realizations are created and simulated. Then, for each reservoir block, the range of possible values is defined by extracting the minimum and maximum S_w value along all the “ m ” possibilities. Therefore, the range [$S_{w_{min}}$ $S_{w_{max}}$] is defined according to the flow conditions and is consistent with the current characterization stage. This range is defined to the production time corresponding to the monitor seismic survey. Note that, according to figure 1, the same procedure was applied for pressure. However, the current work only uses the limits for S_w .

After estimating the range [$S_{w_{min}}$ $S_{w_{max}}$] for every grid block of the model, the volume calibration can be performed. Bellow, a detailed workflow of the volume calibration procedure is proposed:

1. Compute the amount of injected water (in reservoir conditions) present in 4D seismic data according to equation 1:

$$V_{inj_seis} = \sum_{i=1}^{nb} \phi_i V b_i (\Delta_{4D} S w_{seis})_i, \quad (1)$$

where nb is the number of blocks of the model, ϕ is the porosity, Vb is the block volume, $\Delta_{4D} S w_{seis}$ is the time-lapse difference of water saturation estimated from 4D seismic.

2. Compute the correction factor (CF) according to equation 2:

$$CF = V_{inj_seis} / V_{current}, \quad (2)$$

being that $V_{current}$ is the current volume of water:

$$V_{current} = (V_{inj} - V_{prod}) B_w, \quad (3)$$

where V_{inj} is the known volume of injected water, V_{prod} is the known volume of produced water and B_w is the water formation volume factor.

3. Set $i=1$;
4. While $i \leq nb$ calculates the calibrated water saturation value for the i^{th} block by applying the correction factor:

$$(\Delta_{4D} S w_{seis_cali})_i = (\Delta_{4D} S w_{seis})_i / CF. \quad (4)$$

5. Compute the calibrated Sw for the monitor survey:

$$(S w_{seis_cali})_i = (\Delta_{4D} S w_{seis_cali})_i + (S w_{t0})_i; \quad (5)$$

where $S w_{t0}$ is the water saturation value at the initial time (base survey).

6. Verify if the calibrated Sw belongs to the feasible range:

$$(S w_{min})_i \leq (S w_{seis_cali})_i \leq (S w_{max})_i. \quad (6)$$

7. If inequality 6 holds, then the value of the current reservoir block (i^{th} block) is set by equation 5, set $i=i+1$ and return to step 4; else go to step 8.
8. If $(S w_{min})_i > (S w_{seis_cali})_i$ then $(S w_{seis_cali})_i = (S w_{min})_i$, set $i=i+1$ and return to step 4, else go to step 9.
9. If $(S w_{max})_i < (S w_{seis_cali})_i$ then $(S w_{seis_cali})_i = (S w_{max})_i$, set $i=i+1$ and return to step 4.

The steps 2 to 9 can be repeated until a satisfactory volume calibration is reached, namely until $CF-1 < \text{tolerance}$. Another point to highlight is that the steps 1 to 9 can be applied to the whole reservoir or to different reservoir zones, independently.

There are some assumptions to be considered when applying the methodology proposed above:

- 4D seismic data are at the same scale of the reservoir simulation model. Therefore, for real data, an upscaling/downscaling procedure is required to convert data from seismic scale to flow simulation scale.
- 4D base survey was acquired in the pre-production period, so that the time-lapse difference of saturation provides information about the volume of injected water.
- No presence of an aquifer.

3. Application

To evaluate the results of the proposed methodology, all data used in this work are synthetic, as described in the following sections.

The application of the proposed volume calibration procedure is divided into two parts. The first part presents a discussion of the volume calibration on the estimated Sw map from 4D seismic.

Then, the second part shows the importance of using a calibrated Sw map in a history matching procedure.

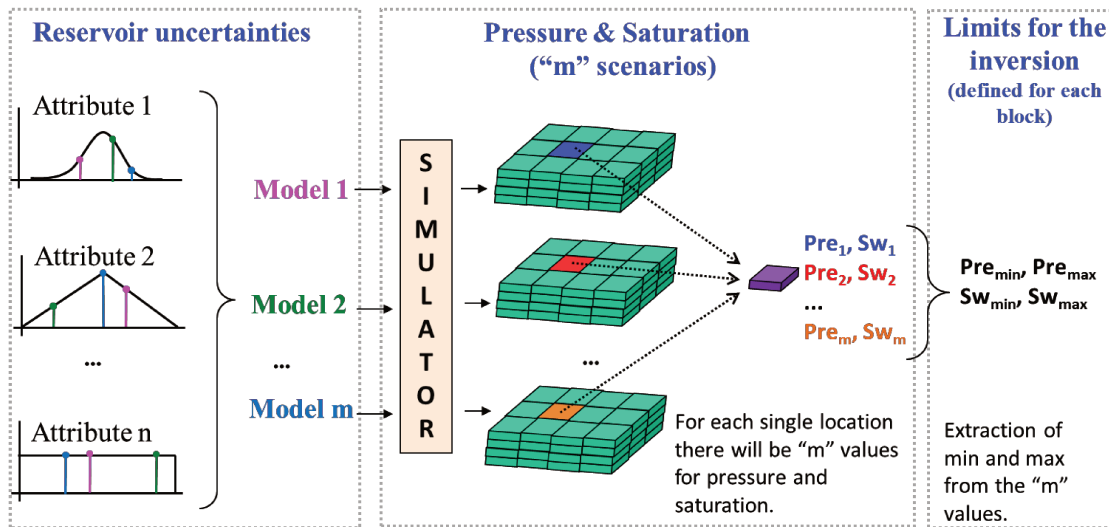


Figure 1: General procedure used to define limits (minimum and maximum) of pressure and saturation for each reservoir block. ‘Attribute 1’, ‘Attribute 2’ and ‘Attribute n’ are generic representations of the reservoir uncertainty and ‘Model 1’, ‘Model 2’ and ‘Model m’ are generic reservoir models, generated from the combination of the reservoir uncertainties (extracted from Davolio et al, 2013a).

3.1. Synthetic dataset construction

This section presents a brief description of the synthetic dataset used in this work, which is the same as that used in Davolio et al (2013a, b); see these references for more details. Some simplifications of these dataset are:

- All data (seismic and reservoir simulation) are at the same scale, which corresponds to a grid with 90x110x5 blocks. Thus, all simulation models used in this work have this grid.
- Initial Sw is considered known (with good estimation of water-oil contact and capillary pressure).
- The seismic data considered here are composed of P and S impedances for two surveys (base and monitor). These impedances were generated by a forward modeling through a petro-elastic model that uses reservoir simulation results and static properties, such as porosity, from the reference simulation model (described below).

3.1.1. Reference simulation model and seismic data

This model represents the true earth model. The static and dynamic model properties represent the answer that the methodologies should reach. Thus, for instance, the closer the estimated Sw map (from 4D seismic) is to the simulation results of the reference model, the better it is. In the same way, when history matching is applied, it is desired that the updated static properties get closer to those of the reference model. Besides validating the results, the reference model is also used to generate the seismic. The seismic dataset is composed of four volumes of impedances, P

and S impedances for two production times (pre-production and 6 years of production). A random noise was added to the impedances, which can be observed in figure 4. The impedances were generated through a petro-elastic model considering the unconsolidated sand model (Mavko et al, 2003) that is described in Davolio et al (2013a). Note that the seismic data considered here are not originated from a pre-stack inversion, as no amplitudes were generated.

3.1.2. Reservoir uncertainties

Reservoir static properties can be divided into two categories: global and local. The former have a global influence on the reservoir, meaning that changes in these properties affect the flow behavior of the whole reservoir (or of a large area of it). The latter have a local effect, i.e., regional changes affect regional flow (around a well, for instance).

The global uncertainties of the dataset used here are fault transmissibility, relative permeability (represented by the Corey exponent) and permeability ratio (vertical/horizontal). The local uncertainties are porosity and horizontal permeability.

The focus of this work is the use of a Sw map to update the reservoir model's properties. Here we propose to use this type of information to update static properties locally, following the history matching methodology presented by Davolio et al (2013b). Before running a local matching, the global uncertainties need to be calibrated. Thus, this work assumes that this calibration has already been performed, as described by Davolio et al (2013b); table 1 shows the true values and the results obtained. Therefore, only local properties (porosity and horizontal permeability) are being assumed as uncertainties in this work. Using the Sequential Gaussian Simulation technique (SGS), 200 realizations of porosity were generated, having the seismic P-impedance volume (base survey) as a secondary variable. Each of these porosity fields was later used as a second variable for the SGS to generate 200 realizations of permeability (figure 2). Each pair of porosity and permeability images was used to generate 200 simulation models. Although the characterization process was not perfect, as it can be seen in table 1 and by comparing figure 2 with figure 5c, the mapping of the uncertainties yielded a satisfactory dispersion in the well production curves. On the top of figure 3, the field average pressure and water rate are displayed for all the 200 models and the history; on the bottom of the same figure the bottom hole pressure (BHP) curves are displayed for two wells.

One important aspect to consider when using several simulation models to constrain 4D seismic information is to ensure that production curves dispersion comprise the history data like the ones shown in figure 3. If a poor uncertainty characterization is performed, generating models that do not comprise the history data (e.g. all models bellow the history curve), the constraints applied to the 4D seismic lead to biased estimations. In the case studied, the proper uncertainties mapping performed was important to improve the estimation of saturation and pressure, as discussed in the following sections.

Table 1: Global parameters before and after the matching applied.

	Fault 1	Fault 2	Fault 3	Fault 4	Kz/Kx	Corey exp.		
						Facies		
Reference	0.4	0.001	0.03	0.8	0.100	4.6	3.1	1.3
After updating	1	0.001	1	1	0.096	4.4	3	1.0

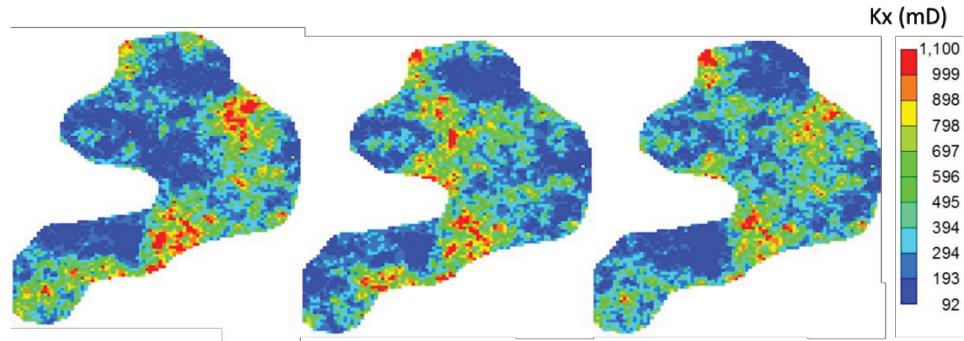


Figure 2: Examples of three realizations of permeability.

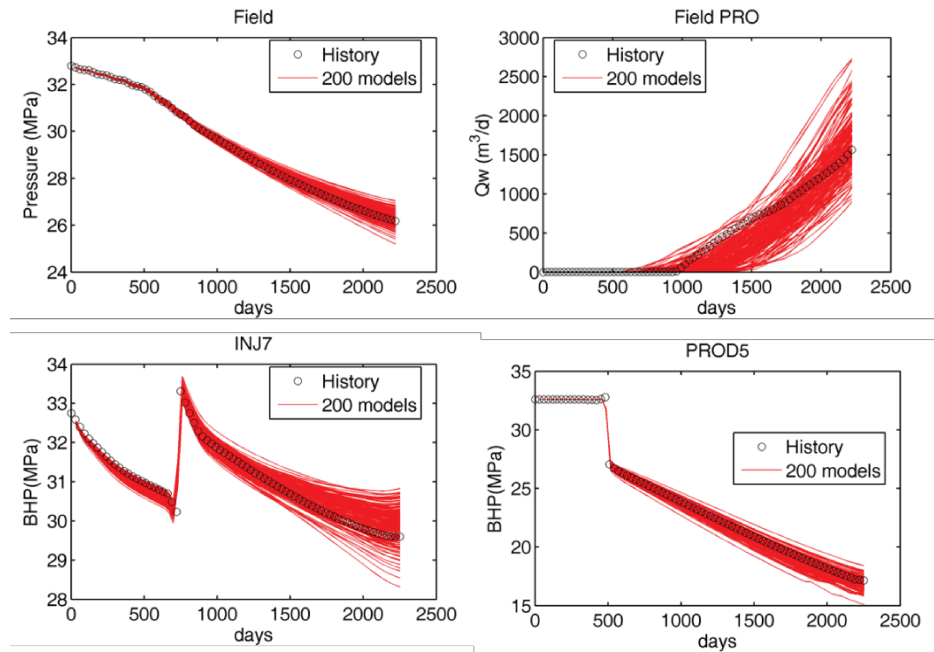


Figure 3: Top: field average pressure and field water rate. Bottom: examples of bottom hole pressure curves for two wells INJ7 (left) and PROD5 (right).

3.1.3. Base simulation model

This model represents the knowledge available regarding the reservoir and needs to be history-matched. The base model was built by a random combination of the uncertainties described above, differentiating it from the reference model. The global uncertainties of these models are already calibrated with well production data (Davolio et al, 2013b) as displayed in table 1. Figure 5 shows the porosity and permeability images for the reference and base model; these properties are calibrated with 4D seismic data, as described in the results.

3.2. Estimating S_w from 4D seismic

The water saturation map used in this work was estimated by a 4D petro-elastic inversion procedure described in Davolio et al (2013a). The inversion is carried out by an optimization process and is performed for each simulation block, independently. As discussed in Davolio et al (2012), this is an optimization problem with only two unknowns (pressure and saturation for each

block) with a well-behaved objective function. So, a gradient-type algorithm is used to search for the solution within the defined solution space.

The input data for the inversion are the time-lapse differences of the noisy synthetic P and S impedances (figures 4c, d). Another important input of the petro-elastic inversion is the porosity field which, in this work, was extracted from the base model (figure 5b). Thus, there are three important sources of errors in the estimation of S_w : the wrong estimative of porosity and overburden pressure and the presence of noise in seismic impedances. The same petro-elastic modeling used to generate the synthetic impedances was used in the inversion process, so no errors are being assumed in this modeling.

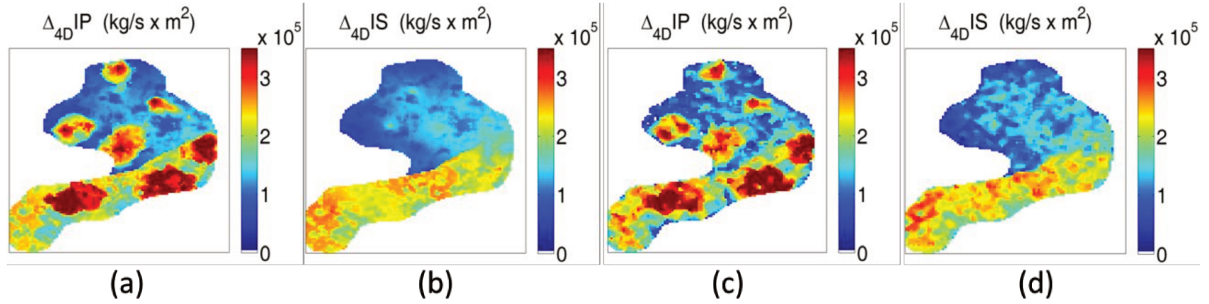


Figure 4: Time-lapse difference of the synthetic seismic attributes without adding noise: (a) P-impedance. (b) S-impedance. Time-lapse difference of the synthetic seismic attributes after noise addition: (c) P-impedance. (d) S-impedance. Layer 3.

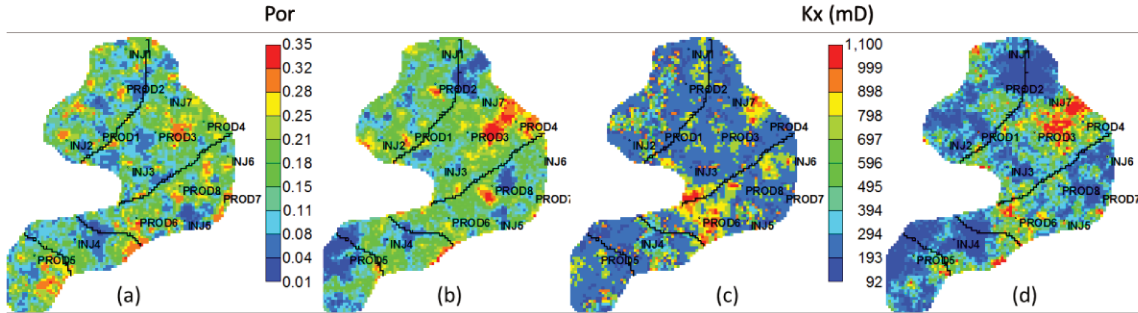


Figure 5: Porosity: reference model (a) and base model (b). Horizontal permeability (mD): reference model (c) and base model (d). Layer 3.

Three inversions were performed (case 1, 2 and 3) in order to highlight different steps of the calibration of 4D seismic information with reservoir simulation results. The calibrations performed are related to the delimitation of the solution space of the petro-elastic inversion process. Thus, the differences among the three cases are:

Case 1: the inversion procedure is performed with “general constraints”, meaning that the solution space is defined by the limits: $S_{w_c} < S_w < 1 - S_{o_r}$ and $Pre_{ProdMin} < Pre < Pre_{InjMax}$.

Case 2: the solution space is defined by the minimum and maximum values $[S_{w_{min}} S_{w_{max}}]$ and $[Pre_{min} Pre_{max}]$ estimated by the methodology proposed in Davolio et al (2013a) that is schematically presented in figure 1. By applying this methodology, the estimated dynamic properties are conditioned to the flow conditions according to the reservoir uncertainties characterization stage.

Case 3: in this case, the calibration of the volume of water proposed in this work is applied. Note that the methodology proposed in this work is using the constraints applied in case 2 ($[Sw_{min}, Sw_{max}]$). Indeed, this work can be seen as an improvement of the methodology proposed in Davolio et al (2013a).

3.3. History matching

The importance of having calibrated water saturation maps estimated from 4D seismic is the incorporation of such data in a history matching procedure, especially in a quantitative way. The history matching procedure applied in this work was proposed by Davolio et al (2013b). The methodology uses 4D seismic information to perform a local matching. The water saturation map estimated from 4D seismic is used as an input to update local properties, such as porosity and permeability, within regions defined around the injector wells. Several model realizations constitute other input data, which, in this work, are the same “ m ” models mentioned before (figure 1).

The local matching starts by dividing the reservoir into regions according to the location of the injector wells and their observed corresponding water saturation error anomaly (figure 6). Then, a simple process of comparing the errors between 4D seismic data and the reservoir model realizations is performed within each region. The models that present the smallest error for each region are selected and a new simulation model is built by a procedure of “copy and paste” of the static properties (porosity and permeability) extracted from the selected models at each region, a process similar to building a patchwork.

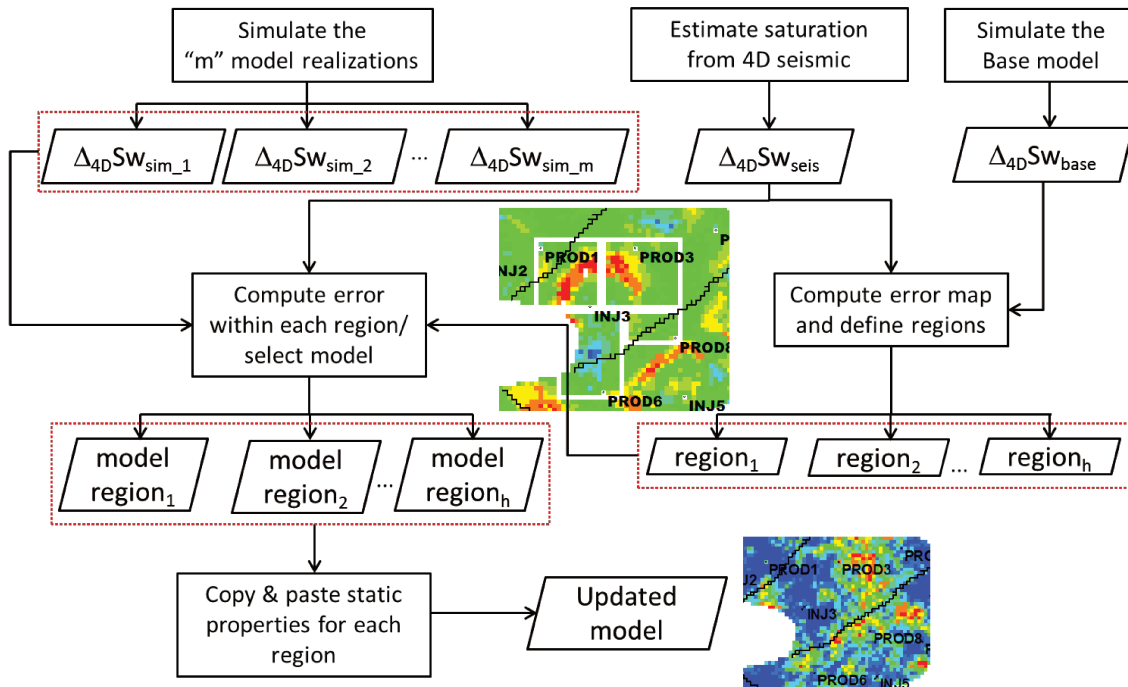


Figure 6: Workflow of the local history matching methodology.

It is important to highlight that before performing this local history matching, the global uncertainties of the reservoir need to be calibrated. As mentioned before, the dataset considered here has its global parameters already matched. The results can be seen in Davolio et al (2013b),

where a methodology that uses well production data was proposed and applied. A satisfactory match for the global uncertainties was reached, although the process was not able to recover the reference model values perfectly. Even so, the global uncertainties were set with the updated values and only local uncertainties needs to be matched. Therefore, the “m” model realizations are only accounting for the local properties (porosity and permeability), yielding a total of 200 models ($m=200$).

This local history matching procedure was applied to three cases, the only difference among them being the input Sw map:

LHM1 = local history matching using as input the estimated Sw map from case 1;

LHM2 = local history matching using as input the estimated Sw map from case 2;

LHM3 = local history matching using as input the estimated Sw map from case 3.

For cases 2 and 3, the limits $[Sw_{min} Sw_{max}]$ were extracted from the 200 simulation results.

4. Results

The volume calibration methodology was applied to the whole reservoir, meaning that all the correction factor calculations considered the volume of water present in the whole reservoir.

4.1. Estimating Sw from 4D seismic

As mentioned in section 2, steps 2 to 9 of the volume calibration proposed can be repeated until a satisfactory calibration is reached. In this work, 15 iterations were enough to reach a good calibration. Figure 7 shows the performance of the volume calibration. The iterations correspond to the execution of steps 2 to 9. The first correction factor computed was: $CF = (4.24 \times 10^7) \text{m}^3 / (3.03 \times 10^7) \text{m}^3 \approx 1.4$. Thus, after the first iteration, the calibrated volume was $\approx 3.32 \times 10^7 \text{m}^3$. This new volume yielded a $CF \approx 1.09$. After applying this second CF, the new volume was $\approx 3.18 \times 10^7 \text{m}^3$ and so on until the 15th iteration that yielded $CF-1=10^{-4}$. Therefore, after 15 iterations, a satisfactory volume calibration was reached for this case.

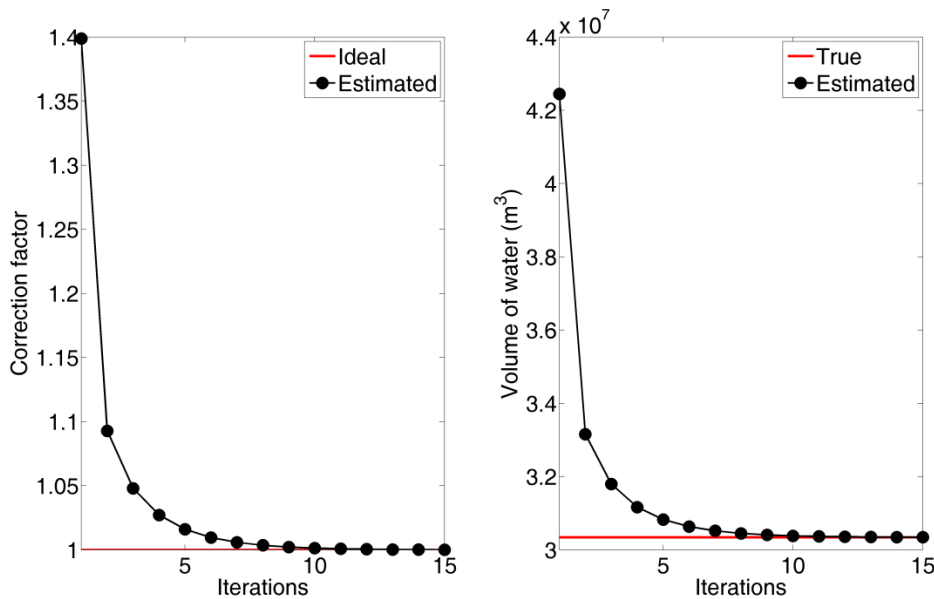


Figure 7: 15 iterations of the proposed volume calibration procedure (steps 2 to 9 in section 2). Left: the correction factor computed per iteration. Right: the calibrated volume of water per iteration.

Figure 8 shows the estimated water saturation map for the three inversions performed and the water saturation map yielded from the simulation of the reference model, which represents the answer that the inversions aim to reach. The same figure also shows the respective error map of the three inversion results. Due to the noise added to seismic impedances and the wrong porosity used as inputs for the petro-elastic inversion, the results of case 1 presented a noisier aspect that is clearly seen in the error map. Note that there is a zone with high errors, indicated by a red arrow; the white region in the error map means that the error is out of scale (bigger than 0.2). The main causes of this error are the low porosity region that was wrongly characterized (compare figures 5a and 5b) together with wrong pressure values; remember that the petro-elastic inversion estimates saturation and pressure, simultaneously. Figure 9 follows the same layout of figure 8 but showing the estimations of pressure for cases 1 and 2; the same noisy behavior of case 1 previously mentioned is observed for pressure as well. In the same way, the region with the highest errors marked in the Sw map presents a high error for pressure too.

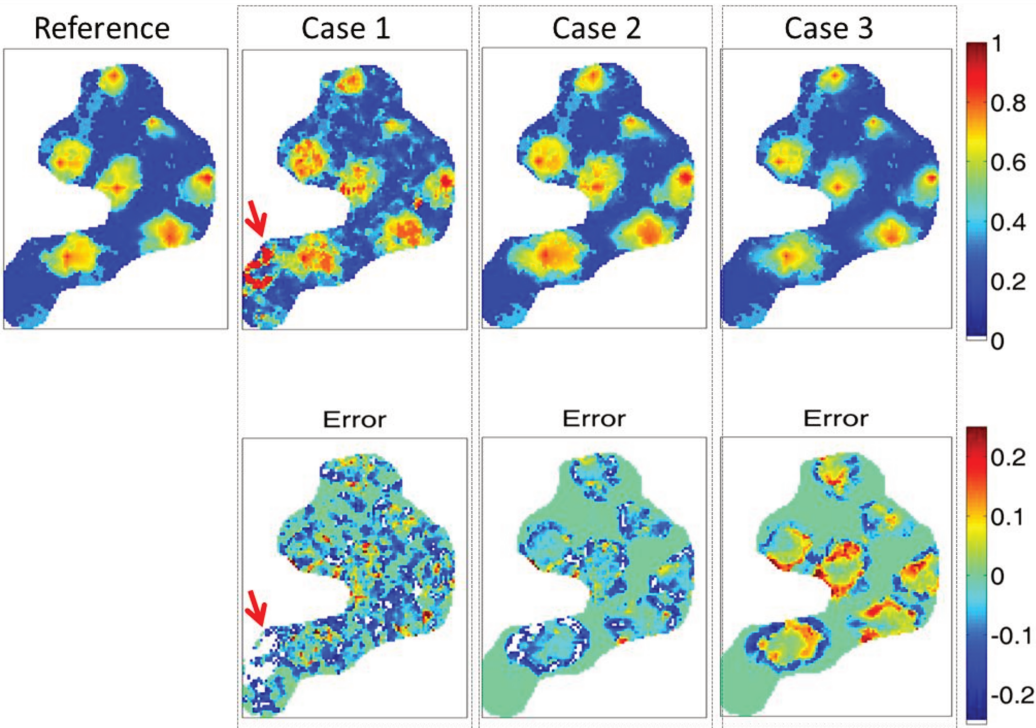


Figure 8: Water saturation maps for the second production time (monitor survey). Top: from left to right, the reference model (answer), the estimated Sw map for cases 1 to 3. Bottom: from left to right, the error (reference – estimated) for the three estimations. Layer 3.

When the estimation of Sw is constrained to flow conditions by imposing the computed limits of case 2, an error reduction is clearly observed in figure 8. Note that the application of these constraints cleaned some areas that were being wrongly estimated due to the seismic noise. Also, the region with high errors observed in case 1 now presents a better response. This happened because the constraints applied to the solution space “forced” the dynamic properties estimations (saturation and pressure) to values more physically consistent, diminishing the effects of wrong static properties characterization. This improvement in the estimation of Sw can also be seen as a consequence of the relevant error reduction observed in the estimation of pressure for case 2 (figure

9). The good estimation of pressure was ensured by the proper uncertainties mapping performed, that was verified with the pressure curves presented in figure 3.

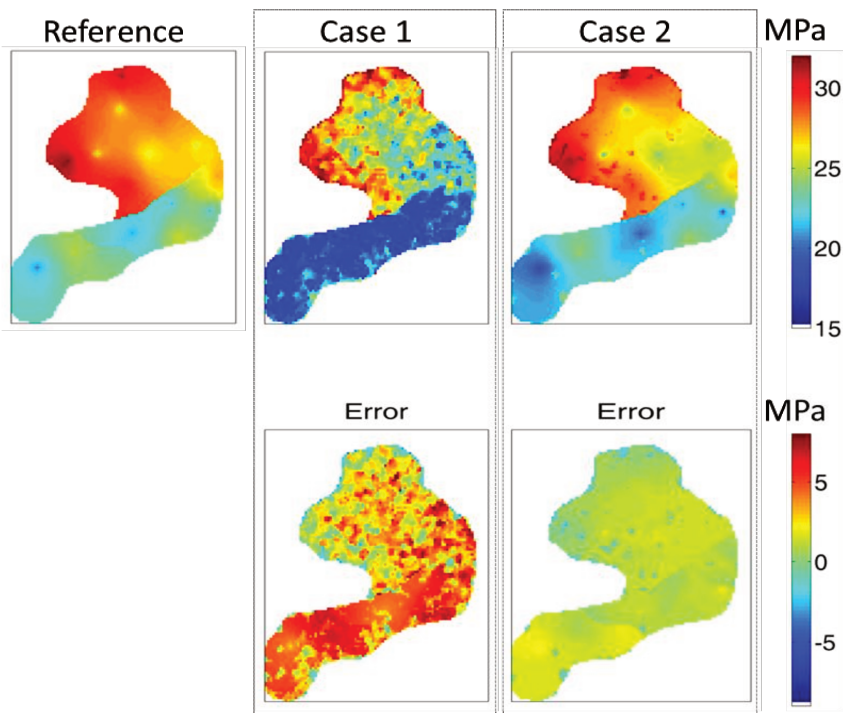


Figure 9: Pore pressure maps for the second production time (monitor survey). Top: from left to right, the reference model (answer), the estimations of cases 1 and 2. Bottom: from left to right, the error (reference – estimated) for the two estimations. Layer 3.

Although the result of case 2 presented a water saturation map closer to the reference, it can be observed that the error anomalies are predominantly negative. This means that the estimated water saturation presents more water than the reference model, showing the necessity of calibrating the volume of water. As in practice, these errors are not available information, this could be checked by a simple computation of the volume of water (equation 1) and comparison with the known volume of injected water.

After applying the volume calibration proposed in this work (case 3), it can be observed that the injection anomalies are better defined. Also, the observed error is indicating that the mass balance is being respected, as it presents positive and negative anomalies, meaning that the error is now more related to an incorrect water front displacement and not with the amount of water.

Figure 10 shows the histogram of the errors observed in figure 8. Aside from the gradual error reduction observed from case 1 to cases 2 and 3, another interesting aspect to highlight is the error distribution of the third case. In case 3, the errors are centralized at zero, with some positive and negative values, indicating again that the amount of water present in the estimated map is better balanced than in the other two cases.

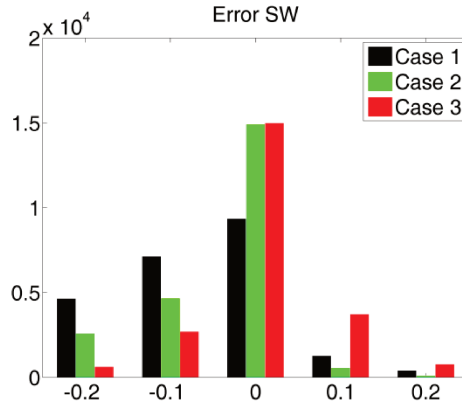


Figure 10: Histogram of the error (reference – estimated) in the estimations of water saturation.

4.2. History matching

The first step in performing the local history matching is to define regions based on the Sw error observed and the location of injector wells. The definition of the regions in this work is illustrated in figure 11. The injector wells that presented the highest errors (for all layers) were selected to perform the local match: INJ1, INJ3, INJ4 and INJ5. See Davolio et al (2013b) for more details about the regions’ definition.

The estimated Sw of case 2 (figure 8) was used to compute the error map shown in figure 11, which is exactly the same input used to define the regions in Davolio et al (2013b). As previously mentioned, the local matching procedure described in section 3.3 was performed for three cases (LHM1, LHM2 and LHM3), the difference among them being the Sw map used as input. Although the region definition is dependent on the input data, in this work, the same regions shown below were used for the three history matchings performed with the goal of comparing the results.

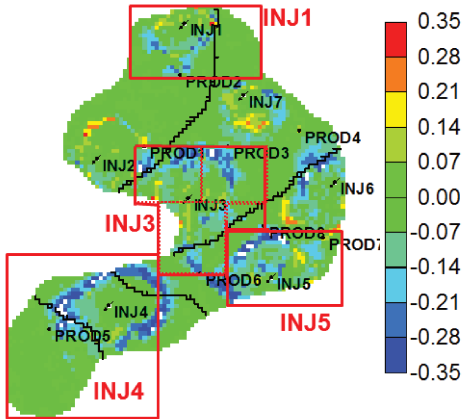


Figure 11: Water saturation error map ($\Delta_{4D}Sw_{base} - \Delta_{4D}Sw_{seis}$) with the regions defined to perform the local matching.

Figure 12a shows the Sw error map (compared to the true answer) of the base model before the local matching. Figures 12b, 12c and 12d show the error maps for the three updated models. The first thing to note is that the updated models LHM1 and LHM2 present more water than they should; observe the predominance of negative anomalies. These results are explained by the fact that the matching procedure is updating the static properties in order to match the Sw maps of case

1 and 2, displayed in figure 8. Figure 13 shows the saturation error (compared to the Sw map estimated from 4D seismic) for each case, i.e., the differences in the base model before and after applying each of the three history matchings. Thus, figure 13 is showing that the local matching procedure is working for LHM1 and LHM2, i.e., the updated models are providing Sw maps that better follow the behavior observed in 4D seismic data. However, these results are not satisfactory, since the matching process is increasing the saturation errors when compared to the true answer as displayed in figures 12b and 12c.

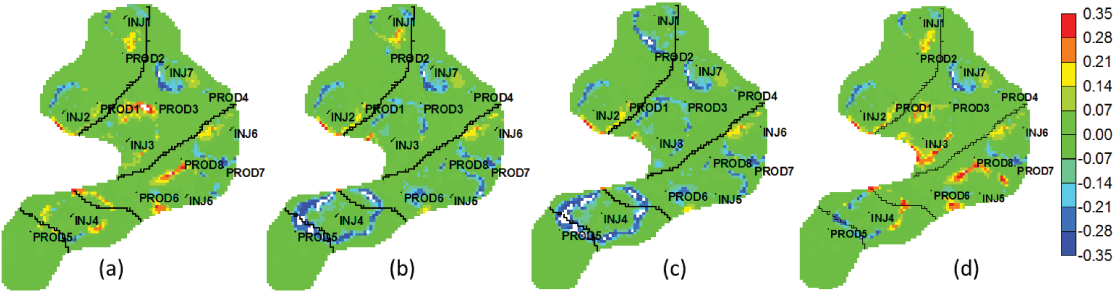


Figure 12: Water saturation error map (reference - simulated) of the base model before (a) and after the local matching LHM1 (b), LHM2 (c) and LHM3 (d). Layer 3.

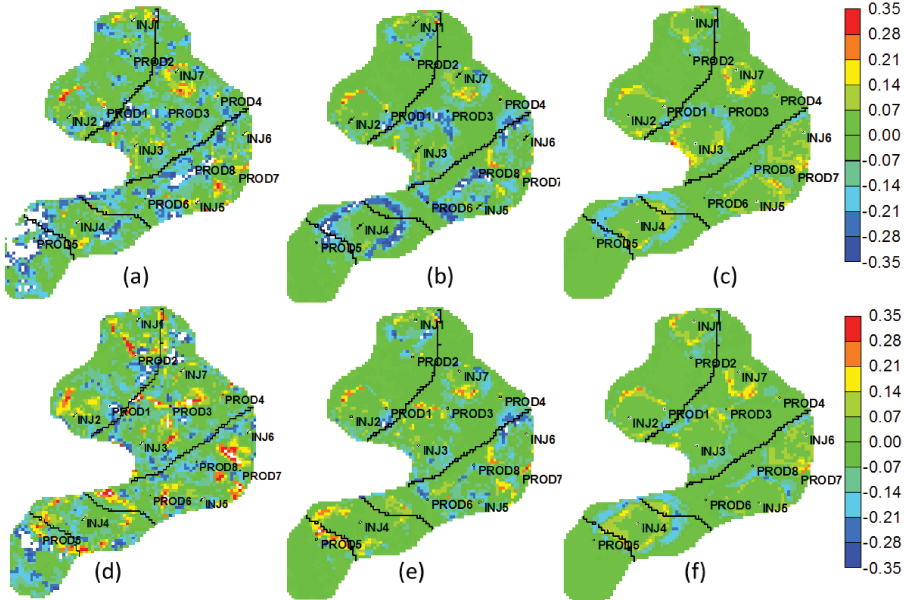


Figure 13: Observed water saturation error map (estimated from 4D seismic – simulated). Top: difference between the estimated saturation for case 1(a), case 2 (b) and case 3(c) and the saturation of the base model before the matching. Bottom: difference between the estimated saturation for case 1(d), case 2 (e) and case 3(f) and the saturation of the base model after the respective history matching (LHM1, LHM2 and LHM3).

The quantitative use of estimated Sw from 4D seismic was successful in the third history matching (LHM3). Figure 12d shows a decrease in the Sw error when compared to LHM1 and LHM2. Some errors are still observed for this case for two reasons: (1) although better calibrated, the Sw map of case 3 still carries some errors and (2) the characterization process is not assumed to

be perfect, i.e., the image realizations of porosity and permeability are not able to reproduce the reference properties. The graph bar displayed in figure 14 corresponds to the sum of the Sw errors at every reservoir location. This graph shows that LHM3 presents a much better balance of errors (positive and negative values).

One can say that the base model (figure 12a) presents the same amount of errors as LHM3 (figure 12d). Indeed, there is a slight error reduction in the Sw map after the local matching LHM3. This could be improved, for instance, by re-defining the regions according to the observed error anomalies specific for this case. But, it is important to highlight that the focus of this work is not to guarantee the best history matching result but to analyze the importance of having better input information when performing such a process. In this sense, the results of figures 12 and 14 demonstrated that the use of the calibrated water saturation map (LHM3) is the safest option.

Looking at the updated properties, especially for the porosity field, the model updated after the matching process LHM3 (figure 15) showed an improvement in the base model and better results than the other matches. The regions marked in figure 15d are examples of a good agreement with the reference porosity field displayed in figure 5a. Concerning the permeability field update, a less pronounced improvement is observed (figure 16). From figure 16, it can also be seen that the characterization process of permeability needs to be improved, since the image realizations do not present the expected features seen in figure 5c. Even so, a better definition of a high permeability zone can be observed, as highlighted in figure 16d.

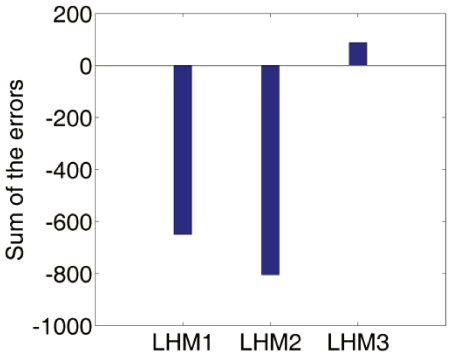


Figure 14: Bar graph indicating the sum of the errors of the water saturation error map (reference - simulated) for the three history matchings applied.

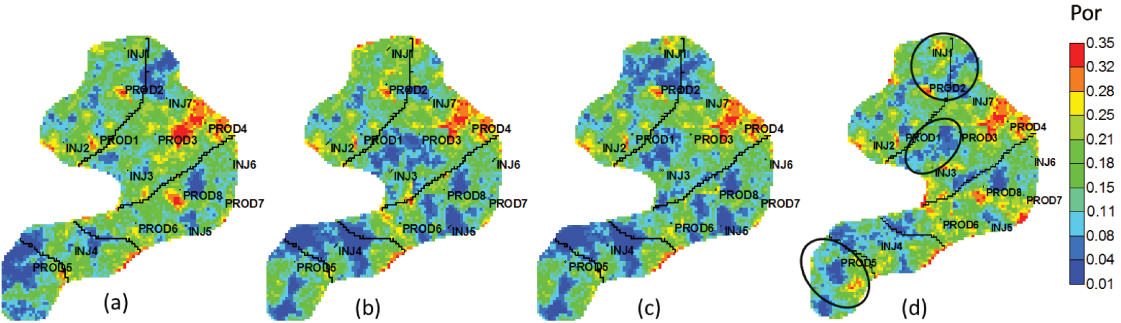


Figure 15: Porosity field of the base model before (a) and after the local matching LHM1 (b), LHM2 (c) and LHM3 (d). Layer 3.

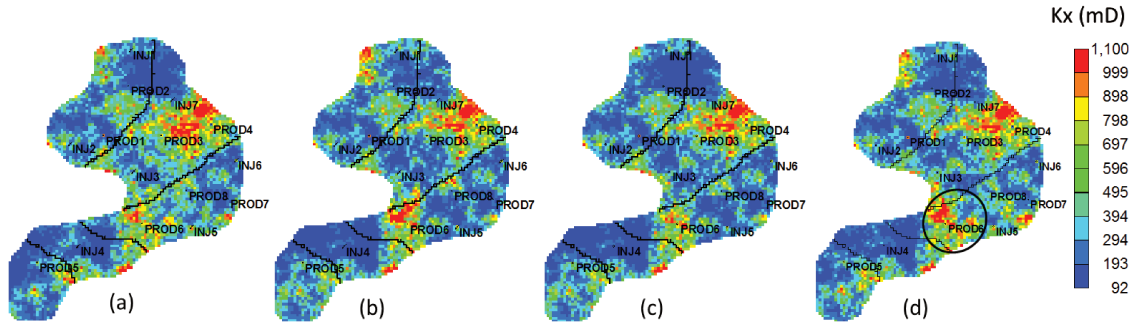


Figure 16: Horizontal permeability field of the base model before (a) and after the local matching LHM1 (b), LHM2 (c) and LHM3 (d). Layer 3.

5 Final remarks

The results presented here showed that it is possible to use reservoir simulation data to better extract dynamic changes from 4D seismic data. The addition of engineering information helps to diminish the effects of poor static properties characterization and problems related to seismic signals. Concerning the history matching process, the results demonstrated that the calibrated estimation of water saturation maps is important to update reservoir models, namely LHM3, which provided the best result when compared to the other two history matchings performed. One point worthy of comment is that, for this dataset, the comparison of the S_w errors in the model before and after the history matching (LHM3) did not show very relevant differences. As already mentioned, this result could be improved by re-defining the regions, for instance. But, again, the result to be highlighted in this work is the comparison among the three history matchings performed, as the focus was not to achieve the best history matching possible.

The methodology proposed to calibrate the volume of water was applied to a synthetic dataset. In this dataset, the S_w map provided by 4D seismic presented more water than it should for the entire reservoir. But, it is important to emphasize that the volume calibration and the history matchings were built to be performed locally. Thus, for more complex cases, it can happen that some regions of the reservoir present a volume bigger or smaller than expected. Then, the correction factor that was computed here and applied to the entire reservoir, in such cases, can be computed/applied individually for each region of interest. In this case, there would be an additional step, which is to identify the water anomalies associated to each injector well in order to compute individual volumes related to each injector.

6 Conclusions

A methodology to calibrate the volume of water present in water saturation maps provided by 4D seismic was proposed. The volume calibration is performed based on reservoir flow conditions imposed by the simulation of several models. As these models account for the uncertainties mapped, the calibrated water saturation map is consistent with flow conditions resulting from the current stage of characterization.

The advantages of applying the proposed methodology were shown in two forms: (1) by comparing the water saturation maps resulted from a petro-elastic inversion process, with and without the volume calibration, and (2) by comparing the results of a history matching that uses the estimated water saturation maps to update static properties locally. Synthetic data was used in both cases and it was important to validate the methodology.

As for the main results, it can be highlighted that: (1) the calibrated water saturation map provided more reliable information to be used for interpretation purposes (qualitatively or quantitatively), since it is more physically consistent (respecting the mass balance); (2) the quantitative use of a calibrated water saturation map in a history matching is very important to ensure a proper static properties updating.

Acknowledgments

The authors would like to thank UNISIM, BG, PETROBRAS, CEPETRO and the Department of Petroleum Engineering for supporting this work. We also thank CMG and Schlumberger for software licenses.

References

- Castro S A, Caers J, Otterlei C M, Meisingset H, Høy T, Gomel P and Zachariassen E 2009 Incorporating 4D seismic data into reservoir models while honoring production and geologic data: a case study *The Leading Edge* **28** (12) 1498-1506.
- Brito D, Moraes R and Emerick A, 2010 The Marlim field: incorporating time-lapse seismic in the assisted history matching, SPE137763 *SPE Latin American & Caribbean Petroleum Engineering Conf.*(Lima, Peru, 1-3 December).
- Davolio A, Maschio C and Schiozer D 2012 Pressure and saturation estimation from P and S impedance: a theoretical study *Journal of Geophysics and Engineering* **9** 447-460.
- Davolio A, Maschio C and Schiozer D 2013a A methodology to constrain pressure and saturation estimation from 4D seismic using multiple simulation models and observed data *Journal of Petroleum Science and Engineering* **105** 51-61.
- Davolio A, Maschio C and Schiozer D 2013b Local history matching using 4D seismic data and multiple models combination, SPE164883 *SPE EUROPEC/EAGE Ann. Conf. Exhibition* (London, United Kingdom, 10-13 June).
- Huang Y, MacBeth C, Barvked O, Gestel J P V and Dybvik O P 2011 Enhanced dynamic interpretation from correlating well activity to frequently acquired 4D seismic signatures *The Leading Edge* **30** (9) 1042-1050.
- Johann P, Sansonowski R, Oliveira R and Bampi D 2009 4D seismic in a heavy-oil turbidite reservoir offshore Brazil *The Leading Edge* **28** (6) 718-729.
- Landa J L and Kumar D 2011 Joint inversion of 4D seismic and production data *SPE Tech. Conf. Exhibition* (Denver, Colorado, 30 October – 2 November).
- Landro M 2001 Discrimination between pressure and fluid saturation changes from time-lapse seismic data *Geophysics* **66** 836-844.

- Lumley D, Adams D, Meadows M, Cole S and Ergas R 2003 4D seismic pressure-saturation inversion at Gullfaks field, Norway *First Break* **21** (9) 49-58.
- MacBeth C, Floricich M and Soldo J 2006 Going quantitative with 4D seismic analysis *Geophysical Prospecting* **54** 303-317.
- Mavko G, Mukerji T and Dvorkin J 2003 *The Rock Physics Handbook: Tools for seismic analysis in porous media* (Cambridge: Cambridge University Press).
- Tolstukhin E, Lyngnes B and Sudan H H 2012 Ekofisk 4D seismic – seismic history matching workflow SPE154347 *EUROPEC/EAGE Ann. Conf. Exhibition (Copenhagen, Denmark, 4-7 June)*.
- Toinet S, Maultzsch S, Souvannavong V and Volnard O 2011 4D pre-stack inversion workflow integrating reservoir model control and lithology supervised classification *First Break* **29** (8) 59-66.

6. CONCLUSIONS

The current work proposed four methodologies: (1) an inversion scheme to estimate pressure and saturation from 4D seismic, (2) a procedure that uses simulation data to better extract variations of dynamic properties from 4D seismic data, (3) a history matching process that uses water saturation maps, generated in the previous papers, in a local matching procedure and (4) a procedure to calibrate the volume of injected water associated to the saturation map estimated from 4D seismic. In addition to the methodologies, which can be seen as the main results of this work, especially the second and the fourth, there are some important results specific to each of the four of them, which should be highlighted.

From the inversion process (paper 1), it could be concluded that:

- The use of only one seismic attribute (P impedance, for instance) is not enough to estimate pressure and saturation variations, since it yields a multiple answer problem. A second attribute with a different response to the changes in dynamic properties should be considered, such as S impedance.
- If an ideal dataset is considered (without any errors/noise and known static properties), a 3D seismic survey would be enough to estimate dynamic properties. However, for more realistic cases, which consider errors in the static properties and noise in seismic data, the time-lapse difference becomes absolutely necessary.
- The inversion was implemented to estimate pressure and saturation for each single block individually. Thus, the optimization procedure is simple, with only two unknowns to be estimated. The objective function considering the 4D approach and P and S impedances simultaneously presented a good behavior with a well-defined global minimum. Thus, the initial guess did not influence the results for the cases studied.
- When noise in seismic data and errors in the static properties are considered, the objective function still presents a global minimum. However, the global minimum is displaced from the expected correct position and does not coincide with the true answer, yielding errors in the estimated pressure and saturation values.

The methodology presented in paper 2 is a relevant result as it proposes an innovative procedure to integrate 4D seismic and simulation models. Some of the results to be highlighted are:

- The proposed procedure applies constraints in the solution space that are derived from the combination of the mapped reservoir uncertainties. Thus, it is a quantitative way of incorporating the knowledge available from the reservoir characterization and simulation processes with 4D seismic signals.
- In the case study presented, the application of the methodology allowed the reduction of errors in some regions of the estimated water saturation map, where, according to the simulations, water should not have reached. Before applying the methodology, these areas had been wrongly estimated from 4D seismic due to the presence of noise in the region. As mentioned before, in these cases, the minimum of the objective function is displaced and does not coincide with the true answer. Thus, the constraints determined by the methodology cut the solution space and now the minimum inside the new space is closer to the true answer.
- The methodology allows checking the flow behavior, taking into account the reservoir uncertainties, to verify that it is in agreement with the time-lapse signals. Thus, it can be useful to identify possible problems with 4D seismic data or with the mapping of uncertainties. Better results are achieved when the most important uncertainties are properly mapped. However, in the cases where this is not achieved as, for instance, in the presence of an "unknown unknown", the methodology might force the inversion limits to the boundaries and this could be used as an indication that the characterization process needs to be improved. This type of situation was not considered in this work but must be considered in future works.

The results obtained from the history matching methodology proposed in paper 3 are:

- A history matching process that uses 4D seismic information locally (regions around injector wells) and that provides updated reservoir properties with geological features.
- It is an easy-to-implement procedure, which can be a good alternative when more sophisticated methods may be unfeasible due to the complexity of implementation or to high computational demand.

- The results obtained in the synthetic case studied showed a considerable error reduction in the water saturation map. This kind of information can play an important role in the decision making process of developing and managing a petroleum field.

Some points to highlight concerning the volume calibration procedure of the fourth and last paper of this work are:

- The proposed methodology allowed the estimation of a saturation map from 4D seismic that respected the expected mass balance. This was verified by observing the saturation errors after the calibration, which presented positive and negative values.
- The history matching results showed that the methodology was able to update reservoir properties and, thus, produce a simulation model that better follows the 4D seismic data. When a poor estimation of the saturation changes was used as input for the history matching, an improper update of the reservoir properties was observed. Thus, the results highlighted the importance of estimating a calibrated map, in order to use it in a quantitative history matching procedure.
- The volume calibration procedure provides a more reliable saturation map and it is important to avoid bias in the amount of water in the updated model after performing a history matching, concentrating the matching procedure in the localization of the water front.

The last aspect to highlight in the current work is that the integration methodologies (papers 2 and 4) could be used in different contexts. For instance, the methodology of paper 2 could be extended to be performed in the impedance domain, instead of the pressure and saturation domain. In the same way, the volume calibration proposed in paper 4 could be applied to saturation maps estimated by other published methodologies (Landro 2001, Lumley et al 2003, and MacBeth et al 2006). Thus, the main contribution of this work is related to the ideas of integration methodologies and not only to the results presented here.

7. FUTURE WORKS

Some points to be addressed to extend the study presented in this work are described below:

- Application of the methodologies in a more challenging dataset, considering, for instance, data with different scales, the presence of gas, the presence of unknown unknowns and uncertainties in the petro-elastic modeling.
- In more complex cases if the spatial correlation of the estimated properties is not respected the petro-elastic inversion must be improved by adding a continuity factor, or by performing the inversion for all the blocks simultaneously. For the latter a more sophisticated optimization algorithm might be necessary.
- Performance of volume calibration locally, around the injector wells, creating an additional step to identify the volume of water corresponding to each selected well.
- Improvement of the proposed local history matching procedure to guarantee continuity in the borders of the regions, generating models more consistent with geologic models.
- Performance of the integration between reservoir simulation models and 4D seismic data in a feedback loop. In this case, the sequence would be: (1) estimation of the dynamic changes from 4D seismic, (2) conditioning/calibration of the estimation with the methodologies presented here, (3) performance of a history matching, (4) use of the new updated static properties to go back to step 1 and repeat all the cycle until a satisfactory matching is reached.
- Extension of the integration methodology (paper 2) to a probabilistic approach. Instead of using only minimum and maximum values, a probabilistic distribution function could be used to condition the estimation of dynamic properties.
- Application of the proposed methodologies to a real dataset.

REFERENCES

Avseth, P., Mukerji, T., Mavko, G., 2005. Quantitative seismic interpretation: applying rock physics tools to reduce interpretations risk. Cambridge University Press, Cambridge.

Batzle, M. and Wang, Z., 1992. Seismic properties of pore fluids. *Geophysics*. 57 (11), 1396-1408.

Brito, D., Moraes, R. and Emerick, A., 2010 The Marlim field: incorporating time-lapse seismic in the assisted history matching. SPE137763. In: Proceedings of the SPE Latin American & Caribbean Petroleum Engineering Conference 1-3 December, Lima, Peru.

Caers, J., 2003. History matching under training-image based geological model constraints. *SPE J.* (7), 218-226.

Castro, S. A., Caers, J., Otterlei, C. M., Meisingset, H., Hoye, T., Gomel, P., Zachariassen, E., 2009. Incorporating 4D seismic data into reservoir models while honoring production and geologic data: a case study. *The Leading Edge*. 28 (12), 1498-1506.

Dadashpour, M., Landrø, M., Kleppe, J., 2008. Nonlinear inversion for estimating reservoir parameters from time-lapse seismic data. *J. Geophys. Eng.* 5, 54-66.

Dadashpour, M., Echeverría-Ciaurri, D., Kleppe, J., Landrø, M., 2009. Porosity and permeability estimation by integration of production and time-lapse near and far offset seismic data. *J. Geophys. Eng.* 6, 325-344.

Davolio, A., Maschio, C., Schiozer, D., 2011. Incorporating 4D seismic attributes into history matching process through an inversion scheme. SPE142946. In: Proceedings of the Annual Conference Exhibition of SPE EUROPEC/EAGE. 23-26 May, Vienna, Austria.

Davolio, A., Maschio, C., Schiozer, D., 2012. Pressure and saturation estimation from P and S impedance: a theoretical study. *J. Geophys. Eng.* 9, 447-460.

Davolio, A., Maschio, C., Schiozer, D., 2013a. A methodology to constrain pressure and saturation estimation from 4D seismic using multiple simulation models and observed data. *J. Petrol. Sci. Eng.* 105, 51-61.

Davolio, A., Maschio, C., Schiozer, D., 2013b. Local history matching using 4D seismic data and multiple models combination. In: Proceedings of the Annual Conference Exhibition of SPE EUROPEC/EAGE. 10-13 June, London, United Kingdom.

Fahimuddin, A., Aanonsen, S., Skjervheim, J. A., 2010. Ensemble based 4D seismic history matching: integration of different levels and types of seismic data. SPE131453. In: Proceedings of the Annual Conference Exhibition of SPE EUROPEC/EAGE. 14–17 June, Barcelona, Spain.

Gervais, V., Roggero, F., 2010. Integration of saturation data in a history matching process based on adaptive local parametrization. *J. Petrol. Sci. Eng.* 73, 86-98.

Gosselin, O., Berg, S. V. D., Cominelli, A. 2001. Integrated History-Matching of Production and 4D Seismic Data. SPE71599. In: Proceedings of the Annual Technical Conference and Exhibition. 30 September- 3 October, New Orleans, Louisiana, USA.

Gosselin, O., Aanonsen, S. I., Aavatsmark, I., Cominelli, A., Gonard, R., Kolasinski, M., Ferdinandi, F., Kovacic, L., Neylon, K. 2003. History Matching Using Time-lapse Seismic (HUTS). SPE 84464. In: Proceedings of the Annual Technical Conference and Exhibition, 5-8 October 2003, Denver, Colorado.

Helgerud, M. B., Miller, A. C., Johnston, D. H., Udoh, M. S., Jardine, B. G., Harris, C., Aubuchon, N., 2011. 4D in the deepwater Gulf of Mexico: Hoover, Madison and Marshall fields. *The Leading Edge*. 30 (9) , 1008-1018.

Huang, Y., MacBeth, C., Barvked, O., Gestel, J. P. V., Dybvik, O. P., 2011 Enhanced dynamic interpretation from correlating well activity to frequently acquired 4D seismic signatures. *The Leading Edge*, 30 (9), 1042-1050.

Hoffman, B. T., Caers, J. 2005. Regional probability perturbations for history matching. *J. Petrol. Sci. Eng.* (46), 53-71.

Ida, M. 2009. Incorporation of Quantitative 4D Seismic Data in the History Matching Process. Master thesis. University of Campinas - UNICAMP.

Jin, L., Alpak, F. O., Hoek, P. V., Pirmez, C., Fehintola, T., Tendo, F., Olaniyan, E., 2011. A comparison of stochastic data-integration algorithms for the joint history matching of production and time-lapse seismic data. SPE146418. In: Proceedings of the Annual Technical Conference Exhibition. 30 October – 2 November, Denver, Colorado, USA.

Johann, P., Sansonowski, R., Oliveira, R., Bampi, D., 2009. 4D seismic in a heavy-oil turbidite reservoir offshore Brazil. The Leading Edge, 28 (6) 718-729.

Kjelstadli, R.M., Lane, H.S., Johnson, D.T, Barkeved, O. I., Buer, K., Kristiansen, T. G. 2005. Quantitative History Match of 4D Seismic Response and Production Data in the Valhall Field. SPE 96317. In: Proceedings of the Offshore Europe. 6-9 September, Aberdeen, United Kingdom.

Kazemi, A., Stephen, K. D., Shams, A., 2010. Seismic history matching of Nelson using time-lapse seismic data: an investigation of 4D signature normalization.. SPE131538. In: Proceedings of the Annual Conference Exhibition of SPE EUROPEC/EAGE. 14–17 June, Barcelona, Spain.

Landa, J. L., Kumar, D., 2011. Joint inversion of 4D seismic and production data. SPE146771. In: Proceedings of the Annual Technical Conference Exhibition. 30 October – 2 November, Denver, Colorado, USA.

Landro, M., 2001. Discrimination between pressure and fluid saturation changes from time-lapse seismic data. *Geophysics* 66, 836-844.

Landro, M., Stronen, L. K., Slheim, O. A., Hilde, E., 2001. Time-lapse seismic as a complementary tool for in-fill drilling. *J. Petrol. Sci. Eng.* 31, 81-92.

Lumley, D., Adams, D., Meadows, M., Cole, S., Ergas, R., 2003. 4D seismic pressure-saturation inversion at Gullfaks field, Norway. *First Break*, 21 (9), 49-58.

MacBeth, C., Floricich, M., Soldo, J., 2006. Going quantitative with 4D seismic analysis. *Geophysical Prospecting*, 54, 303-317.

Maschio, C., Carvalho, C. P. V., Schiozer, D. J., 2010. A new methodology to reduce uncertainties in reservoir simulation models using observed data and sampling techniques. *J. Petrol. Sci. Eng.* 72, 110-119.

Mavko, G., Mukerji, T., Dvorkin, J., 2003. *The Rock Physics Handbook: Tools for seismic analysis in porous media*. Cambridge University Press, Cambridge.

Neal, R. M., 2003. Slice Sampling. *The Annals of Statistics*, 31(3), 705-767.

Nunes, J.P., Santos, M. S., Maciel, N., Davolio, A., Formento, J. L., 2009. Separation of pressure and saturation effects using AVO 4D in Marlim Field. In: *Proceedings of the 11th International Congress of the Brazilian Geophysical Society*, 24-28 August, Salvador, Brazil.

Sedighi, F., Stephen, K.D., 2009., Faster Convergence in Seismic History Matching by Efficient Parameter Searching. SPE121210. In: Proceedings of the Annual Conference Exhibition of SPE EUROPEC/EAGE, 8-11 June 2009, Amsterdam, The Netherlands.

Schiozer, D.J., Ligeró, E.L., Suslick, S.B., Costa, A.P.A., Santos, J.A.M., 2004. Use of representative models in the integration of risk analysis and production strategy definition. J. Petrol. Sci. Eng. vol. 44 (1–2), 131–141.

Stephen, K., D., Soldo, J., MacBeth, C., Christie, M., 2005. Multiple model seismic and production history matching: a case study. SPE 94173. SPE EUROPEC/EAGE. In: Proceedings of the Annual Conference Exhibition of SPE EUROPEC/EAGE, 13-16 June, Madrid, Spain.

Souza, R. M., Machado, A. F., Muneratto, F. P., Schiozer, D. J., 2010. Iterative history matching technique for estimation reservoir parameters from seismic data. SPE131617. In: Proceedings of the Annual Conference Exhibition of SPE EUROPEC/EAGE. 14–17 June, Barcelona, Spain.

Souza, R. M., Muneratto, F. P., D. J. Schiozer, 2011. Quantitative integration of time-lapse derived information in a history matching procedure. SPE143009. In: Proceedings of the Annual Conference Exhibition of SPE EUROPEC/EAGE. 23-26 May, Vienna, Austria.

Tolstukhin, E., Lyngnes, B., Sudan H. H., 2012. Ekofisk 4D seismic – seismic history matching workflow. SPE154347. In: Proceedings of the Annual Conference Exhibition of SPE EUROPEC/EAGE, 4-7 June, Copenhagen, Denmark.

Toinet, S., Maultzsch, S., Souvannavong, V., Volnard, O., 2011, 4D pre-stack inversion workflow integrating reservoir model control and lithology supervised classification. *First Break* 29 (8), 59-66.

Tura, A. and Lumey, D., 1999. Estimating pressure and saturation changes time-lapse AVO data. *SEG Technical Program Expanded Abstr.* pp. 1655–1658.

Tuttle, C., Pelissier, M., Barnes, M., Tribe, J., Persad, K., 2009. A seismically constrained reservoir modeling workflow: case study. *The Leading Edge*, 28 (12), 1492-1497.

APPENDIX A

Complementary results of the paper “*Pressure and saturation estimation from P and S impedances: a theoretical study*”

Paper 1 presents some discussions concerning the objective function behavior of the petro-elastic inversion proposed. To visualize the optimization aspects of the inversion, all discussions were presented assuming one single reservoir location (one grid block). The results presented here complement those discussions by showing the inversion results in an entire reservoir model. These new results allow verification of the reflection of the optimization issues in an entire reservoir model, evaluating different combinations of static and dynamic variables.

These results were extracted from the published paper Davolio et al (2011), which is attached at the end of this appendix. The goal of this appendix is to highlight the relationship between the studies presented for one single block in paper 1 and the results for the entire reservoir, presented in Davolio et al (2011). For more details, see the respective references.

The relationship between the results of the two works is shown in the figures below that follow the layout: the results in a single reservoir location are displayed on the top (some images were extracted from paper 1) and the results of the same inversion process are displayed at the bottom, under the same optimization conditions, for an entire reservoir (images extracted from Davolio et al, 2011). In order to check the accuracy of the results, Figure A-1 presents the true answer to the problem for the entire reservoir.

1. 3D approach: the non-uniqueness issue

The first result of the petro-elastic inversion presented in paper 1 highlights the non-uniqueness problem when changes in pressure and saturation are estimated from P impedance. These results are displayed at the top of Figure A-2. At the bottom of the same figure, the manner in which this problem affects different locations of a reservoir is presented.

Given that the expected solution (true answer) is displayed in Figure A-1, Figure A-2 shows that the dynamic properties are being poorly estimated. The saturation anomalies are not being recovered and the pressure map is influenced by these water anomalies,

indicating that this process could not differentiate the effects of the two dynamic properties from seismic data (IP).

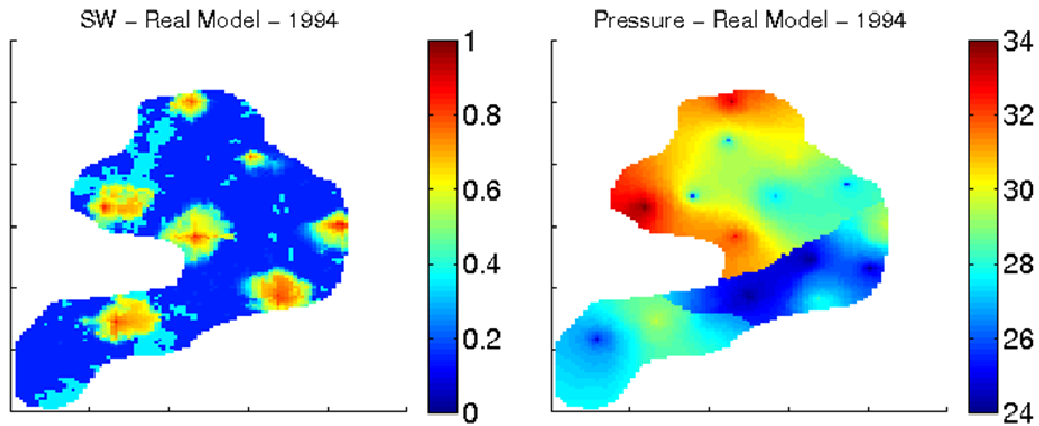


Figure A-1: Expected inversion response for saturation and pressure (MPa).

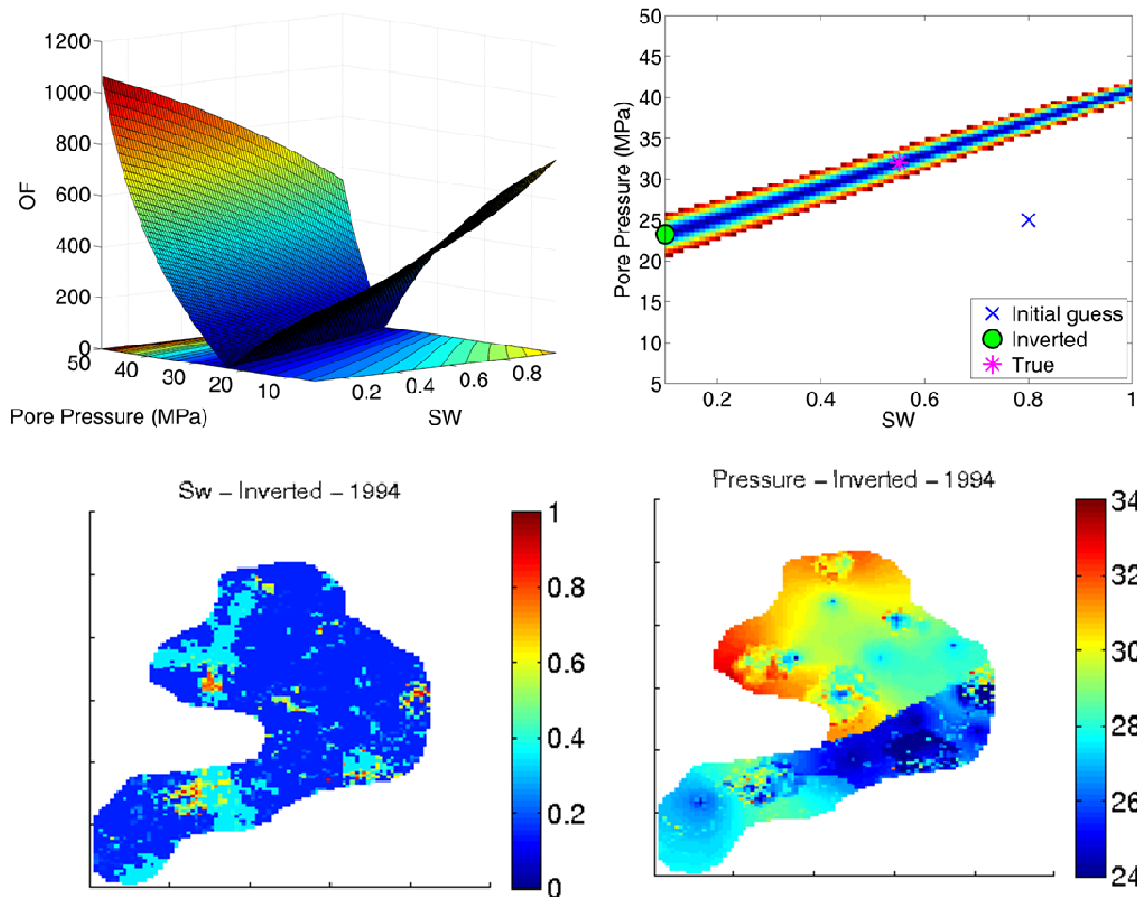


Figure A-2: 3D inversion results, assuming only the P impedance in the objective function: $OF=f(IP)$. Top: considering one single reservoir location (extracted from Davolio et al, 2012). Bottom: estimated pressure (MPa) and saturation considering the entire reservoir (extracted from Davolio et al, 2011).

For an ideal dataset (no errors/noise), the non-uniqueness problem can be solved by considering, simultaneously, P and S impedances in the objective function. This is illustrated in Figure A-3. The exact solution found by the 3D algorithm, which is observed for the single block location, is explained by the very well-behaved objective function that holds a well-defined global minimum. This situation is observed for the entire reservoir. As illustrated in Figure A-3, the estimation of pressure and saturation for the entire reservoir was very precise.

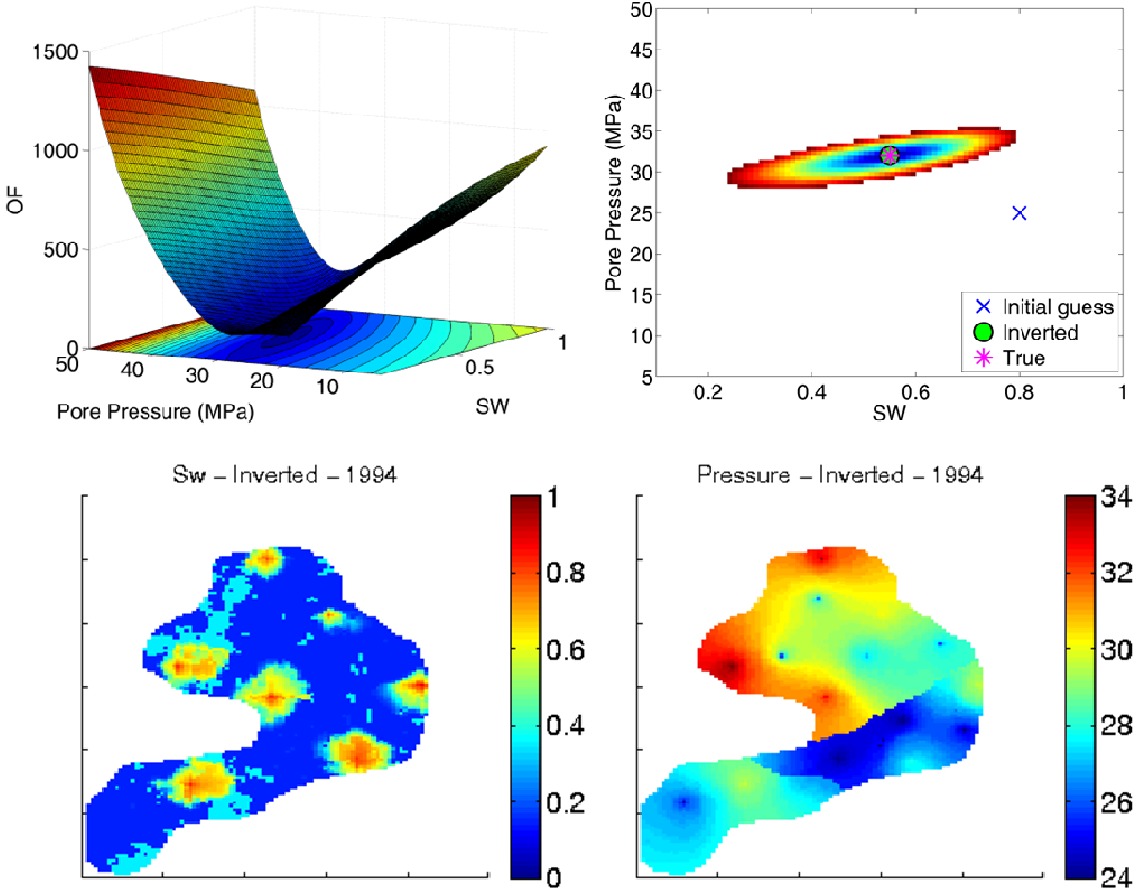


Figure A-3: 3D inversion results, assuming P and S impedance in the objective function: $OF=f(IP,IS)$. Top: considering one single reservoir location (extracted from Davolio et al, 2012). Bottom: estimated pressure (MPa) and saturation considering the entire reservoir (extracted from Davolio et al, 2011).

2. 3D approach: assuming an incorrect porosity

When a non-ideal dataset is assumed, the 3D inversion starts to fail. The non-ideal dataset was represented in paper 1 by assuming an inaccurate value of porosity, which is an important input for petro-elastic inversion. For the inversion performed in the entire reservoir, this inaccuracy was added by multiplying the true porosity image by a constant (1.15).

For this case, the global minimum of the objective function does not coincide with the expected answer, as illustrated in Figure A-4. The results of the inversion in the entire reservoir also reflect this poor estimation.

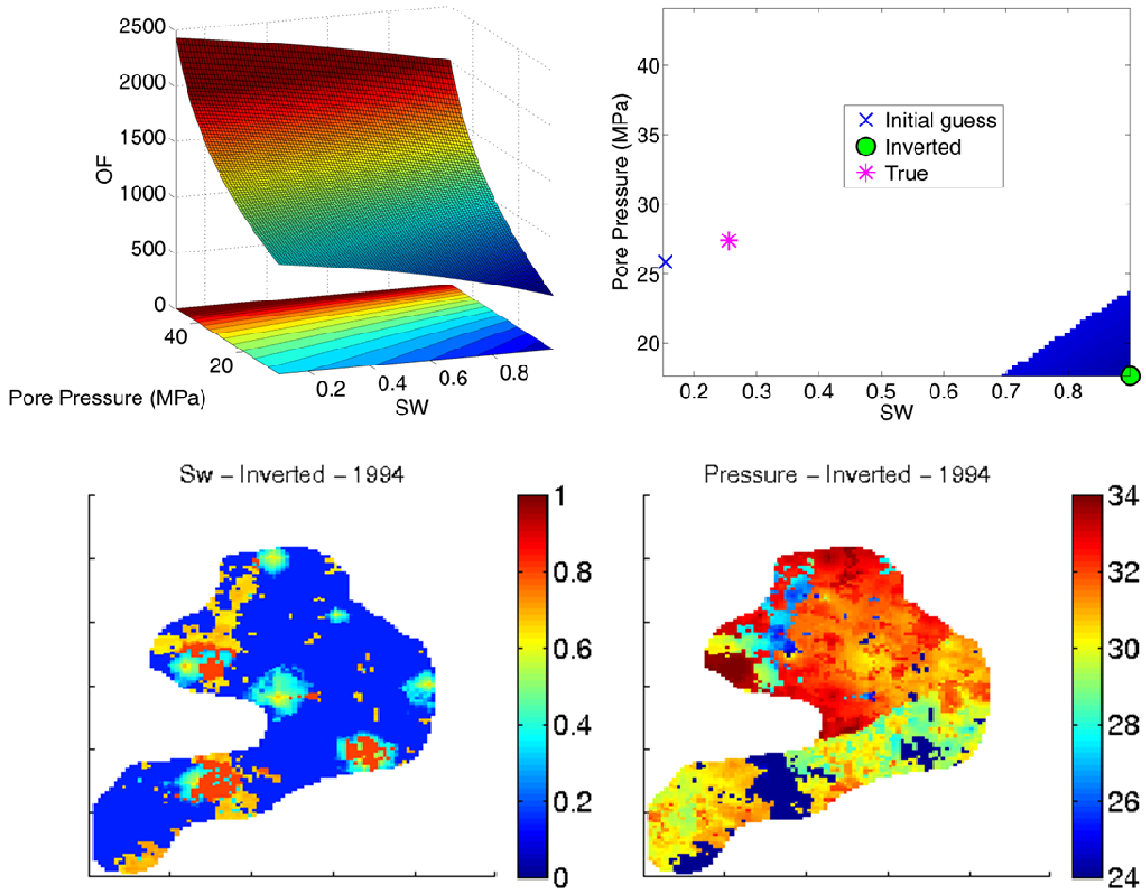


Figure A-4: 3D inversion results assuming P and S impedance in the objective function, $OF=f(IP,IS)$, and an incorrect porosity as input. Top: considering one single reservoir location (extracted from Davolio et al, 2012). Bottom: estimated pressure (MPa) and saturation considering the entire reservoir (extracted from Davolio et al, 2011).

3. 4D approach

The problem of imperfect static properties to be used as input for the petro-elastic inversion can be mitigated by using the 4D approach. The objective function for this case presents a well-defined global minimum again (Figure A-5). As a consequence, the results of the entire reservoir also present acceptable errors. Indeed, these errors are smaller than 6%, as illustrated in Davolio et al, 2011 – Figure 7.

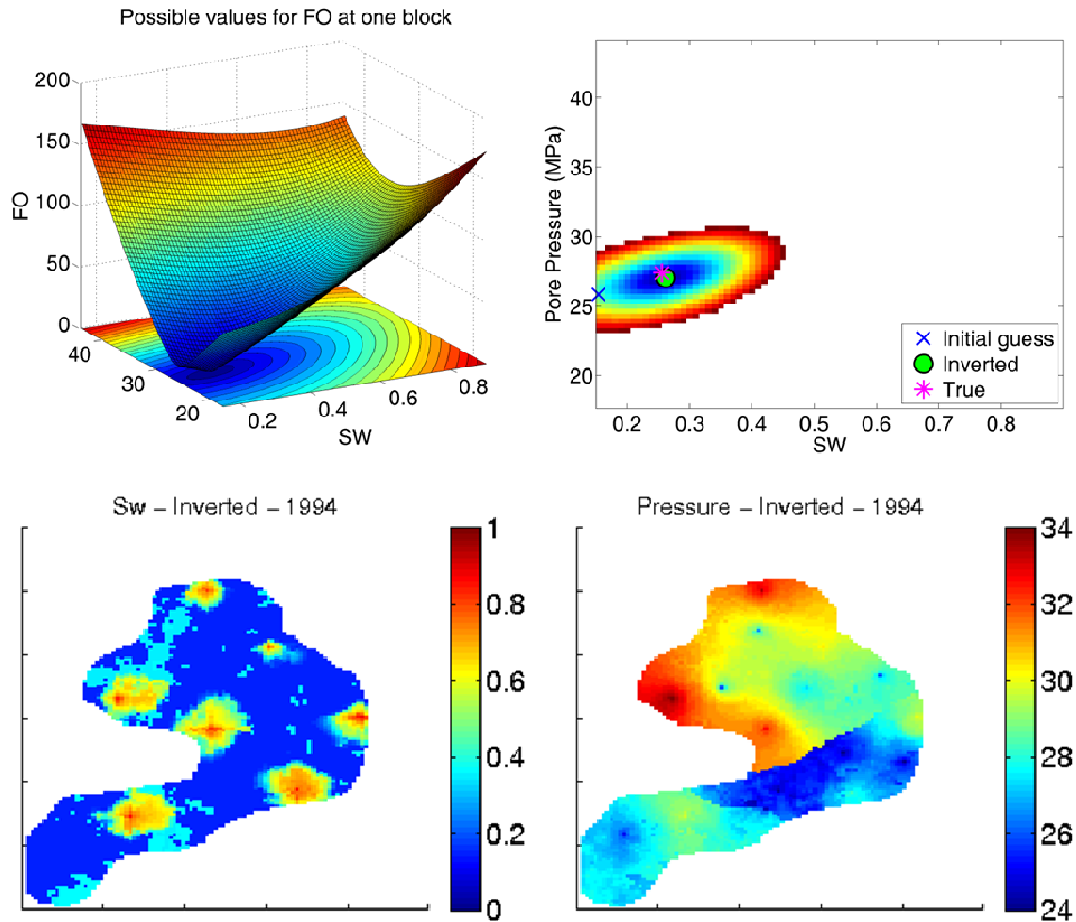


Figure A-5: 4D inversion results, assuming wrong porosity as input. Top: considering one single reservoir location (extracted from Davolio et al, 2012). Bottom: estimated pressure (MPa) and saturation considering the entire reservoir (extracted from Davolio et al, 2011).

4. 4D approach: assuming uncertainties in the initial reservoir conditions

The last result presented here concerns the assumption of knowledge regarding the initial reservoir conditions. The images below were not extracted from Davolio et al (2011)

but were generated with the same dataset presented in that paper. One of the premises of this thesis is that the first seismic survey was acquired in the pre-production period and that pressure and saturation are known at that time, given the equilibrium conditions. In this part of the appendix, an example is presented, where this condition is not satisfied. To illustrate this example, an incorrect facies characterization was considered, which yielded the incorrect initial water saturation (connate water) displayed in Figure A-6b. The initial pressure is not totally correct either, as it is assuming the constant value of 32MPa (Figure A-6d).

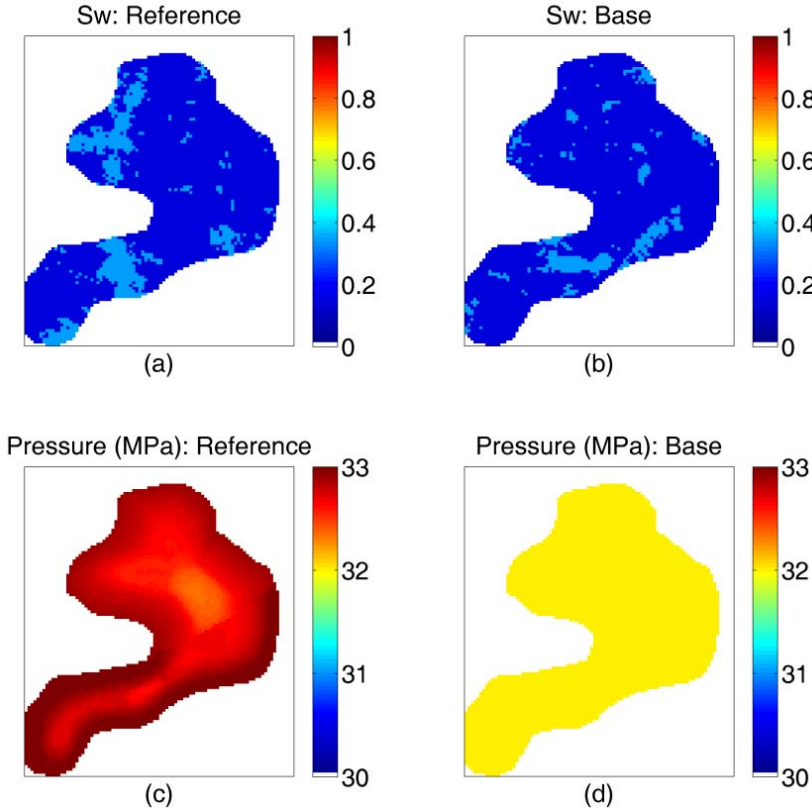


Figure A-6: Water saturation and pressure at the initial time (first survey). (a) and (c) represent the true properties. (b) and (d) represent the available knowledge.

To illustrate the effect of these uncertainties in the inversion process, the other input properties of the inversion were considered correct and no noise was added to seismic data. The inversion results are shown in Figure A-7. Looking at the error at the bottom of the image, it is possible to see that the main problem regarding the saturation map is related to the initial water saturation (compare with Figure A-6). Note that the injection anomalies were properly recovered and that the relevant errors are concentrated at the locations where

the initial saturation was wrong (Figures A-7c). The pressure is also presenting some influence on the error considered at time 0; observe the differences between the expected image (Figure A-1) with the estimated one (Figure A-7b).

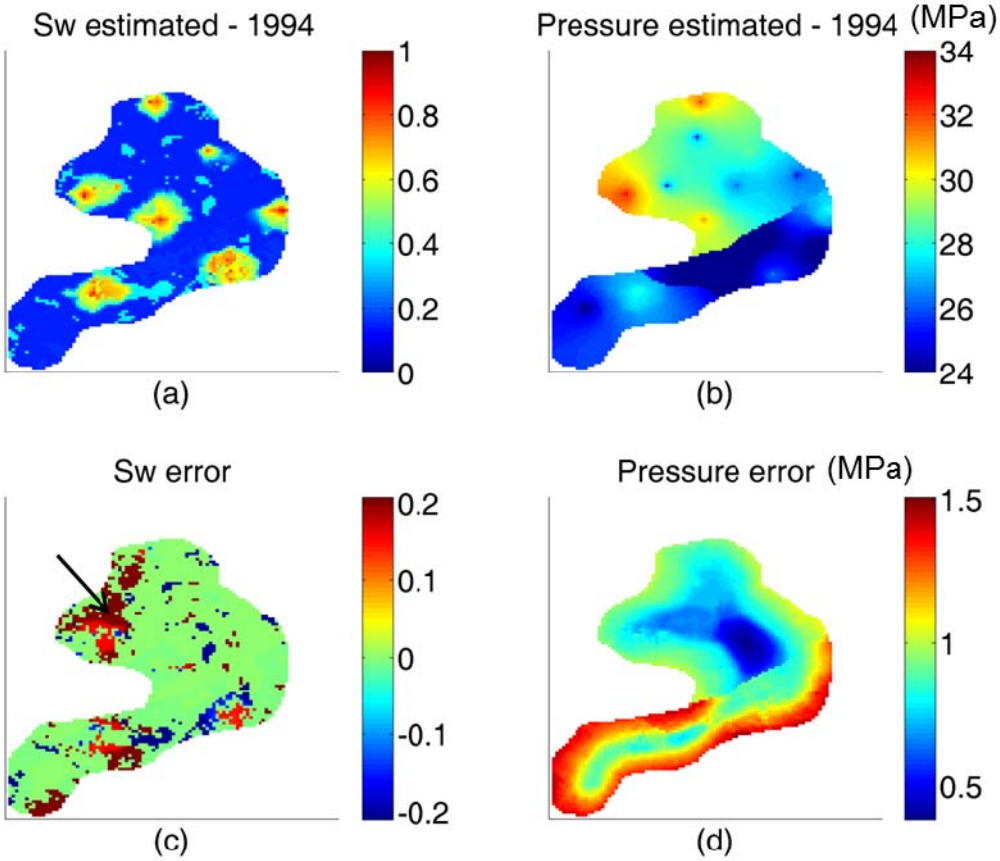


Figure A-7: Estimated saturation (a) and pressure (b) maps for the second seismic survey time. Saturation (c) and pressure (d) errors (estimated – reference).

To visualize the objective function behavior for this case, one point in the reservoir was selected (indicated by the arrow in Figure A-7c) and the same type of analysis shown before was repeated. Figure A-8 shows that, when this type of uncertainty is assumed, the minimum of the objective function does not coincide with the expected answer. This behavior was also observed, in a less pronounced form, in Figure A-5 (where porosity was not totally correct). More generally, it can be said that any source of error considered in the inversion (uncertainties in the static properties, inaccuracy in the seismic impedances etc.) will cause a displacement in the minimum of the objective function, and more problematic cases can yield very wrong estimates of the dynamic properties. Appendix C presents an

example of this kind of situation and how the methodologies of papers 2 and 4 help to improve the estimations.

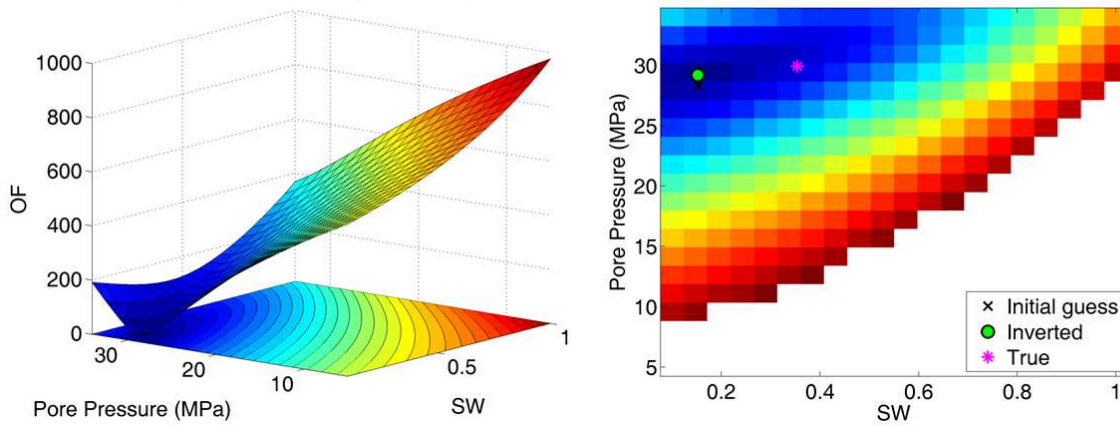


Figure A-8: Objective function behavior for one grid block (indicated in Figure A-7c).

The dynamic properties of the base model (pressure and saturation) are used as input for the inversion. These properties at the initial time (corresponding to the first survey) are kept constant during the optimization process and those corresponding to the second time (second survey) are modified in order to minimize the objective function. Thus, if the dynamic properties at the initial time carry some errors, these errors are reflected in the response of the optimization process, i.e., the estimated pressure and saturation for the second time (remember that the objective function minimizes the time lapse difference). This explains the errors observed in Figure A-7.

However, these errors are substantially diminished when the time lapse difference of the estimated dynamic properties is analyzed, as shown in Figures A-9 and A-10. The true change in saturation and pressure are shown in Figures A-9a and A-10a, respectively. The second column of these images displays the changes observed according to the available information (represented in this work by the so-called Base model) and the third column displays the estimated changes. The errors displayed in Figures A-9e are totally acceptable for saturation and the same can be said for pressure, which yielded error values smaller than 1MPa (Figure A-10e). Thus, Figures A-9 and A-10 show that, even if the properties at the initial time are inaccurate, the pressure and saturation changes are being properly recovered, which is, indeed, the information needed for reservoir monitoring.

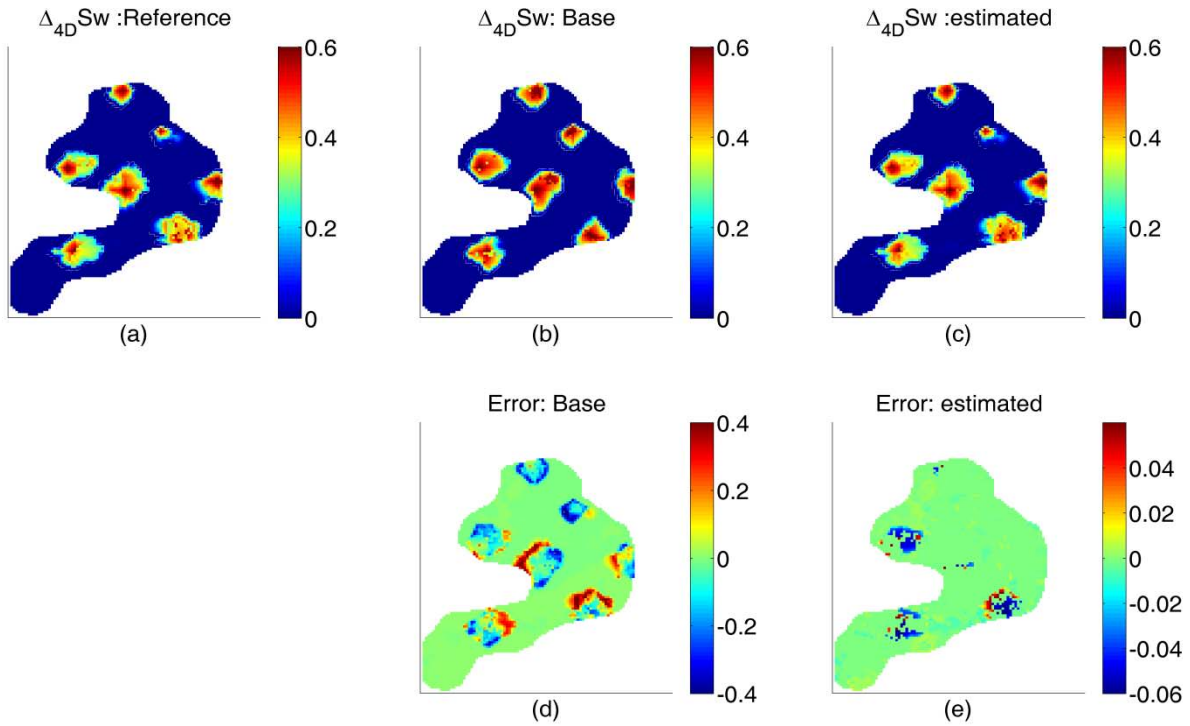


Figure A-9: Time lapse difference of water saturation maps: (a) true answer, (b) base model used as input for the inversion and (c) estimated. Map error: (d) = (b) – (a) and (e) = (c) – (a).

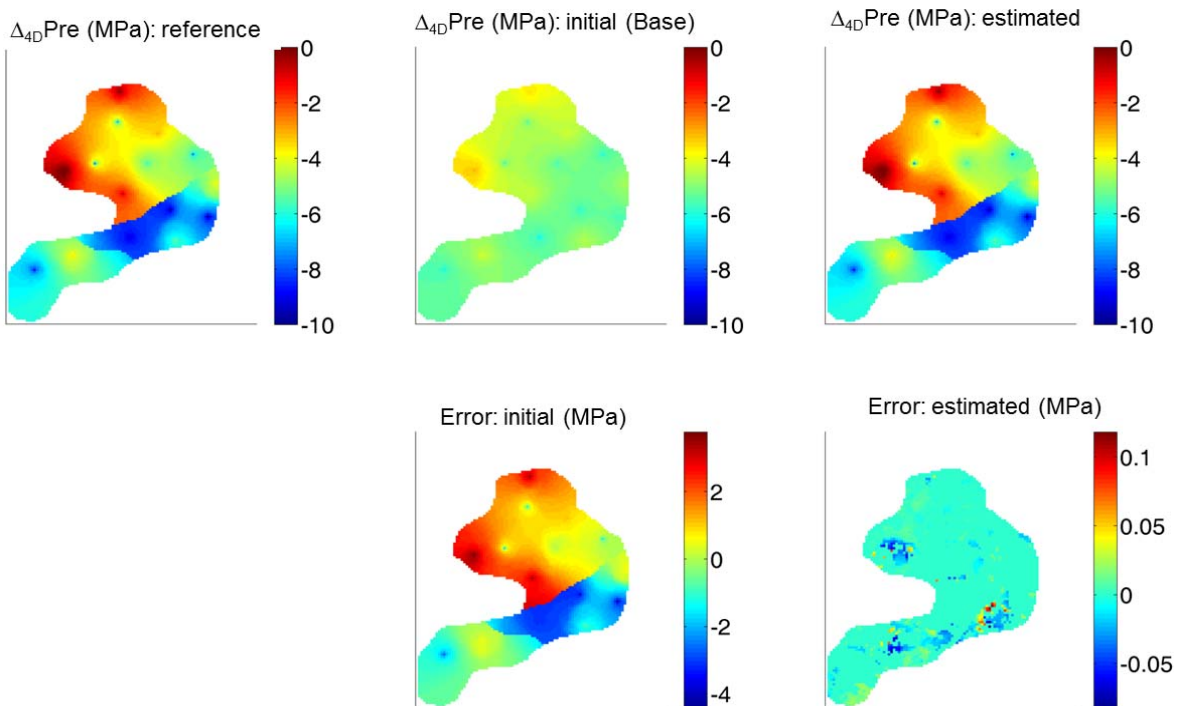


Figure A-10: Time lapse difference of pressure maps: (a) true answer, (b) base model used as input for the inversion and (c) estimated. Map error: (d) = (b) – (a) and (e) = (c) – (a).



SPE 142946

Incorporating 4D Seismic Attributes Into History Matching Process Through An Inversion Scheme

A. Davolio, C. Maschio, D. J. Schiozer, UNISIM - UNICAMP

Copyright 2011, Society of Petroleum Engineers

This paper was prepared for presentation at the SPE EUROPEC/EAGE Annual Conference and Exhibition held in Vienna, Austria, 23–26 May 2011.

This paper was selected for presentation by an SPE program committee following review of information contained in an abstract submitted by the author(s). Contents of the paper have not been reviewed by the Society of Petroleum Engineers and are subject to correction by the author(s). The material does not necessarily reflect any position of the Society of Petroleum Engineers, its officers, or members. Electronic reproduction, distribution, or storage of any part of this paper without the written consent of the Society of Petroleum Engineers is prohibited. Permission to reproduce in print is restricted to an abstract of not more than 300 words; illustrations may not be copied. The abstract must contain conspicuous acknowledgment of SPE copyright.

Abstract

Time-Lapse seismic attributes has been showed as a promising tool to be used in the history matching process. The most common seismic attribute used to integrate these data is P-impedance. The procedure usually made is a minimization of the differences between the seismic P-impedance and the synthetic P-impedance computed from the flow simulation data through a forward modeling. On this paper, we propose a methodology that goes in the opposite way. We invert the seismic data to pressure and saturation and then incorporate these results in the history match procedure in order to integrate the inversion process with the flow simulator, using the results of the reservoir simulation to guide the process. Another feature is that instead of using only the P-impedance in our inversion procedure we are also taking into account a second seismic attribute the S-impedance, which is more sensitive to pressure than saturation variations. A discussion is presented regarding the results obtained using a model with characteristics similar to the Brazilian offshore fields and synthetic seismic data. The main contribution of this work is the integration of the seismic attributes inversion and reservoir simulation processes. We also show the advantages of the inversion procedure to obtain pressure and saturation considering prediction of petroleum production and the details used in the methodology to avoid multiple combinations of saturation and pressure in the inversion process.

Introduction

Traditional history matching uses production and pressure data measured in the wells, such as oil, water and gas rate, flowing and static pressures etc, for conditioning of reservoir simulation model in order to reproduce the observed data. The utilization of survey seismic derived data, such as pressure and saturations maps, in the history matching is relative new. Although this practice is relative new it has become increasingly common due to the improvement generally observed when it is compared to the traditional workflow using only production data. Gosselin et al (2001) and Gosselin et al (2003) presented a methodology in which the fluid flow simulator was coupled with a petro-elastic model to convert the simulated saturation/pressure and static rock properties into simulated elastic properties and run the history matching on the elastic domain. Kjelstadli (2005) showed the use of seismic surveys acquired through permanent ocean-bottom seismic cables. Sedighi and Stephen (2009) worked on a fast method based on neighbourhood algorithm using time-lapse seismic to effectively condition saturation and pressure changes in history matching. Dadashpour (2009) proposed a computer aided history matching methodology for porosity and permeability estimation integrating production and time-lapse seismic data in the form of zero offset amplitudes and amplitude versus offset (AVO) gradients. Another work that concerns integration of 4D seismic data into the history matching process by a forward modeling is Ida (2009), where the author proposes a methodology that matches the data in the elastic domain, adjusting impedance maps. Thus, there are several ways to integrate these two set of data, Fahimuddin et al (2010) addressed this question presenting a discussion regarding which kind of seismic data and at which level of history matching process these data should be integrated. The authors compare the integration of seismic data in the elastic and amplitude domains and conclude that the elastic domain performs better than the other one.

Most of the works found in the literature utilize the acoustic impedance or seismic amplitudes in the history matching process through a forward petro elastic modeling and the matching is done in the seismic domain (elastic or amplitudes). The idea of using pressure and saturation maps, the purpose of second part of this work, has as main motivation on the use of reservoir parameters as input of the process, which it seems to be a more natural way from the point of view of reservoir behavior understanding. The point is that extracting pressure and saturation information from seismic data is not a trivial task. It can be found in the literature several works aiming to recovery dynamic properties from 4D seismic data. Tuna and Lumley

(1999) showed that it is possible to estimate changes on pressure and saturation through P-wave and S-wave impedances seismic derived. On Landro (2001) the author derived mathematical expressions that can be used to extract pressure and saturation changes using 4D AVO data, he also shows that the application of his technique to real 4D seismic data was made successfully. Later on the work of Nunes et al (2009) shows an application of Landro's (2001) method in a real Brazilian field, with good results. MacBeth et al (2006) also proposed a methodology to identify pressure and saturations changes using time lapse seismic amplitudes. The work of Dadashpour et al (2008) presented a petro-elastic inversion methodology that uses zero offset 4D seismic amplitudes to recovery pressure and saturation changes. Following this line, this work presents a methodology that estimates pressure and saturation from P and S impedances through a petro-elastic inversion. Then on the second part, these estimated dynamic properties are coupled into history matching process.

Petro-elastic modeling

The methodology proposed in this work is divided in two parts, the first one attempt to generate saturation and pressures maps inverting seismic attributes and the second one attempt to use these data in the history matching process.

The inversion algorithm is made through an optimization procedure where the differences between the seismic attributes and the simulation derived seismic attributes are minimized. To generate seismic attributes from simulation data, a petro elastic modeling (PEM), which is a set of relationships that relates fluid/rock and elastic properties, is required. Follows below the relationship that composes the PEM considered in this work.

The seismic attributes that are used in the inversion are compressional and shear impedances, also called P-impedance (IP) and S-impedance (IS), respectively. Considering ρ , V_p and V_s the density, compressional and shear wave velocities of the medium the impedances can be written as:

$$IP = V_p \rho, \quad (1)$$

$$IS = V_s \rho. \quad (2)$$

Seismic velocities depend on rock saturated bulk (K_{sat}) and shear (μ_{sat}) modulus according to the equations:

$$V_p = \sqrt{\frac{K_{sat} + \frac{4}{3}\mu_{sat}}{\rho}}, \quad (3)$$

$$V_s = \sqrt{\frac{\mu_{sat}}{\rho}}. \quad (4)$$

The most used theoretical approach to determine the rock saturated bulk and shear modulus are the Gassmann equations that can be described as follows (Avseth et al. 2005):

$$K_{sat} = K_{dry} + \frac{(1 - \frac{K_{dry}}{K_{min}})^2}{\frac{\phi}{K_{fl}} + \frac{1 - \phi}{K_{min}} - \frac{K_{dry}}{K_{min}^2}}, \quad (5)$$

$$\mu_{sat} = \mu_{dry}, \quad (6)$$

where K_{dry} , K_{min} and K_{fl} are the bulk modulus of the rock frame, the mineral and the fluid mixture. μ is the shear modulus and ϕ is the porosity. Note that Gassmann equations predict that the rock bulk modulus change if the fluids change, but the rock shear modulus do not.

To compute the dry bulk and shear modulus the known friable, or uncemented, sand model (Mavko et al. 2003) is used in this work. This model makes use of the Hertz-Mindlin contact theory and a heuristic modified Hashin – Strikman lower bound, according to the equations:

$$K_{dry} = \left[\frac{\phi/\phi_c}{K_{HM} + 4\mu_{HM}/3} + \frac{1 - \phi/\phi_c}{K + 4\mu_{HM}/3} \right]^{-1} - \frac{4}{3}\mu_{HM}, \quad (7)$$

$$\mu_{dry} = \left[\frac{\phi/\phi_c}{\mu_{HM} + z} + \frac{1 - \phi/\phi_c}{\mu + z} \right]^{-1} - z, \quad (8)$$

where

$$z = \frac{\mu_{HM}}{6} \left(\frac{9K_{HM} + 8\mu_{HM}}{K_{HM} + 2\mu_{HM}} \right), \quad (9)$$

being that K_{HM} and μ_{HM} are the bulk and shear modulus at critical porosity ϕ_c given by the contact Hertz-Mindlin theory,

$$K_{HM} = \left[\frac{n^2(1-\phi_c)^2\mu^2}{18\pi^2(1-\nu)^2} P_{eff} \right]^{\frac{1}{3}}, \quad (10)$$

$$\mu_{HM} = \frac{5-4\nu}{5(2-\nu)} \left[\frac{3n^2(1-\phi_c)^2\mu^2}{2\pi^2(1-\nu)^2} P_{eff} \right]^{\frac{1}{3}}, \quad (11)$$

where P_{eff} is the effective pressure; μ and ν are the mineral shear bulk modulus and Poisson ratio and n is the coordination number.

Proposed Petro-elastic inversion

The link between simulation and seismic data is done through the equations presented above, i.e., given saturation/pressure pairs provided by simulation and rock and fluids properties the elastic parameter such as P and S impedances can be computed through forward modeling. So, in the opposite direction the inversion is done when the elastic parameters are provided and the dynamics properties are estimated.

The minimization of the objective function is carried out through an optimization algorithm based on numerical gradients computation and sequential quadratic programming, available in MatLab software (*fmincon*). In this work three different approaches of the objective function is presented. The main objectives are to verify the improvement when more than one seismic attribute is used into the objective function and also how to handle time lapse data set into that.

For the first two algorithms proposed the objective function can be generally described as:

$$OF = \|SA^{obs} - SA^{cal}\| \quad (12)$$

where *obs* and *cal* stands for observed and calculated, respectively; SA means seismic attribute, which can be $SA=IP$ or the vector $SA = [IP \ IS]$.

The objective function of the third algorithm is given in terms of dSA instead of SA which means time lapse difference of the seismic attributes so,

$$OF = \|dSA^{obs} - dSA^{cal}\| \quad (13)$$

where again d is the 4D difference between two vintages and the vector dSA is defined as $dSA = [dIP \ dIS]$.

In order to better control the inversion scheme synthetic seismic data is used, so the petro elastic modeling will be also used to generate the synthetic seismic attributes. To do so two simulation models have to be considered, the one used to create the synthetic seismic, called reference model and the second one called base model that represents the model we want to adjust.

Pressure and saturations derived from the base model simulation are used as initial guess to all inversion algorithms and the inversion is run for each reservoir model cell independently.

Algorithm 1: inversion algorithm using IP

The first algorithm built follows the ideas presented in (Souza et. al, 2010). The main input data for this algorithm are the observed seismic P-impedance (in equation 12, $SA=IP$) and the initial guess. Before running the inversion the base model (the one that will be adjusted) is simulated and the pressure and saturations values estimated are used as initial. Then, using the petro elastic modeling the optimization algorithm finds the saturation and pressures values that best match the two P-impedances, the one coming from seismic and the one computed from the simulation data.

Assuming that the initial reservoir conditions are known the inversion aims to work only with the second production time, so the algorithm uses only one time production data.

Algorithm 2: inversion algorithm using IP and IS

As stated in (Souza et. al, 2010) estimating pressure and saturation from P-impedance end up in a no uniqueness problem. In order to better handle this issue the second algorithm we propose incorporate more seismic information into the inversion process. The use of two different kind of seismic data simultaneously (P and S impedances), instead of only using the well known P-impedance, helps to differentiate between pressure and saturation effects since these attributes have different answers when the dynamic properties change (Tuna et al, 1999). One reason for this difference is that S-impedance is not as

sensitive to fluids change as P-impedance, remembering that shear modulus does not depend on pore fluids contents as mentioned before. So, the 4D changes observed on shear impedance data should be more related to pressure than saturation and that makes the difference compared to the P-impedance, which is sensitive to both effects. Figure 1 shows this behavior, where it can be seen that big changes for saturation yields very small changes in IS, the opposite is observed for IP. The values of IP and IS shown on figure 1 were calculated through the petro elastic modeling previously presented, so it represents the sensitivity of the elastic properties to pressure and saturation changes considering those relationships.

Following the same scheme defined in algorithm 1, the difference now is that SA in the objective function (equation 12) is the vector $SA=[IP \ IS]$. The same assumption about the date considered in the previous algorithm is used here and the whole procedure is done with only one seismic survey.

Algorithm 3: inversion algorithm using IP and IS and a 4D approach

One of the best arguments to work with time lapse seismic data is that making the difference between two vintages allows mitigating the effect of noise, or uncertainty in the reservoir properties when synthetic seismic needs to be modeled. Following our study, if we start to consider uncertainties in the reservoir model the two algorithms presented before may fail. To try to overcome these issues the third algorithm proposes to minimize the 4D impedances differences. This code, as the one defined before, keeps the use of both impedances (IP and IS) into the objective function and a different aspect compared to the previous methodology is that now the evaluation of 4D differences requires two seismic surveys as input data. Here the objective function is defined by equation 13.

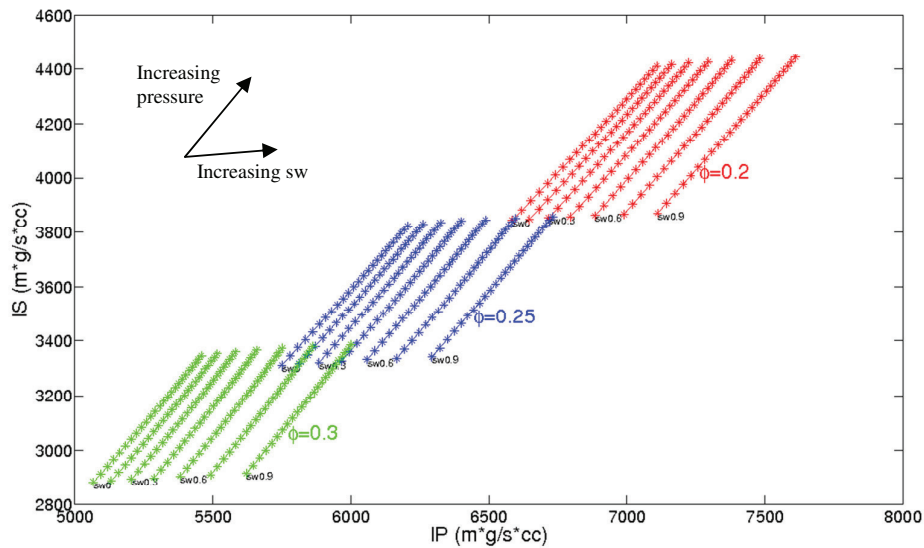


Figure 1- P and S impedances sensitivity to saturation and pressure changes, considering three values of porosity (0.2, 0.25 and 0.3). Note that S-impedance is almost insensitive to saturation effects.

Constraints

All the inversion procedures are limited by known boundaries that come from engineering data. The water saturation values are constrained by connate water saturation and one minus irreducible oil saturation:

$$S_{wc} \leq S_w \leq 1 - S_{or} \quad (14)$$

The water saturation boundaries vary according to the facies reservoir distribution.

As no gas will be considered another constraint applied to S_w is that the sum of the oil and water saturations is equal to one,

$$S_o + S_w = 1 \quad (15)$$

For the pressure range we are assuming the pressure bubble point and the overburden pressure,

$$P_{bub} \leq P \leq P_{over} \quad (16)$$

As this work concerns only synthetic seismic data we are not dealing with scaling issues.

Model description

The reservoir was discretized in a corner-point grid with 90×110×5 blocks, 60 meters in size in x and y direction (5400 m × 6600 m) and 15 meters (in average) in z direction. The model was generated through geostatistical techniques. There are three facies characterized according to three permeability ranges. The reservoir also comprises four faults, as can be seen in Figure 2. The transmissibility of each fault was included as uncertain attribute in the study. The reservoir is drained by eight vertical producer wells supported by seven water injector wells. A reference reservoir model (chosen from the possible combinations of the 16 uncertain attributes) was simulated to generate a history of 3600 days. The description of the 16 attributes considered is shown in Table 1. For the generation of Base model, multiplier values for the parameters 1 to 9 was set to 1. For the four faults (parameters 10 to 13), multipliers equals to 0.5 were used. For relative permeability (parameters 14 to 16), exponent of water phase (Corey Model) was set to 3. Oil rate of the production wells and water rate of the injection wells (obtained from the reference model - history) are imposed to the Base model.

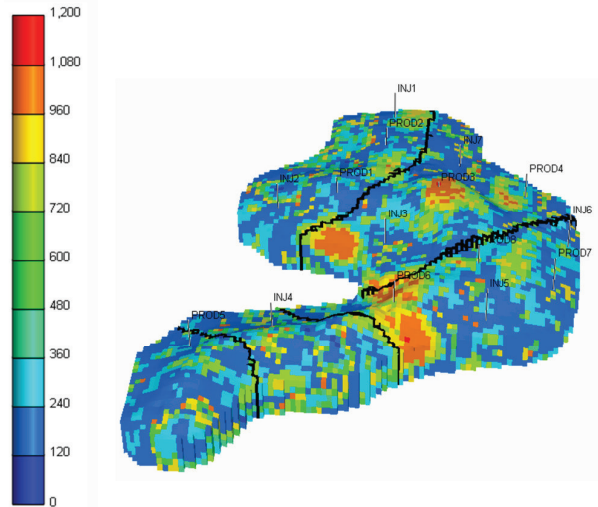


Figure 2 - Horizontal permeability (mD) of model studied

Table 1 - Description of the model parameters

Attribute number	Description	Type	Min	Max
1 to 3	Porosity	Multiplier	0.85	1.15
4 to 6	Horizontal Permeability (Kx)	Log Multiplier	0.75	1.1
7 to 9	Vertical Permeability (Kz)	Percent of Kx (%)	4	25
10 to 13	Fault transmissibility	Multiplier	0	1
14 to 16	Relative permeability	Exponent of water phase (Corey Model)	1	5

Concerning time-lapse seismic data, it will be considered as the base data the synthetic seismic generated from the reference simulation model at the initial production time (year 1990), when no fluids neither pressure changes has occurred. The monitor surveys will be assumed after 4 and 8 years of production, represented by the years 1994 and 1998 of the same simulation model. All the inversion schemes proposed aim to find pressure and saturation values for the monitor surveys.

Application: Petro-elastic Inversion

Remembering that the static reservoir properties used as input to run the petro elastic model, such as porosity, fluid properties, compressibility, etc, were the same for both models (base and reference), when we apply the inversion procedures proposed we are evaluating the possibility of recovery pressure and saturation information from seismic attributes assuming we know these static reservoir parameters. Figure 3 shows the saturation and pressure maps for the reference model for the third layer after four years of production, these data were used to generate the seismic impedances and they represent the answer we want to reach.

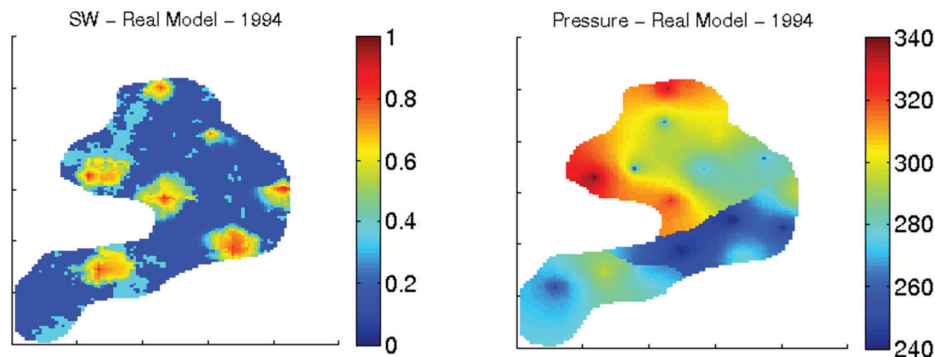


Figure 3 – Water saturation and pressure (kgf/cm2) maps of layer 3 of the reference model after four years of production.

Algorithm 1

Application of Algorithm 1 intends to show how much information about pressure and saturation effects it is possible to recovery when only P-impedance data is available. Figure 4 shows the results for the third layer of the model. Comparing qualitatively these maps with the ones shown on Figure 3 it can be noticed that the inversion algorithm was not able to capture the water saturation anomalies. Also, the pressure map presented some influence of the saturation behavior showing that the effects of both dynamic properties could not be properly differentiated from P-impedance data. Although some information especially about the pressure field could be recovered the results were not very satisfactory.

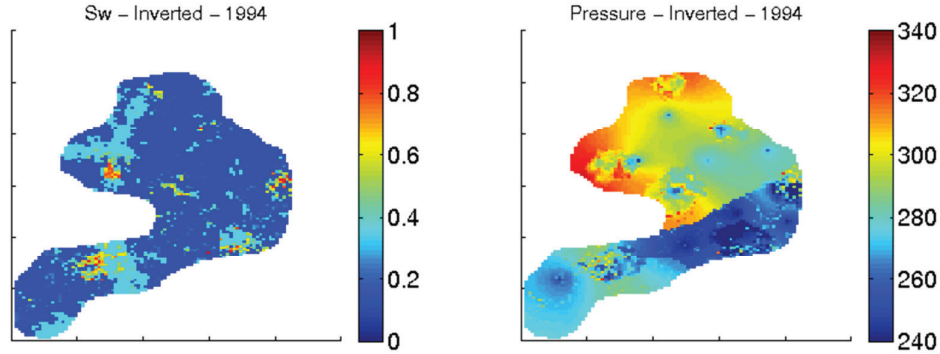


Figure 4 - Inverted water saturation and pressure (kgf/cm²) maps of the third reservoir layer at year 1994. Results obtained by the application algorithm 1.

Algorithm 2

This second case aims to evaluate the contribution of shear impedance for the inversion when it is included into the objective function. Incorporation of this new seismic attribute is the only difference between the results provided by running algorithm 2 and the ones obtained through algorithm 1. Observing Figure 5 we clearly see the improvement of the inversion results when IS is considered together with IP in the objective function, showing that now the inversion was able to discriminate pressure and saturation effects. Further, the error maps shown in the same figure reveals that the results were very close to the answer we wish to reach, giving a percentage error < 1%. This means that the problem of non-uniqueness was reduced by incorporating IS into the process.

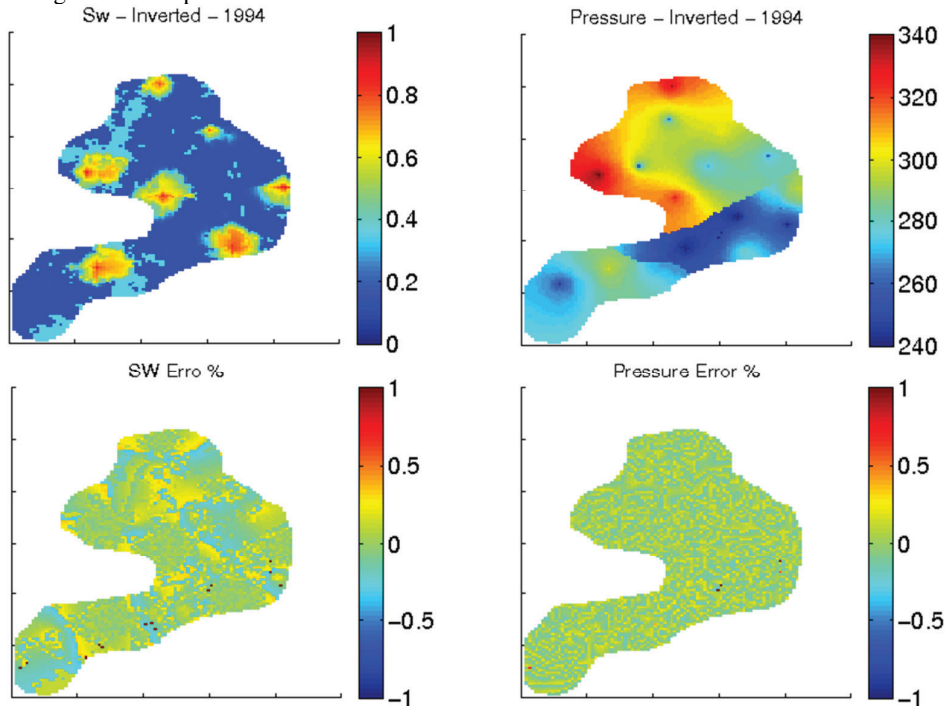


Figure 5 - On top: inverted water saturation and pressure (kgf/cm²) maps of the third reservoir layer at year 1994. On bottom: percentual error maps. Results obtained by the application algorithm 2.

Algorithm 2 – applied in a modified porosity model

Knowing that the use of both impedances improves the inversion algorithm response being quantitatively close to the solution, we start to consider uncertainties in the reservoir base model. The generation of seismic attributes was done exactly as before, using the reference model. However the base simulation model is now composed by a modified porosity field, where a constant multiplier was applied to it. So, the inversion algorithm uses this modified porosity field as input and the simulated pressure and saturations values used as initial guess were generated incorporating this change. This case would be closer to a field case, where the reservoir simulation model does not accurately represent the real porosity values. Saturation and pressure maps resulted from this case can be seen on Figure 6.

We do not even need to look at the error maps to realize that this small change in one reservoir property messed up the inversion process, yielding results very far from the expected. This result shows the instability of the process when recovering saturation and pressure information by a petro elastic inversion. A good sign is that the general trend was kind of recovered, what means that some improvements could be done in the process to guide the inversion and produce better results.

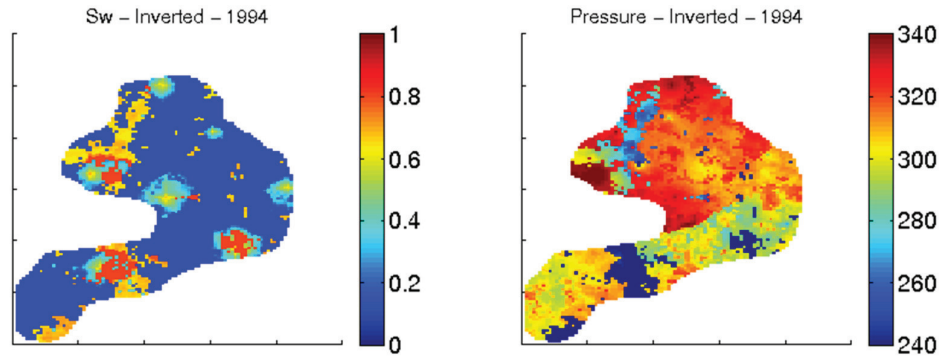


Figure 6 - Inverted water saturation and pressure (kgf/cm²) maps of the third reservoir layer at year 1994. Results obtained by the application algorithm 2 considering a modified porosity field in the base model.

Algorithm 3 – applied in a modified porosity model

In the previous application it was noted the instability of the inversion when the porosity field is disturbed. This third algorithm we are proposing deals with this issue by defining the objective function concerning time lapse differences. As mentioned before this methodology is based on a minimization between the 4D differences of the seismic and simulation derived impedances, where the main objective is to mitigate the error in the porosity field by subtracting the seismic attributes.

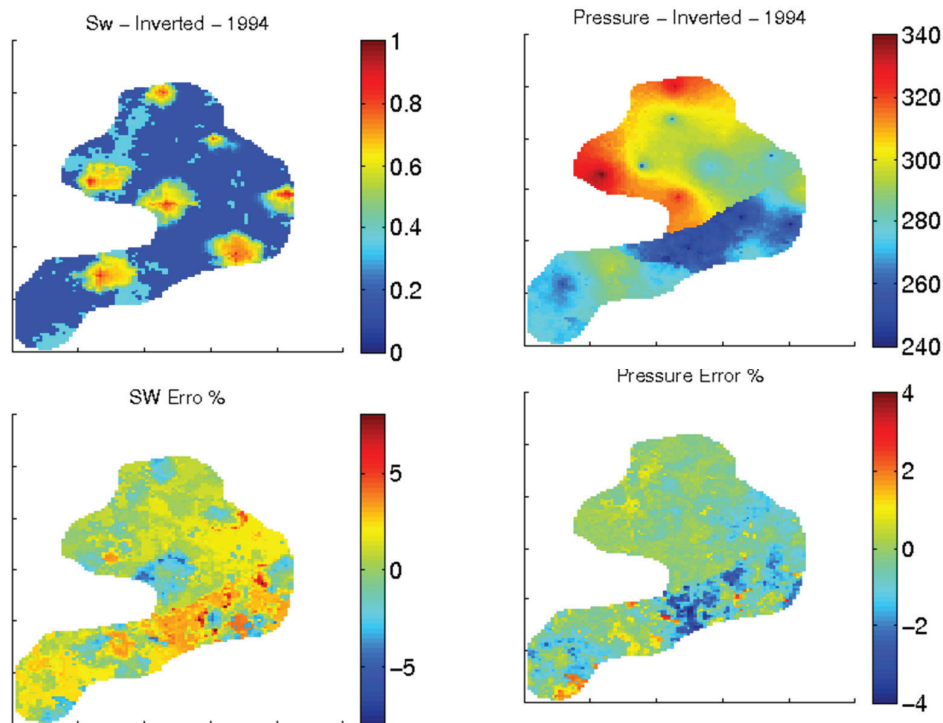


Figure 7 - On top: inverted water saturation and pressure (kgf/cm²) maps of the third reservoir layer at year 1994. On bottom: percentual error maps. Results obtained by the application algorithm 3 considering a modified porosity field in the base model.

The application of this methodology requires a minimum of two seismic vintages. Remember that in this work the base survey corresponds to the initial state of the field, i.e., the production has not started. The results for this case are illustrated on Figure 7 and as it can be seen the 4D approach really improves the inverted saturation and pressure maps, mitigating the effect of inaccuracy in the porosity field. The errors are now acceptable (see the bottom of the same figure) presenting values less than 6%.

Comparing the results shown so far one can say that the use of S and P impedance together allows to quantitatively recovery pressure and saturations information. If uncertainties in the reservoir static properties are considered, the 4D difference of seismic attributes helps to minimize this error on the inversion results. On the second part of this work the results provided by the application of algorithm 3 are used in the history matching process as described below.

History matching

Saturation and pressure maps obtained from the application of Algorithm 3 are used in the history matching process. The minimization of the objective function is carried out through an optimization algorithm based on numerical gradients computation and sequential quadratic programming, available in MatLab software (*fmincon*). The objective function is mathematically represented by the Equation 17:

$$OF = w_p \frac{1}{s} \sum_{j=1}^s \left[D_p / (D_p)_B \right] + w_m \left[Ems / (Ems)_B + Pms / (Pms)_B \right] \quad (17)$$

in which

$$D_p = \sum_{i=1}^n (obs_i - sim_i)^2, \quad Ems = \sum_{k=1}^b (Sobs_k - Ssim_k)^2 \quad \text{and} \quad Emp = \sum_{k=1}^b (Pobs_k - Psim_k)^2$$

In Equation 17, obs_i and sim_i represent observed and simulated production data, respectively, n is the number of production data and s is the number of data series (well water rate, for example) and w_p is a weight factor for production data. $Sobs$ and $Ssim$ are observed and simulated saturation maps and $Pobs$ and $Psim$ are observed and simulated pressure maps, w_m is a weight factor for pressure and saturation data and b is the number of grid blocks. D_p , Ems and Emp are differences related to production data, saturation and pressure maps, respectively. Remembering that observed pressure and saturation maps considered here is those ones obtained from the inverse procedure (Algorithm 3).

The subscript "B" in previous equations represents quantities (differences) computed for Base model. Therefore, the division by Base model quantity represents normalization in order to combine data with different magnitude (production rates, pressure and saturation maps) in the objective function. This signifies that if a given modified model has a OF value greater than 1, it has a match worse than the Base case. Conversely, if OF is lower than 1, the model has a match better than the Base case.

Eight situations considered in the history matching process are shown in Table 2. The processes are classified according to the following three aspects: (1) the amount of data considered in the history period (2940 and 3600 days); (2) the composition of the objective function (with and without the use of the pressure and saturation maps and (3) the number of parameters considered in the history matching. In the third one, the objective is to show, in a simplified way, how pressure maps can be used to identify reservoir compartmentalization, in this case, the pressure error maps (Figure 8) reveals clearly the presence of the two sealing faults (transmissibility multipliers near from zero in the reference model). Therefore, the history matching processes with 16 parameters consider the presence of these two faults and the processes with 14 parameters do not consider. The objective function was composed by water rate of the eight producer wells plus four maps: pressure and saturation for 1470 and 2940 days.

Table 2 - Description of the history matching processes

History matching process	History (days)	Objective function	Parameters
HM16P_2940	2940	Production	16
HM16P_3600	3600		
HM16PM_2940	2940	Production + pressure and saturation maps	
HM16PM_3600	3600		
HM14P_2940	2940	Production	14
HM14P_3600	3600		
HM14PM_2940	2940	Production + pressure and saturation maps	
HM14PM_3600	3600		

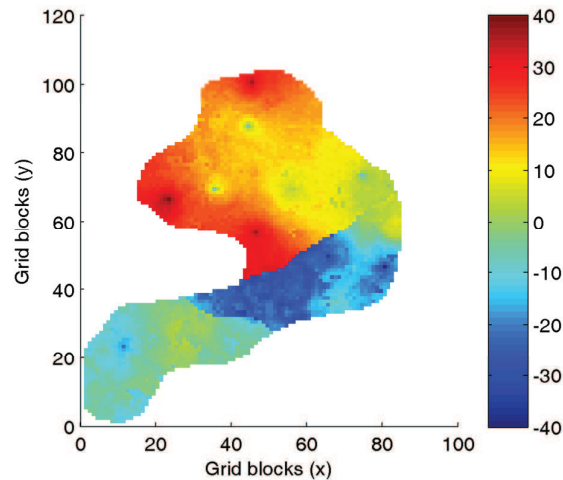


Figure 8 - Difference in pressure map (1470 days) related to the Base model (Observed-Base)

The water rate of 4 wells of the best model resulted from the Processes “HM16PM_2940” and “HM16P_2940” (with and without the use of pressure and saturation maps in the objective function, respectively) is shown in Figure 9. The difference in saturation maps related to the best model is shown in Figure 10. Both analysis show that the use of pressure and saturation maps in the objective function produced better results. Regarding the convergence of the minimization process, it can be observed in Figure 11-a that HM16PM_2940 used more simulation, however, the reduction of the objective function was much higher.

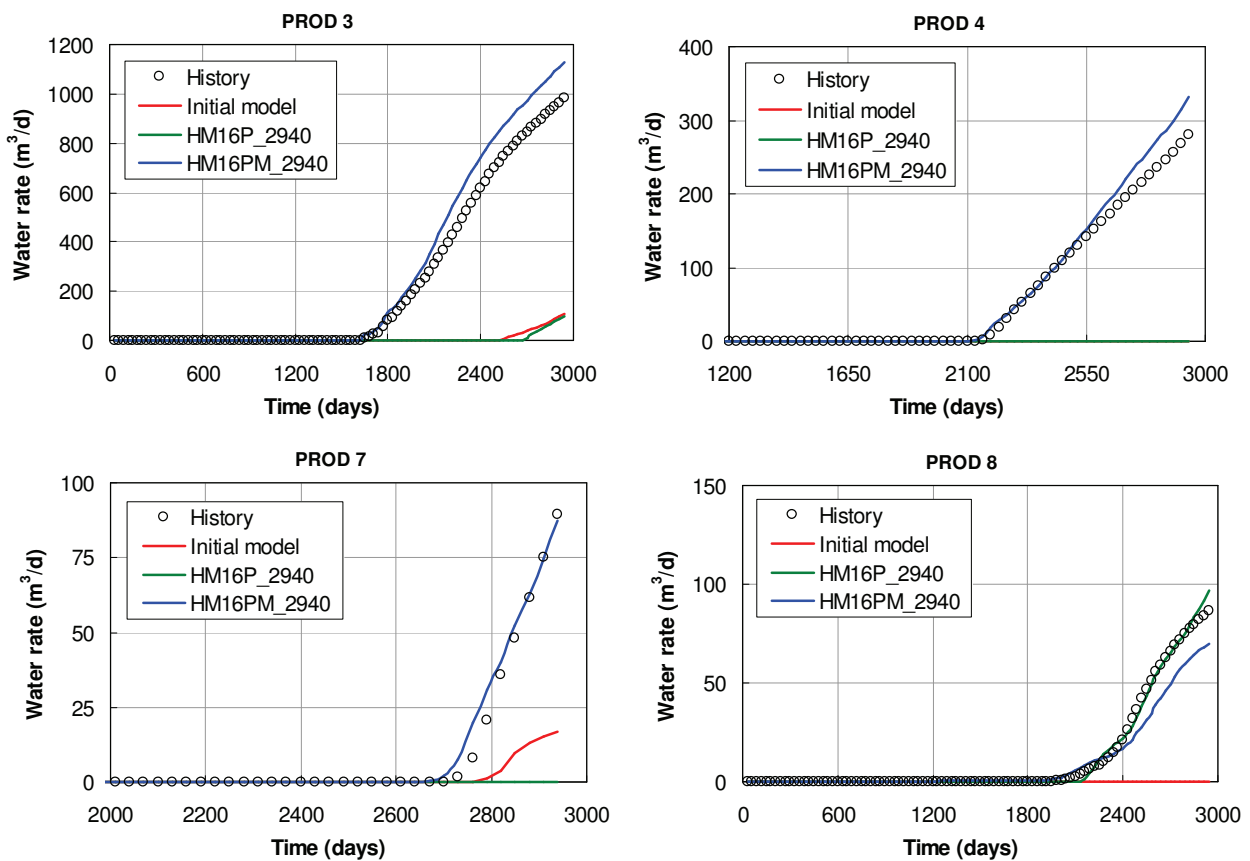


Figure 9 - Wells water rate: comparison of history matching processes with (HM16PM_2940) and without (HM16P_2940) pressure and saturation maps in the objective function

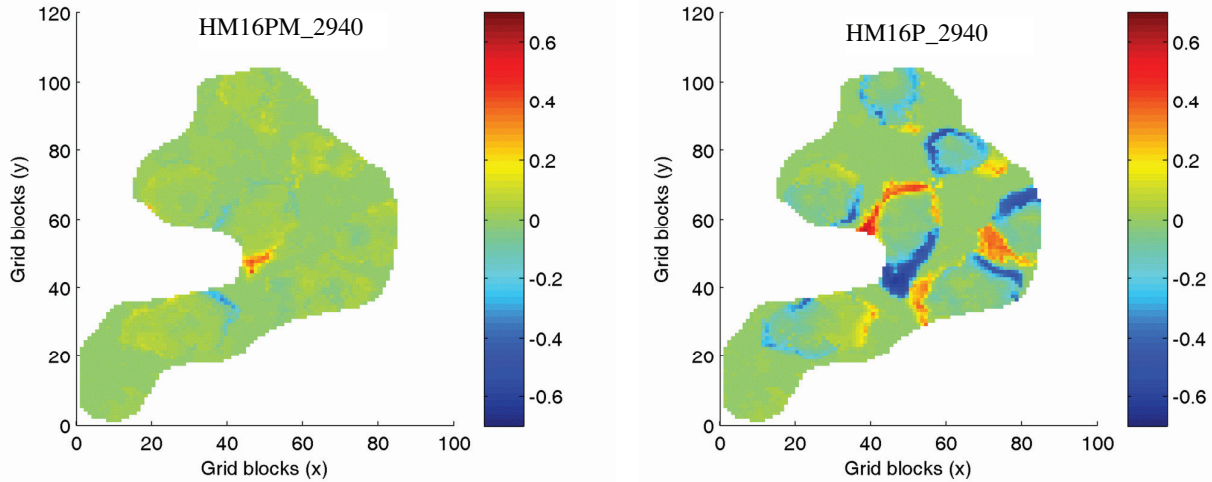


Figure 10 - Difference in saturation maps related to the best solution: comparison of history matching process with (HM16PM_2940) and without (HM16P_2940) pressure and saturation maps in the objective function

In Figure 12 is presented results from the history matching process considering 3600 days of production. In this case, the increase in amount of production data improves the results for well PROD7 obtained from the process using only production data in the objective function. However, the number of simulation was greater as can be seen in the convergence behavior (Figure 11-b) and the reduction of the objective function was smaller. It can also be seen from Figure 11 that the use of pressure and saturation maps in the objective function stabilizes the optimization process, considering the similar number of simulations and similar (and expressive) reduction of the objective function in both cases (2940 and 3600 days). A summarized quantitative analysis of the best solution of each history matching process is shown in Table 3. As would be expected, the assumption of 14 parameters (without the two sealing faults) gives a worse result, mainly for the wells PROD4 and PROD7, near the region comprising the sealing main fault.

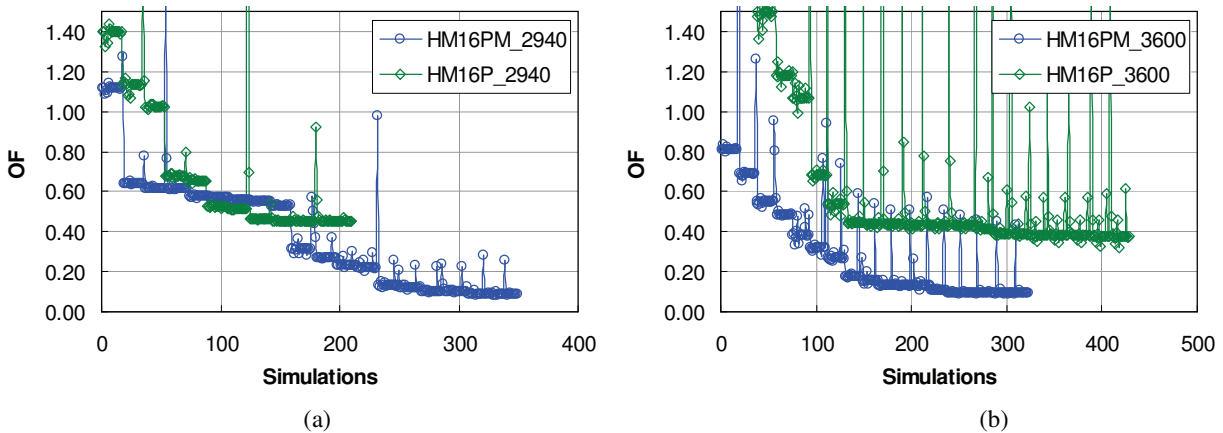


Figure 11 - Comparison of the convergence behavior of four minimization processes

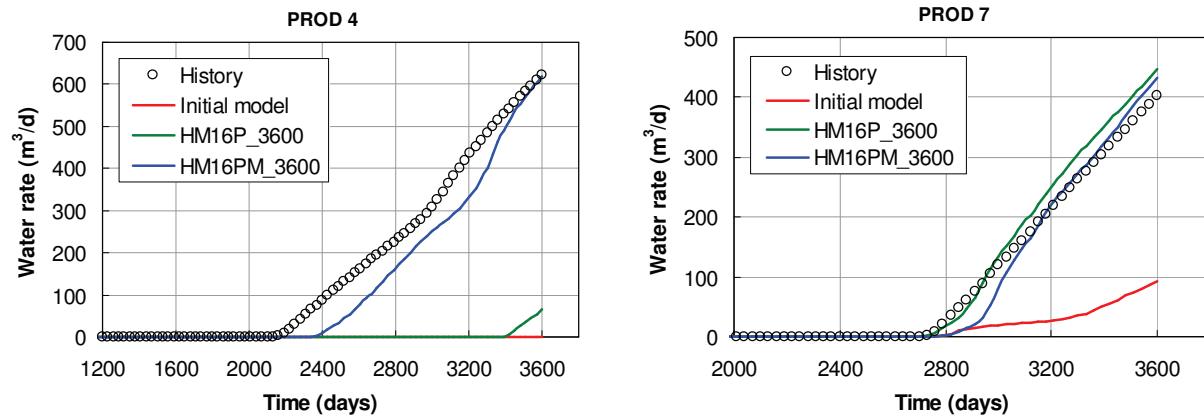


Figure 12 - Wells water rate: comparison of history matching processes with (HM16PM_3600) and without (HM16P_3600) pressure and saturation maps in the objective function

Table 3 - Summarized quantitative analysis of the best solution of each history matching process

Process	Difference (%) in production data ($(1-Dp/DpB) \times 100$) for the producers wells								Difference (%) in saturation and pressure maps ($100 \times (1-E_{ms}/E_{msB})$ and $100 \times (1-E_{mp}/E_{mpB})$)			
	P1	P2	P3	P4	P5	P6	P7	P8	Sw1470	Sw2940	P1470	P2940
HM16P_2940	74.6	97.1	-2.8	0.0	96.1	64.9	-51.6	99.5	-5.4	3.0	-16.4	33.4
HM16P_3600	95.4	93.8	77.0	4.9	96.2	-1007.0	97.3	98.4	59.5	58.7	62.9	86.6
HM16PM_2940	85.9	95.5	96.5	97.9	99.4	78.1	97.7	94.4	90.8	89.5	92.0	88.7
HM16PM_3600	97.4	99.3	93.1	96.2	76.8	10.4	98.0	92.8	68.4	45.4	73.4	73.5
HM14P_2940	67.4	96.1	32.8	0.0	97.3	-60.0	-51.6	96.4	9.3	-13.2	-3.5	47.3
HM14P_3600	8.9	23.5	2.9	0.0	96.8	-157.5	98.1	67.0	-6.3	11.5	-13.1	33.8
HM14PM_2940	89.0	93.7	61.6	0.1	99.5	-83.7	-51.6	97.8	55.2	26.9	33.9	52.6
HM14PM_3600	55.6	10.4	19.7	0.0	98.7	-11.6	94.5	87.0	23.4	-6.0	9.5	25.5

Conclusions

Regarding the inversion the main result observed is the big contribution that shear impedance brings to the petro elastic inversion when it is simultaneously considered with P-impedance into the objective function. Another relevant point is that the time-lapse difference should be considered in order to minimize the error caused by uncertainties in the reservoir model. It has to be highlighted as well that the methodology makes the assumption that the base survey corresponding to the initial reservoir state when time lapse differences is computed. This supposition takes advantage of using a data with less uncertainty once there is no fluid movement or pressure changes at this time.

Concerning the initial guess some tests were run comparing constant values and model base simulated values of pressure and saturation and it was noted that the results did not presented big differences. This happen because of the constraints applied during the inversion, so these restrictions plays an important role guiding properly the inversion; even more than the initial guess. Another point to highlight is that this process is not time consuming as the inversion is run independently for each reservoir grid cell.

For the cases studied in this work, the use of pressure and saturation maps in the objective function improves the history matching process, mainly when less production data is available. Differences between observed and simulated pressure maps can be useful to identify reservoir compartmentalization, aiming the reservoir parameterization for posterior history matching.

This work is a preliminary study of a seismic/simulation integration study that is being developed. We are currently working on adding more uncertainty at model properties aiming to build a more robust set of constraints through the definition of regions where some knowledge is proved by field measured data.

References

Avseth, P.; Mukerji, T. and Mavko, G. 2005. "Quantitative seismic interpretation: applying rock physics tools to reduce interpretations risk". Cambridge University Press, Cambridge, U.K.

- Dadashpour, M.; Landrø, M.; Kleppe, J. 2008. "Nonlinear inversion for estimating reservoir parameters from time-lapse seismic data", *Journal of Geophysics and Engineering*, vol 5; pp. 54-66.
- Dadashpour, M.; Echeverria-Ciurri, D.; Kleppe, J.; Landrø, M. 2009. "Porosity and permeability estimation by integration of production and time-lapse near and far offset seismic data", *Journal of Geophysics and Engineering*, vol 6; pp. 325-344.
- Fahimuddin A.; Aanonsen S.; Skjervheim J. A. 2010. "Ensemble Based 4D Seismic History Matching: Integration of Different Levels and Types of Seismic Data". (SPE131453), Annual Conference and Exhibition, 14-17 June 2010, Barcelona, Spain.
- Gosselin, O.; van den Berg, S.; Cominelli, A. 2001. "Integrated History-Matching of Production and 4D Seismic Data" (SPE 71599), Annual Technical Conference and Exhibition, 30 September-3 October 2001, New Orleans, Louisiana.
- Gosselin, O.; Aanonsen, S.I.; Cominelli, A. et al. 2003. "History Matching Using Time-lapse Seismic (HUTS)" (SPE 84464), Annual Technical Conference and Exhibition, 5-8 October 2003, Denver, Colorado.
- Ida, M. (2009). "Incorporation of Quantitative 4D Seismic Data in the History Matching Process". Master thesis. State University of Campinas - UNICAMP. (in Portuguese).
- Kjelstadli, R.M.; Lane, H.S. Johnson, D.T et al.; 2005. "Quantitative History Match of 4D Seismic Response and Production Data in the Valhall Field" (SPE 96317), Offshore Europe, 6-9 September 2005, Aberdeen, United Kingdom.
- Landro M. 2001. "Discrimination between pressure and fluid saturation changes from time-lapse seismic data". *Geophysics*. vol 66; pp 836-844.
- MacBeth, C.; Floricich, M. and Soldo, J. 2006. "Going quantitative with 4D seismic analysis". *Geophysical Prospecting*. vol 54, pp 303-317.
- Mavko, G., Mukerji, T. and Dvorkin, J.2003. "*The Rock Physics Handbook: Tools for seismic analysis in porous media*". Cambridge University Press.
- Nunes, J.P.; Santos, M.S.; Maciel, N.; Davolio, A.; Formento, J. L. 2009. "Separation of pressure and saturation effects using AVO 4D in Marlim Field", 11th International Congress of the Brazilian Geophysical Society, Salvador, Brazil, 24-28 August 2009.
- Sedighi, F.; Stephen, K.D. 2009. "Faster Convergence in Seismic History Matching by Efficient Parameter Searching" (SPE 121210), EUROPEC/EAGE Conference and Exhibition, 8-11 June 2009, Amsterdam, The Netherlands.
- Souza, R. M., A. F. Machado, F. P. Muneratto, D. J. Schiozer. 2010. "Iterative History Matching Technique for Estimation Reservoir Parameters from Seismic Data" (SPE131617), Annual Conference and Exhibition, 14-17 June 2010, Barcelona, Spain.
- Tuna, A. and Lumley, D. E. 1999. "Estimating pressure and saturation changes from time-lapse AVO data", SEG Expanded Abstracts.

APPENDIX B

Complementary results of the paper “*Local history matching using 4D seismic data and multiple models combination*”

Pressure matching

The local history matching methodology proposed in paper 3 uses Sw maps to estimate static reservoir properties, such as porosity and permeability. The Sw map is provided by 4D seismic and, for the dataset used in this work, it was also possible to estimate pressure maps from 4D seismic (according to the results presented in papers 1 and 2). Thus, pressure maps could also be considered an input parameter for the history matching. The choice of not using this information came from the results obtained after the application of the global matching procedure. For the dataset of this work, the global matching procedure, which uses only well production data (BHP and water rate), provided an updated model with a satisfactory pressure matching. Thus, there was no need to extend the methodology to incorporate pressure map information. This appendix shows the results that led to this conclusion. It is important to point out that, in cases where a satisfactory pressure matching is not achieved using only well data, a procedure similar to the one presented in paper 3 could be applied for estimated pressure maps as well.

From Figure B-1, it can be observed that the average reservoir pressure of the model after global matching (black diamond) is considerably better than the one from the base model (solid blue). The average pressure curve of this updated model closely follows the expected behavior of the history data (red circles).

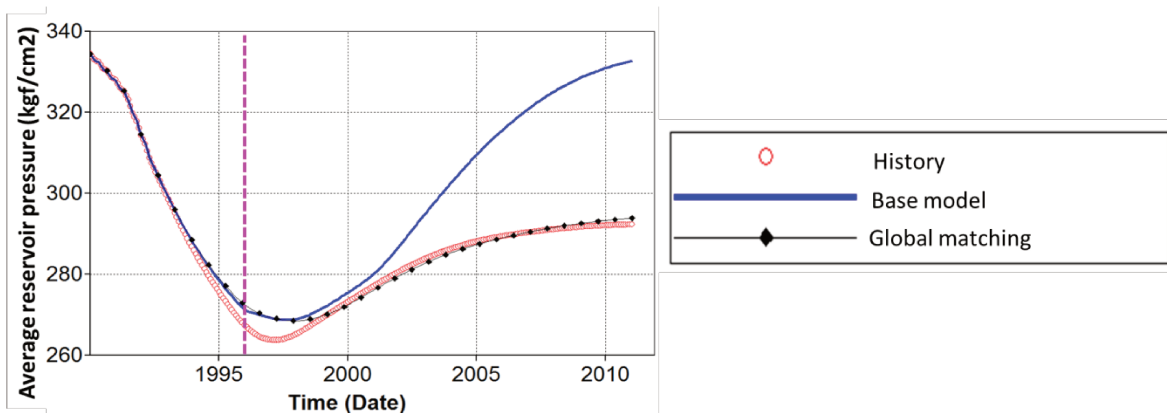


Figure B-1: Average reservoir pressure. The magenta vertical line indicates the two periods: history and forecast.

The pressure map of the model after the global matching (Figure B-2d) also shows an improvement when compared to that of the base model (Figure B-2c). Although differences can be observed around some wells such as INJ1, INJ2, INJ3, the pressure distribution along the reservoir grid is following the expected trend from 4D seismic (Figure B-2b). Figure B-2a shows the true pressure map from which it can be verified that the estimation from 4D seismic was reliable.

Figure B-3 shows the percentage errors of the pressure maps for the base model and this same model after the global matching, compared to the map estimated from 4D seismic. After global matching, the majority of errors observed are smaller than 10%. Thus, the pressure maps are already close to the one estimated from 4D seismic and, again, it is clear that there is no need to include this information in the history matching.

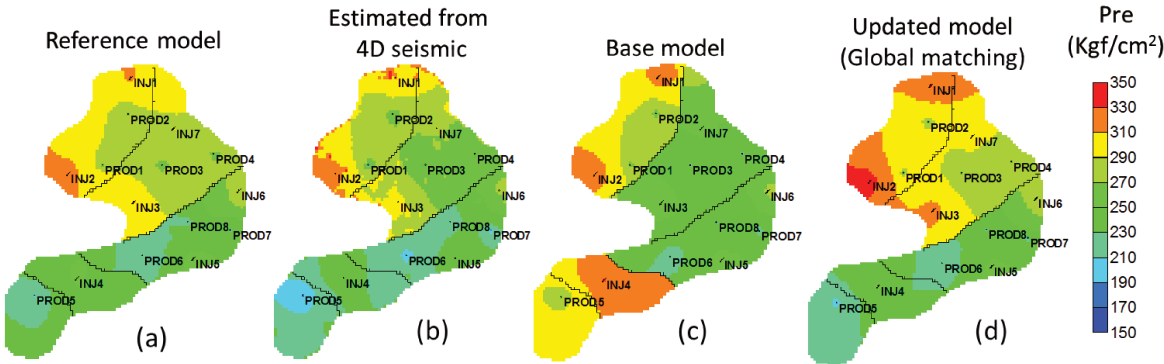


Figure B-2: Pressure maps (layer 3) of the reference model (a), the estimation from 4D seismic (b), the base model (c) and the model after global matching (c).

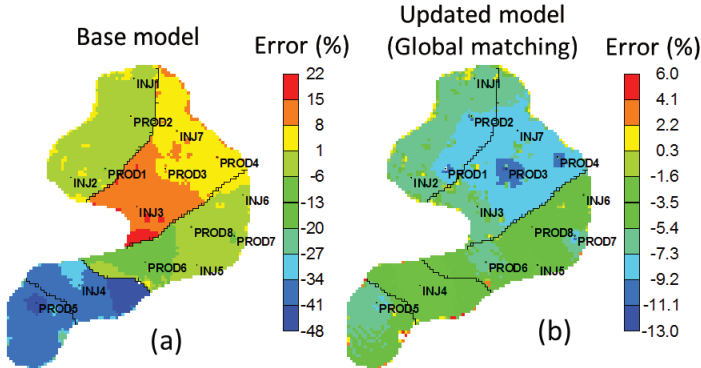


Figure B-3: Pressure percentage error maps (layer 3) of the base model (a) and the model after global matching (b). The error is computed among the pressure map estimated from 4D seismic (Figure A2-b) and the simulation models.

The BHP curves for the individual wells (Figure B-4) also confirm the same results. This information is complementary to the results discussed in the paper. Based on these results, the local matching methodology was proposed to incorporate only water saturation maps. Indeed, this assumption is also in agreement with the difficulty to extract pressure maps from 4D seismic in real cases and with the fact that, usually, engineering data is enough to calibrate the pressure behavior.

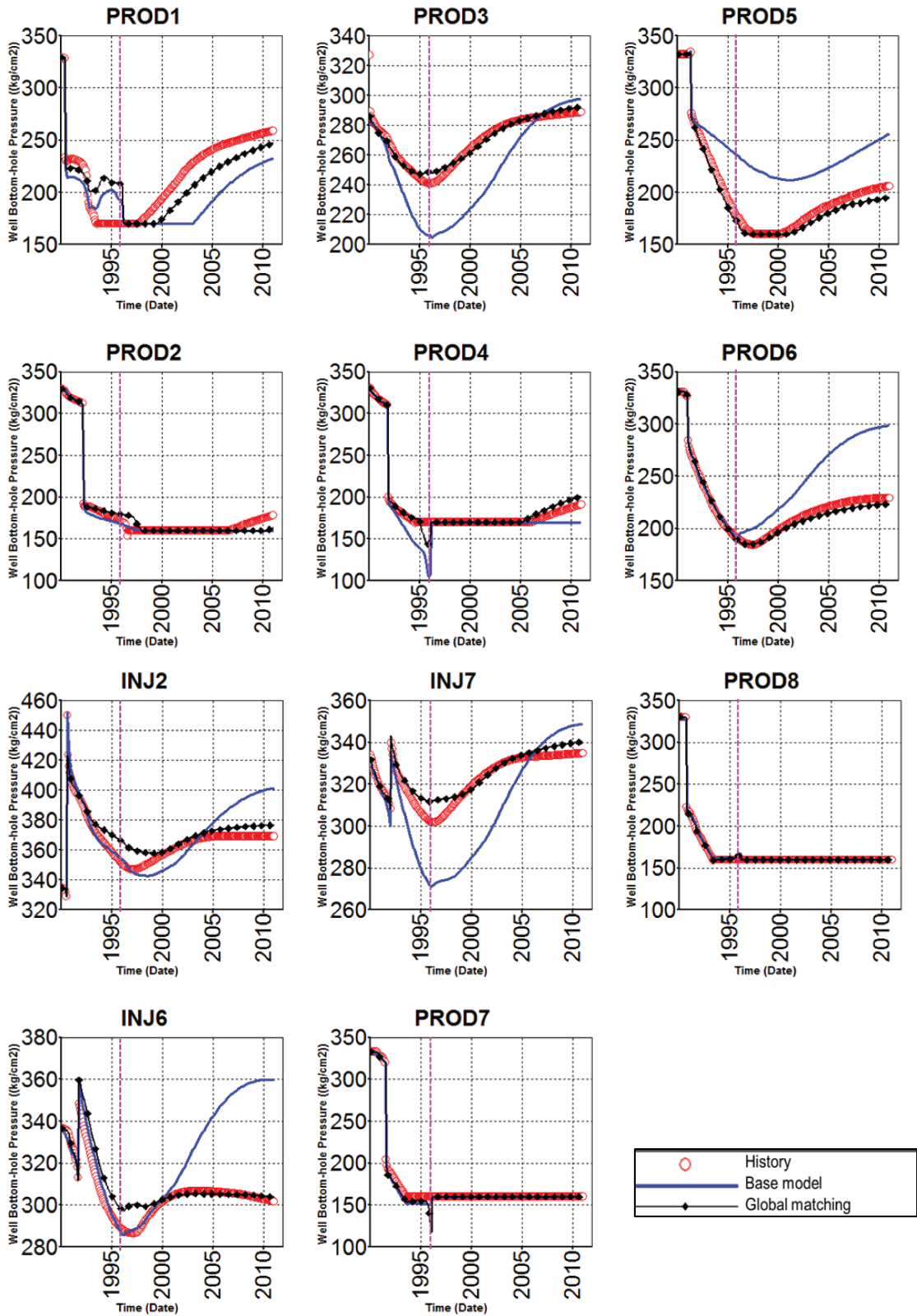


Figure B-4: Bottom-hole pressure for injectors and producers. The magenta vertical line indicates the two periods: history and forecast.

APPENDIX C

Complementary results of the paper “*A methodology to calibrate water saturation estimated from 4D seismic*”

This appendix presents some complementary results and discussions that comprise the two parts of paper 4: the first one is related to the estimation (and calibration) of a saturation map and the second is focused on the use of the estimated map in a history matching process.

1. Estimation of saturation from 4D seismic

The first part of this appendix presents a discussion on the 4D petro-elastic inversion defined in paper 1, which is used as a tool to estimate saturation and pressure maps in all the subsequent papers. Here, the discussion is focused on how the constraints applied to the solution space of the optimization process help to improve the solutions. These constraints are the base of the most important results of this thesis, which are the methodologies, presented in papers 2 and 4.

Paper 1 presents a discussion concerning the objective function behavior of the 4D petro-elastic inversion proposed, considering one single grid block (Figures 10a and 10b in the paper). These images show that, if an ideal dataset is used (without any error/noise), the objective function is very well-behaved, with a global minimum that can be easily found by any optimization process (Figure 10a). However, when an imperfect scenario is assumed by adding some errors in one of the input parameters of the inversion (porosity), the objective function still presents a global minimum, though this point does not coincide with the expected answer (Figure 10b). Actually, the inversion result presented in Figure 10b is very accurate, although not exactly correct. However, when greater inaccuracy or another source of errors (noise in seismic data, for instance) is assumed, the location of the global minimum of the objective function can be very different from the true answer of the problem. In this type of situation, the use of the constraints proposed in paper 2 plays an important role to improve the estimation of pressure and saturation.

This appendix shows an analysis similar to the one presented in paper 1, concerning the details of the optimization, but highlighting the role of the constraints to improve the

solutions. To do this, one point of the model grid was selected, based on the inversion results shown in Figure 6 of paper 4. In this sense, Figure C-1 displays a zoom in the region highlighted with the red arrow in Figure 6 in paper 4; the error maps presented here are exactly the same; only the color scale has been modified. The point marked with a yellow star was selected to perform the analysis of the objective function behavior, in order to understand the improvement seen, especially from Case 1 to Case 2. As stated in paper 4, the sources of error for the inversion are: the wrong estimate of porosity and overburden pressure and the presence of noise on seismic impedances. These errors are described in Table C-1 for this selected grid location.

Remember that the only difference among these inversions is the definition of the solution space due to new constraints. These differences are described in Table C-2, where the constraints applied to the selected grid location for each of the inversions are displayed. Note that Cases 2 and 3 have the same values, because Case 3 corresponds to the estimated saturation of Case 2 with the volume calibration.

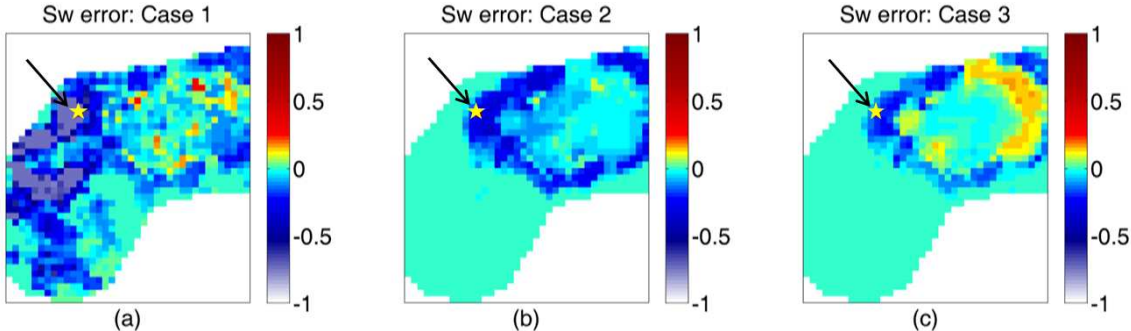


Figure C-1: Zoom in the water saturation errors presented in Figure 6 of paper 4. The point marked with the yellow star was selected to analyze the objective function behavior of the three inversions performed (Cases 1, 2 and 3).

Table C-1: Data related to the point marked in Figure C-1.

	$\Delta_{4D}IP$ (Kg/s x m ²)	$\Delta_{4D}IS$ (Kg/s x m ²)	ϕ	P_over (MPa)
Input for inversion (with noise)	212.98 x10 ³	285.71 x10 ³	0.0266	60
True value (without noise)	232.30 x10 ³	242.94 x10 ³	0.0480	70
Percentage error (%)	-9.07	14.97	-80.45	16.6

Table C-2: Definition of the solution space for the inversions analyzed here for the single location marked in Figure C-1.

	Sw		Pre (MPa)	
	Min	Max	Min	Max
Case 1	0.35	0.8	17.65	44.13
Case 2	0.36	0.57	21.24	23.97
Case 3	0.36	0.57	21.24	23.97
Case ApC	0	1	1	50

Besides the inversions shown in Figure C-1, another test was run as an illustrative example, where the solution space is defined according to more general values: $0 \leq Sw \leq 1$ and $1 \leq Pre \leq 50$ (MPa). Here, this test is called ApC (appendix C). The results of this case are shown in Figure C-2. Following the same layout of the images of paper 1, Figure C-2a shows the objective function behavior and Figure C-2b the location inside the solution space of the estimated values, the initial guess and true answer. This example clearly demonstrates the fact that when errors are considered, such as those in Table C-1, the global minimum is displaced and it does not coincide with the true answer.

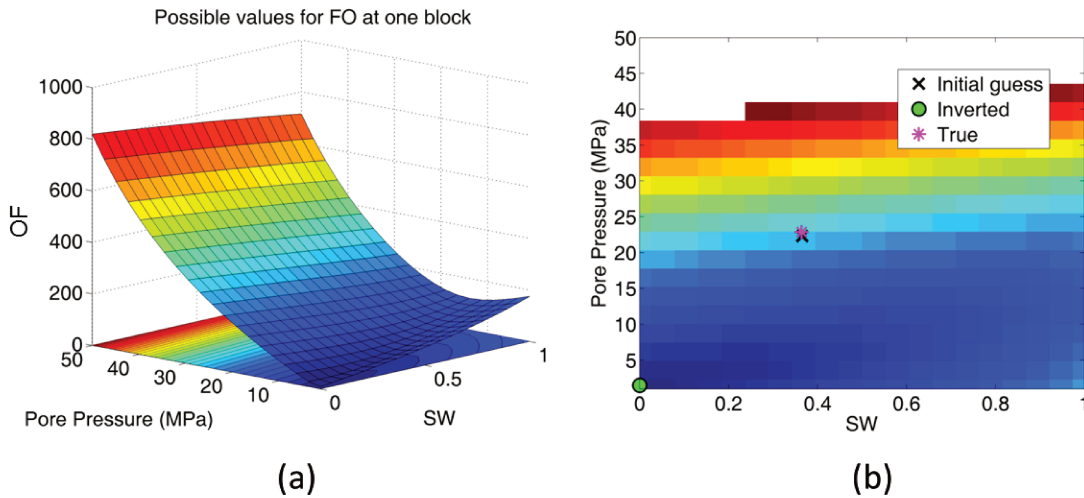


Figure C-2: Inversion results for one grid block location (yellow star marked in Figure C-1) for Case ApC (Table C-1). (a) Possible values of the objective function. (b) Lower values of the objective function, where hot colors stand for higher values; initial guess (black cross), estimated (green circle) and true answer (magenta asterisk).

In the second inversion, the solution space is constrained with the values presented in paper 4 (Case 1 in Table C-2) that are defined by: $Sw_c < Sw < 1 - So_r$ and $Pre_{ProdMin} < Pre < Pre_{InjMax}$. The inversion behavior of this case is shown in Figure C-3. Note that, by

cutting the solution space, the feasible values of pressure are closer to the expected value, which caused a better response of the optimization (compare the pressure values of Cases ApC and 1 in Table C-3).

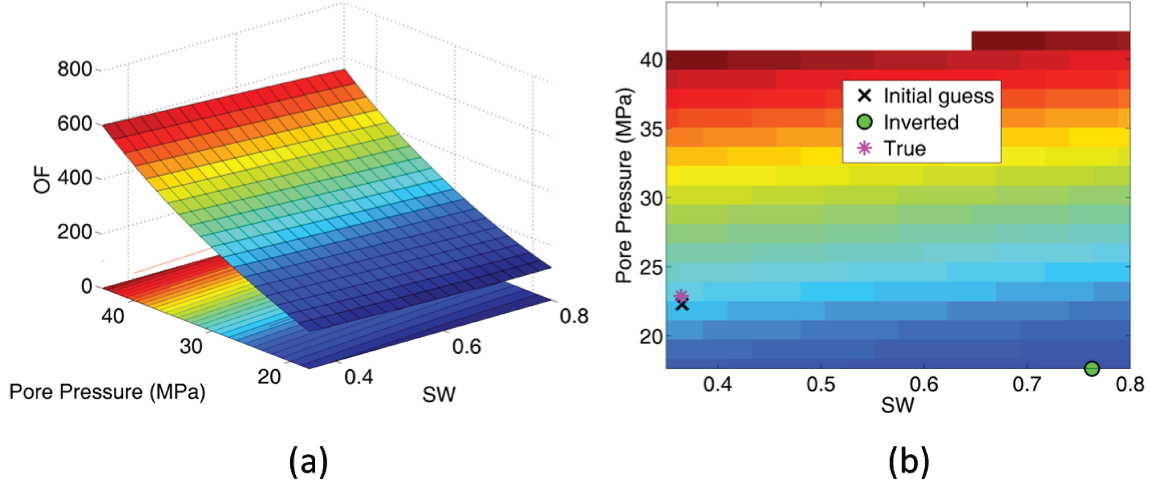


Figure C-3: Inversion results for one grid block location (yellow star marked in Figure C-1); Case 1 in Figure C-1. The solution space is defined as $Sw_c < Sw < 1 - So_r$ and $Pre_{ProdMin} < Pre < Pre_{InjMax}$. (a) Possible values of the objective function. (b) Lower values of the objective function, where hot colors stand for higher values; initial guess (black cross), estimated (green circle) and true answer (magenta asterisk).

The third inversion performed for the selected single location considered the solution space of Case 2 in Table C-2. This means that the range for saturation and pressure are estimated by the methodology proposed in paper 2. Figure C-4 shows the results for this case. Again, it can be observed that, as the solution space is stricter now, a better estimation is reached.

Table C-3 summarizes all the inversion results discussed here. Note that the last row corresponds to the third inversion performed with the volume calibration presented in paper 4 (Case 3 in Table C-2). The last column corresponds to the norm of the error of the solution found:

$$\left\| \begin{matrix} 100(Sw_{true} - Sw_{estimated}) \\ Pre_{true} - Pre_{estimated} \end{matrix} \right\|. \quad (B1)$$

The norm values indicate a gradual improvement obtained from the first inversion (assuming a general solution space) to the last case that considers a stricter and more consistent range, together with the water volume calibration applied to S_w .

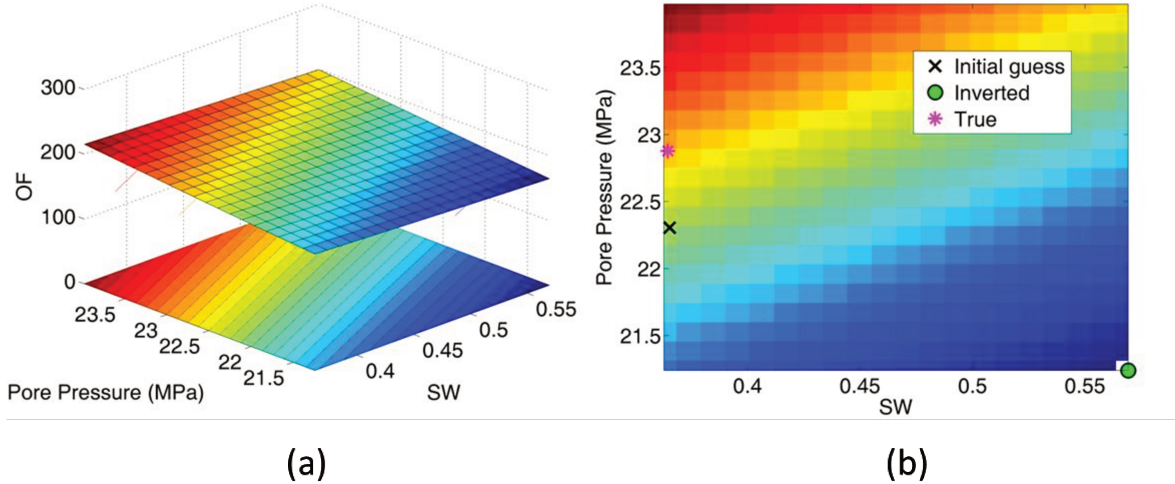


Figure C-4: Inversion results for one grid block location (yellow star marked in Figure C-1); Case 2 in Figure C-1. The solution space is defined as $S_{wc} < S_w < 1 - S_{or}$ and $PreProdMin < Pre < PreInjMax$. (a) Possible values of the objective function. (b) Lower values of the objective function, where hot colors stand for higher values; initial guess (black cross), estimated (green circle) and true answer (magenta asterisk).

Table C-3: Summary of the inversion tests presented for the selected single block location.

	S_w	Pre (MPa)	Norm
True	0.3645	22.88	-
Case ApC	0	1.47	42.27
Case 1	0.7630	17.70	40.18
Case 2	0.5690	21.20	20.52
Case 3	0.4310	21.20	6.86

2. History matching results: well curves

The discussions presented in paper 4, concerning the history matching process applied to the data, were focused on the improvement of the saturation map yielded from the updated simulation model. To complement those results, this appendix displays the well curves of the simulation model before and after the history matching. To tie these results with paper 3 as well, the images below follow the same pattern of curves (color and style) presented in paper 3:

1. History (red circles)
2. Base model (blue solid line): represents the initial model without any matching;
3. Base + GL (black diamond): base model after the global matching presented in paper 3. This model was used as input to perform the (local) history matching of paper 4.
4. LHM2 (dashed green): base model + GL after the local matching presented in paper 3 that was called LHM2 in paper 4.
5. LHM3 (yellow solid circles): base model + GL after the local matching that uses the calibrated saturation map as input for the local history matching (paper 4).

As already mentioned in paper 4, after applying the local history matching (LHM3) slight changes were observed in the simulation results, before and after this matching. One point to be highlighted is that the goal of the last paper was not to achieve the best history matching, but to show that LHM3 was the best option among the three local history matching presented there. In general, the well curves presented below show a relevant improvement from the initial base model and the model after global matching. Then, small changes are observed among the model after the global matching and the two models LHM2 and LHM3.

Figure C-5 shows the field water rate and average pressure. Observing the water rate curves, it can be said that the best model is LHM3, as it presents an excellent production forecast. For the average field pressure, in the history period, LHM3 also provided the best match; in the forecast period, LHM2 and LHM3 have a similar performance.

The curves for the individual wells are shown in Figures C-6 and C-7. As already mentioned, generally there are not significant differences among the models after the matching. Some wells can be pointed out, where LHM3 performed better than LHM2 as, for instance, the wells PROD5 and PROD6 of Figure C-6.

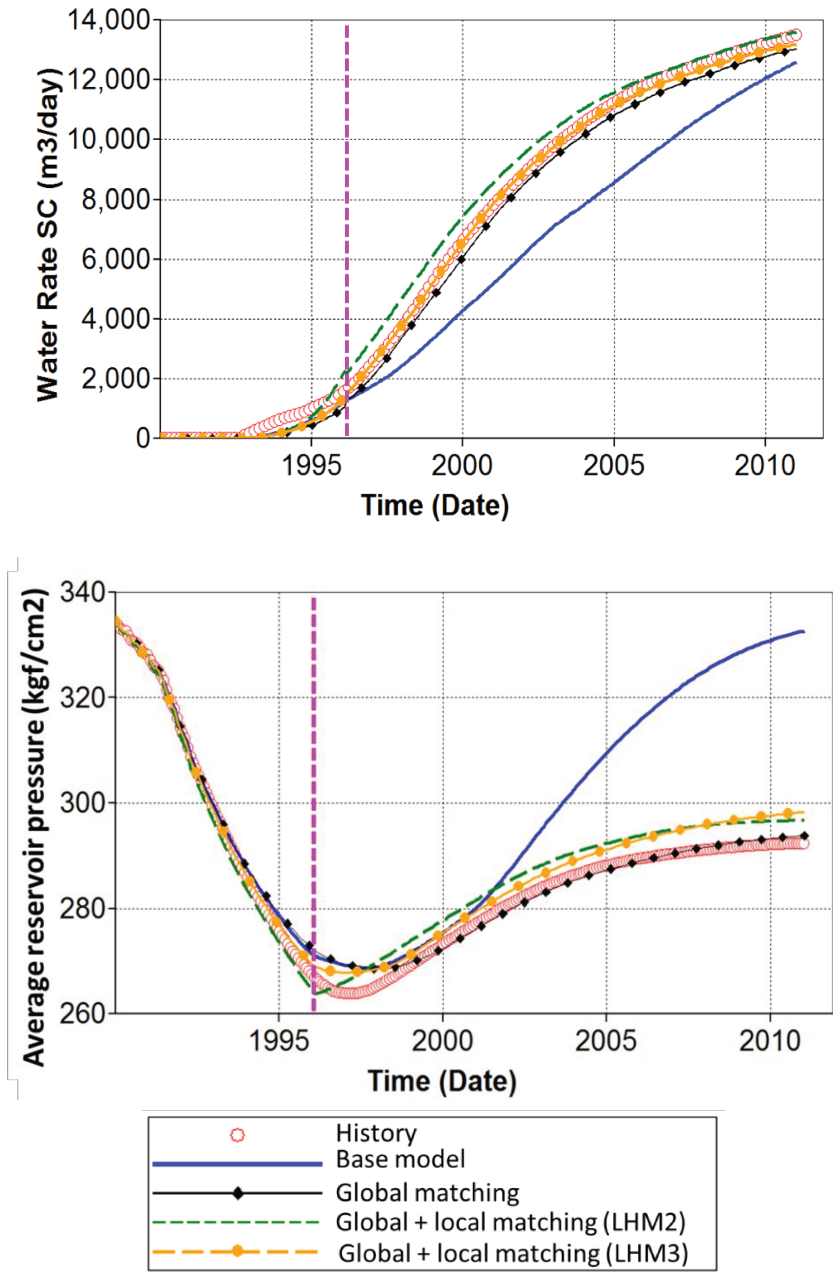


Figure C-5: Top: field water rate (m3/day). Bottom: average reservoir pressure (Kgf/cm2).

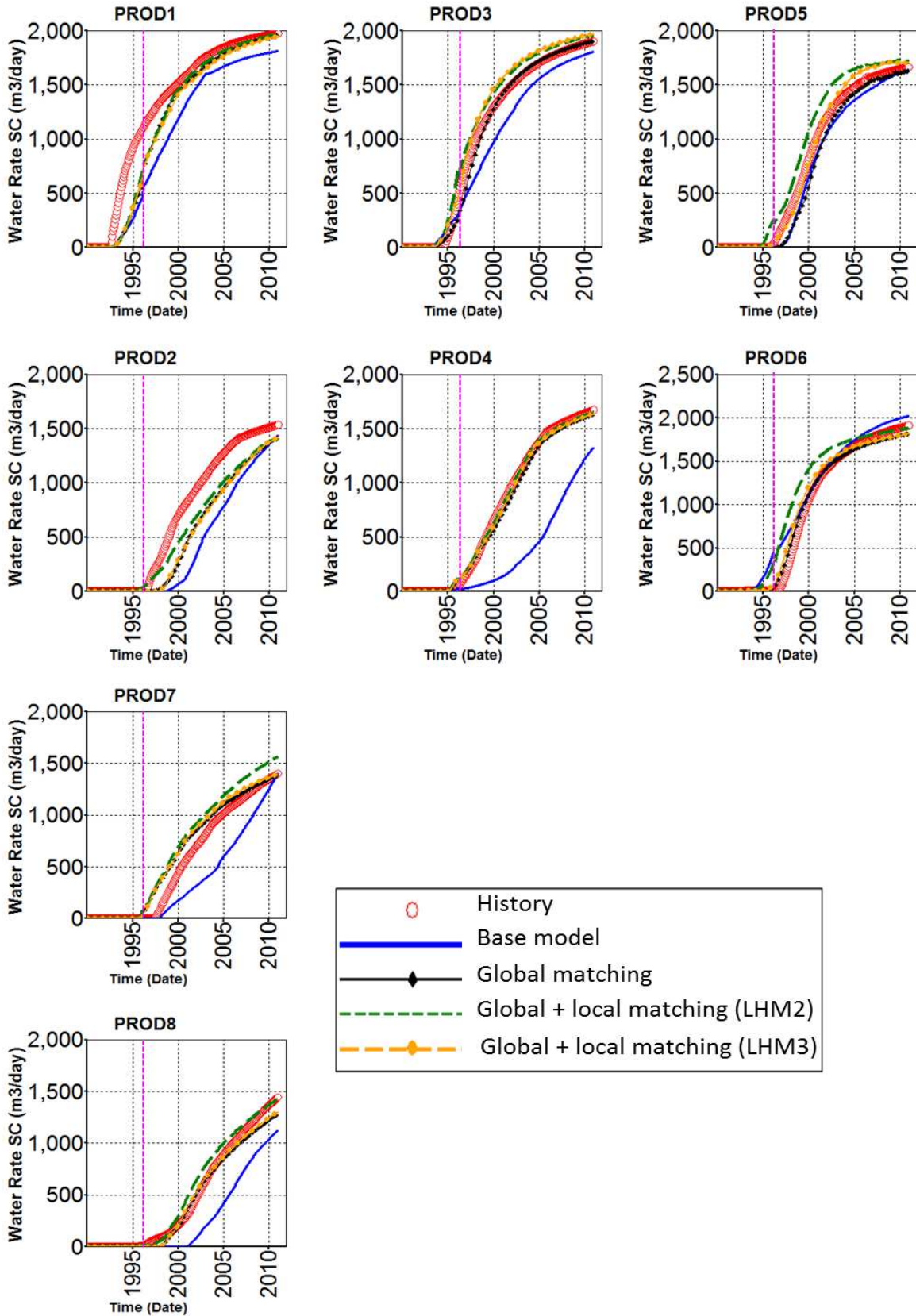
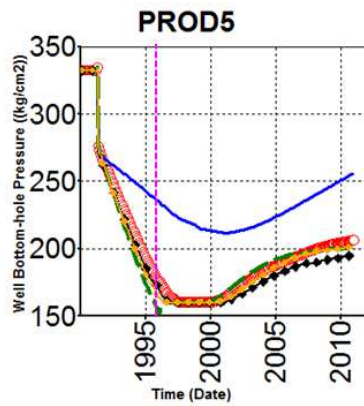
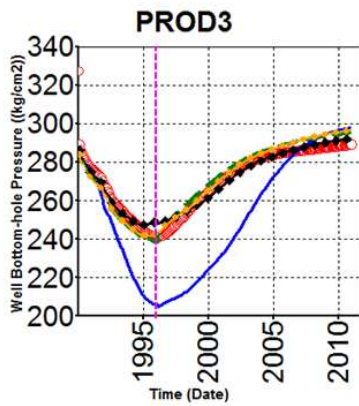
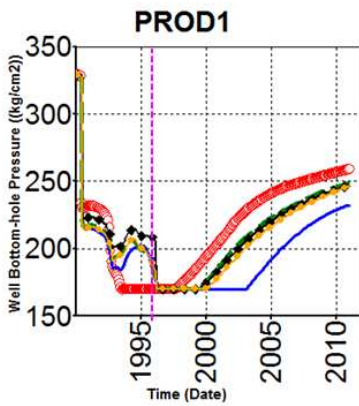
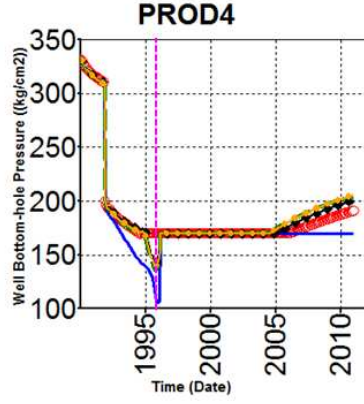
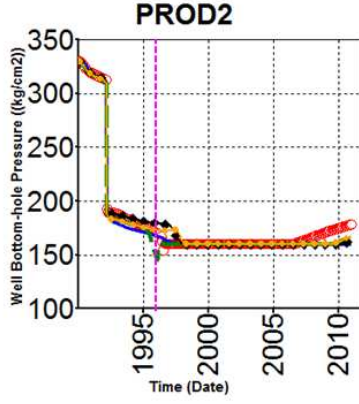
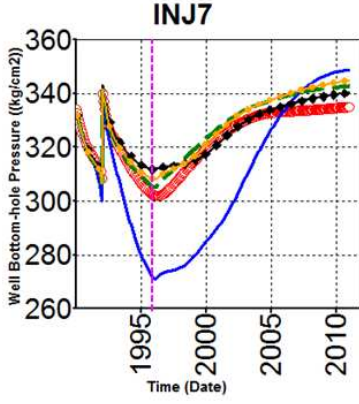
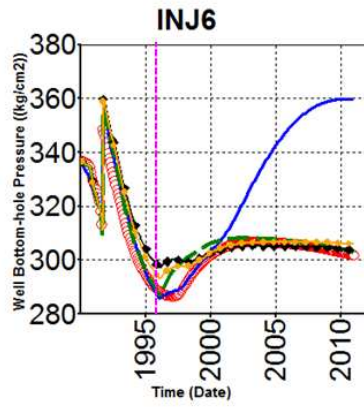
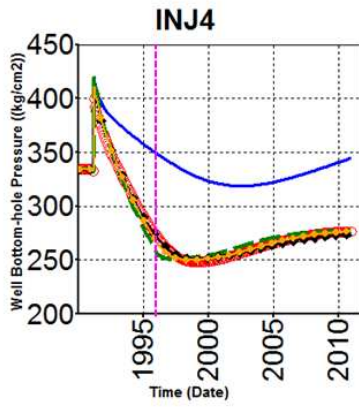
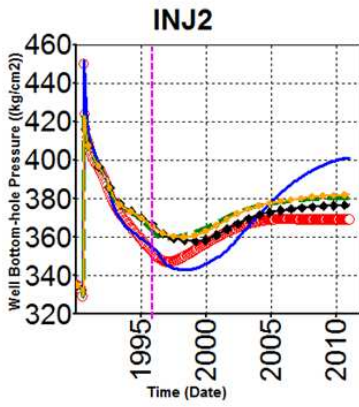
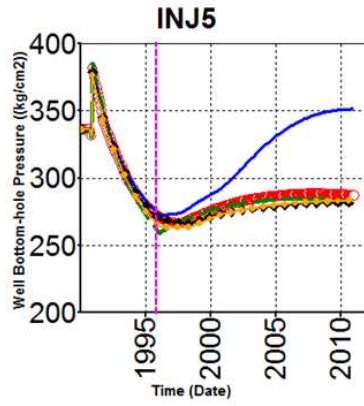
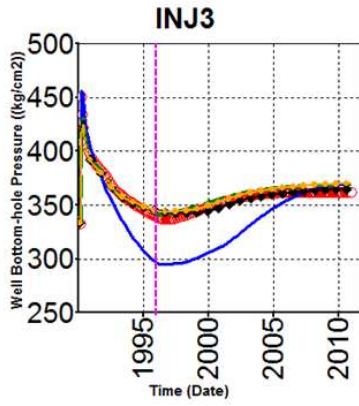
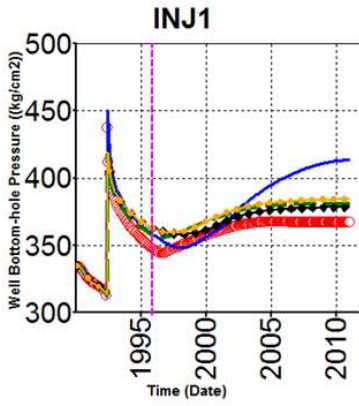


Figure C-6: Water rate (m³/day) for all producer wells.



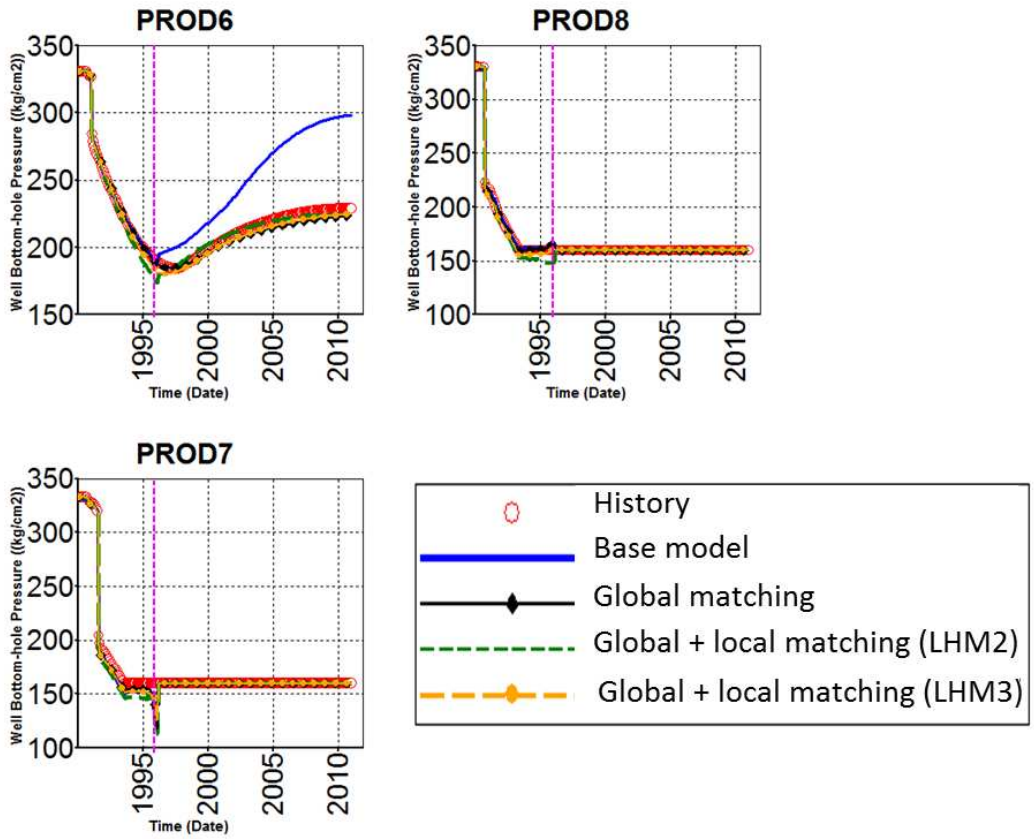


Figure C-7: Bottom-hole pressure (kgf/cm²) for all wells (injectors and producers).